U.S. Department
of Commerce

Volume 121
Number 1–2
January–April 2023

Fishery Bulletin

Pacific Islands Fisheries
Science Center Library

Received on: 6/23

U.S. Department of Commerce

Gina M. Raimondo
Secretary

National Oceanic and Atmospheric Administration

Richard W. Spinrad
Administrator

National Marine Fisheries Service

Janet Coit
Assistant Administrator
for Fisheries

Fishery Bulletin

Scientific Editor
José I. Castro
National Marine Fisheries Service, NOAA
263 13th Avenue South
Saint Petersburg, Florida 33701

Managing Editor
Kathryn Dennis
Scientific Publications Office
National Marine Fisheries Service, NOAA
1845 Wasp Boulevard, Building 176
Honolulu, Hawaii 96818

Associate Editor
Cara Mayo
Scientific Publications Office
National Marine Fisheries Service, NOAA
7600 Sand Point Way NE
Seattle, Washington 98115-0070

Editorial Board

Henry L. Bart Jr.	Tulane University, New Orleans, Louisiana
Katherine E. Bemis	National Systematics Laboratory, Washington, DC
Matthew D. Campbell	National Marine Fisheries Service, Pascagoula, Mississippi
William B. Driggers III	National Marine Fisheries Service, Pascagoula, Mississippi
Gretchen L. Grammer	South Australian Research and Development Institute, Adelaide, Australia
Richard Langton	National Marine Fisheries Service, Walpole, Maine (retired)
J. Fernando Márquez-Farías	Universidad Autónoma de Sinaloa, Mazatlán, México
Richard S. McBride	National Marine Fisheries Service, Woods Hole, Massachusetts
Richard L. Merrick	National Marine Fisheries Service, Falmouth, Massachusetts (retired)
Richard D. Methot	National Marine Fisheries Service, Seattle, Washington
Lisa J. Natanson	National Marine Fisheries Service, Narragansett, Rhode Island (retired)
Mark S. Peterson	University of Southern Mississippi, Ocean Springs, Mississippi
André E. Punt	University of Washington, Seattle, Washington
Joseph M. Quattro	University of South Carolina, Columbia, South Carolina
John F. Walter III	National Marine Fisheries Service, Miami, Florida

***Fishery Bulletin* website: https://spo.nmfs.noaa.gov/fb.htm**

Fishery Bulletin (ISSN 0090-0656) is published quarterly by the Scientific Publications Office, National Marine Fisheries Service, NOAA, 7600 Sand Point Way NE, Seattle, WA 98115-0070.

Although the contents of this publication have not been copyrighted and may be reprinted entirely, reference to source is appreciated.

The Secretary of Commerce has determined that the publication of this periodical is necessary according to law for the transaction of public business of this Department. Use of funds for printing of this periodical has been approved by the Director of the Office of Management and Budget.

For Sale by the Superintendent of Documents, U.S. Government Publishing Office, Washington, DC 20401. Subscription price per year: $32.00 domestic and $44.80 foreign. Cost per single issue: $19.00 domestic and $26.60 foreign. **See back for order form.**

Fishery Bulletin carries original research reports on investigations in fishery science, engineering, and economics. It began as the Bulletin of the United States Fish Commission in 1881; it became the Bulletin of the Bureau of Fisheries in 1904 and the *Fishery Bulletin* of the U.S. Fish and Wildlife Service in 1941. Separates were issued as documents through volume 46; the last document was no. 1103. Beginning with volume 47 in 1931 and continuing through volume 62 in 1963, each separate appeared as a numbered bulletin. A new system began in 1963, with volume 63, in which papers are bound together in a single issue. Beginning with volume 70, number 1, January 1972, *Fishery Bulletin* became a periodical, issued quarterly. In this form, it is available by subscription from the Superintendent of Documents, U.S. Government Publishing Office, Washington, DC 20401. It is also available free in limited numbers to libraries, research institutions, and state and federal agencies and in exchange for other scientific publications.

U.S. Department of Commerce
Seattle, Washington

Volume 121
Number 1–2
January–April 2023

Fishery Bulletin

Contents

Articles

1–16 **Kyne Krusic-Golub and Lisa Ailloud**

Evaluating otolith increment deposition rates in bigeye tuna (*Thunnus obesus*) and yellowfin tuna (*T. albacares*) tagged in the Atlantic Ocean

17–29 **Long V. Nguyen, Dat X. Mai, Quang M. Thai, and Tuan S. Vo**

Juvenile yield and adult abundance, genetic diversity and structure, and linkages among marine habitats for goldlined spinefoot (*Siganus guttatus*) in the coastal waters of Vietnam

Note

30–35 **Bobbie M. Buzzell, Adrianne M. Akmajian, and Alejandro Acevedo-Gutiérrez**

Exploring the biotic resistance of the invasive green crab (*Carcinus maenas*) by examining the diet of North American river otters (*Lontra canadensis*)

Articles

36–49 **Michael V. Cyrana, Alexander J. Ledet, and Henry L. Bart Jr.**

Ovarian masculinization and reproductive impairment in 3 species of groundfish in and around the hypoxic zone in the Gulf of Mexico

50–66 **Paul G. von Szalay, Stan Kotwicki, Lewis A. K. Barnett, Lou J. Rugolo, and Kotaro Ono**

Reducing uncertainty in survey abundance estimates by considering alternative designs and estimators: a case study with 3 species in the Gulf of Alaska

67 **Errata**

69–72 **Guidelines for authors**

The National Marine Fisheries Service (NMFS) does not approve, recommend, or endorse any proprietary product or proprietary material mentioned in this publication. No reference shall be made to NMFS, or to this publication furnished by NMFS, in any advertising or sales promotion that would indicate or imply that NMFS approves, recommends, or endorses any proprietary product or proprietary material mentioned herein or that has as its purpose an intent to cause directly or indirectly the advertised product to be used or purchased because of this NMFS publication.

The NMFS Scientific Publications Office is not responsible for the contents of the articles.

National Marine Fisheries Service
NOAA

Fishery Bulletin
established in 1881

Spencer F. Baird
First U.S. Commissioner of Fisheries and founder of *Fishery Bulletin*

Evaluating otolith increment deposition rates in bigeye tuna (*Thunnus obesus*) and yellowfin tuna (*T. albacares*) tagged in the Atlantic Ocean

Kyne Krusic-Golub[1]
Lisa Ailloud (contact author)[2]

Email address for contact author: lisa.ailloud@noaa.gov

[1] Fish Ageing Services
28 Swanston Street
Queenscliff, Victoria 3225, Australia

[2] International Commission for the Conservation of Atlantic Tunas Secretariat
Calle Corazón de Maria 8
28002 Madrid, Spain

Present address for contact author: Southeast Fisheries Science Center
National Marine Fisheries Service, NOAA
75 Virginia Beach Drive
Miami, Florida 33149

Abstract—A recent Atlantic-wide tag-recapture experiment run by the International Commission for the Conservation of Atlantic Tunas was an opportunity to directly validate otolith increment deposition rates for bigeye tuna (*Thunnus obesus*) and yellowfin tuna (*T. albacares*) in the region. Age and time at liberty were estimated by using annual and daily increment counts for sectioned otoliths from sampled fish previously injected with oxytetracycline and later recaptured. The use of annual increment counts resulted in greater age estimates than those from daily increment counts for fish >55 cm straight fork length (SFL). Use of daily increment counts led to underestimation of time at liberty for fish >55 cm SFL at recovery, compared with known times at liberty. In contrast, predictions based on annual increment counts are accurate across the entire size range of sampled fish, validating the notion that increments are deposited annually. We therefore recommend that counting annual increments be the preferred method for aging yellowfin and bigeye tuna from the Atlantic Ocean and that the use of daily increments for aging be limited to young of the year. Aging fish accurately is important for stock assessments in which data on age and growth play an increasingly essential role in examining population dynamics. It is crucial that otolith reading practices and analyses based on age data reflect the most up-to-date recommendations for age estimation.

Manuscript submitted 25 April 2022.
Manuscript accepted 18 November 2022.
Fish. Bull. 121:1–16 (2022).
Online publication date: 22 December 2022.
doi: 10.7755/FB.121.1.1

The views and opinions expressed or implied in this article are those of the author (or authors) and do not necessarily reflect the position of the National Marine Fisheries Service, NOAA.

Fish otoliths (or ear stones) are metabolically inert structures whose concentric growth rings have been widely used as indicators of fish age. Although the exact physiological and biochemical processes of increment formation in otoliths are not well understood, it is generally accepted that the rate of deposition is regulated by variations in both biotic (e.g., growth, feeding, reproduction, and stress) and abiotic (e.g., light and water temperature) factors (Morales-Nin, 2000). For many species, the otolith increment deposition rate has been validated. However, for tropical bigeye tuna (*Thunnus obesus*) and yellowfin tuna (*T. albacares*), validation studies have been limited (Table 1), and the protocols accepted for age determination are not the same across stocks and are applied inconsistently across the size spectrums of stocks.

The results of many studies indicate that the technique of using daily increment counts is not suitable for species that are medium- to long-lived. The outer daily increments become very narrow once fish reach a certain size, making them difficult to discern (Campana, 1992; Jones, 1992). In addition, otolith increments may not be deposited daily after fish reach a certain age or size (Neilson and Campana, 2008). Annual increments, on the other hand, are generally visible throughout the life of a fish; therefore, counts of these increments are often deemed more accurate than daily increment counts, especially once a fish reaches a certain age or size (Casselman, 1983; Francis et al., 1992; Williams et al., 2013). However, until recently, scientists thought that fish inhabiting tropical environments could not be aged reliably by using this technique because their environment lacks clear seasonal signals. Increased expertise and results of recent studies validating the rate of deposition of annual increments in otoliths of fish in tropical environments have shifted that notion (Newman et al., 1996; Cappo et al., 2000; Pilling et al., 2000; Morales-Nin and Panfili, 2005; Fowler, 2009).

Annual growth increments in otolith sections have successfully been

Table 1

Summary of studies, adapted from Williams et al. (2013), in which the periodicity of the formation of growth increments in otoliths was directly validated for yellowfin tuna (YFT) (*Thunnus albacares*) and bigeye tuna (BET) (*T. obesus*) sampled in the Atlantic, Pacific, and Indian Oceans. The age validation methods used in these studies to determine the deposition rate of daily and annual increments in otoliths included oxytetracycline (OTC) mark-recapture experiments, captive experiments (captive), bomb radiocarbon dating (^{14}C), and strontium chloride ($SrCl_2$) mark-recapture experiments. LM=light microscope; SEM=scanning electron microscope; SFL=straight fork length.

Region (ocean)	Species	Sample size	Validation method	Increment type	Reading method	Time at liberty (d)	Length range (cm SFL)	Age range (years)	Source
Eastern Pacific	YFT	53	OTC	Daily	Whole otolith, LM	3–389	40–110	–	Wild and Foreman, 1980
Eastern Pacific	YFT	74	OTC	Daily	Whole otolith, LM	<515	<148	–	Wild et al., 1995
Western Pacific	YFT	12	Captive	Daily	Whole otolith, LM	3–39	25–40	–	Yamanaka, 1990[a]
Western Pacific	YFT	3	OTC	Daily	Sectioned otolith, SEM and LM	21–175	39–91	–	Lehodey and Leroy[6]
Eastern Atlantic	BET	83	OTC	Daily	Sectioned otolith, LM	10–412	44–95	–	Hallier et al., 2005
North Pacific	YFT	2	Captive	Daily	Whole otolith, LM	24–30	52	–	Uchiyama and Struhsaker, 1981
Eastern Pacific	BET	70	OTC	Daily	Sectioned otolith, LM	15–551	38–135	–	Schaefer and Fuller, 2006
Western Pacific	BET	10	$SrCl_2$	Annual	Sectioned otolith, SEM	207–2420	79–159	2–9	Farley et al., 2006
Western Indian	BET	116	OTC	Daily	Sectioned otolith, LM	3–1166	46–142	–	Sardenne et al., 2015
Western Indian	YFT	112	OTC	Daily	Sectioned otolith, LM	8–969	48–135	–	Sardenne et al., 2015
Western Atlantic	BET	12	^{14}C	Annual	Sectioned otolith, LM	–	130–175	3–17	Andrews et al., 2020
Western Atlantic	YFT	34	^{14}C	Annual	Sectioned otolith, LM	–	100–180	2–18	Andrews et al., 2020

[a] Yamanaka, K. L. 1990. Age, growth and spawning of yellowfin tuna in the southern Philippines. Indo-Pac. Dev. Manag. Program., IPTP Work. Pap. 21, 87 p.

used to age a number of tuna and billfish species (Gunn et al., 2008; Griffiths et al., 2010; Farley et al., 2013; Wells et al., 2013; Secor et al., 2014; Farley et al.[1]; Lang et al., 2017; Murua et al., 2017; Farley et al.[2]; Pacicco et al., 2021). The annual rate of increment deposition has been recently validated for bigeye and yellowfin tuna in the Atlantic Ocean by using bomb radiocarbon dating (Table 1) (Andrews et al., 2020; Pacicco et al., 2021) and for bigeye tuna in the western Pacific Ocean by using strontium chloride in mark-recapture experiments (Farley et al.[3]). Direct comparison of ages based on annual increment counts versus daily increment counts have also been carried out for tropical tuna species, and the results indicate that age estimates from daily increment counts are negatively biased compared with age estimates from annuli (Griffiths et al., 2010; Williams et al., 2013).

In the eastern Pacific Ocean, daily increment counts are used for aging yellowfin and bigeye tuna up to ~150 cm in straight fork length (SFL) (Wild and Foreman, 1980; Schaefer and Fuller, 2006; Minte-Vera et al., 2020; Xu et al., 2020). No direct aging is carried out for fish larger than 150 cm SFL, even though the longevity for bigeye tuna has been estimated to be at least 15–16 years on the basis of tagging data (Langley et al., 2008).

[1] Farley, J., N. Clear, D. Kolody, K. Krusic-Golub, P. Eveson, and J. Young. 2016. Determination of swordfish growth and maturity relevant to the southwest Pacific stock. West. Cent. Pac. Fish. Comm. WCPFC-SC12-2016/SA-WP-11, 90 p. [Available from website.]

[2] Farley, J., K. Krusic-Golub, P. Eveson, N. Clear, F. Roupsard, C. Sanchez, S. Nicol, and J. Hampton. 2020. Age and growth of yellowfin and bigeye tuna in the western and central Pacific Ocean from otoliths. West. Cent. Pac. Fish. Comm. WCPFC-SC16-2020/SA-WP-02, 27 p. [Available from website.]

[3] Farley, J., K. Krusic-Golub, N. Clear, P. Eveson, N. Smith, and J. Hampton. 2019. Project 94: workshop on yellowfin and bigeye age and growth. West. Cent. Pac. Fish. Comm. WCPFC-SC15-2019/SA-WP-02, 14 p. [Available from website.]

In the western and central Pacific Ocean, Indian Ocean, and Atlantic Ocean, the ages of yellowfin and bigeye tuna are now routinely estimated by using a combination of counting daily increments, hereafter referred to as *daily aging* (restricted to small fish <80 cm SFL or at age 1), and counting annual increments, hereafter referred to as *annual aging* (Farley et al.[4]; Farley et al.[2]; Allman et al., 2020; Pacicco et al., 2021).

Differences in aging methods result in divergent assumptions regarding the life history of fish of the same species. The oldest aged specimens of yellowfin tuna from the Atlantic Ocean and from the western and central Pacific Ocean have been estimated to be 18 years old (Andrews et al., 2020) and 15 years old (Farley et al.[2]), respectively, and both ages are based on annual aging. In contrast, the oldest aged specimen of yellowfin tuna from the eastern Pacific Ocean is estimated to be 4 years old, an age based on daily aging (Wild, 1986). Although differences in maximum age could result from geographical differences in historical fishing pressure (i.e., age truncation of exploited populations caused by sustained, size-selective fishing), in this case, they are more likely the result of differences in aging protocols (i.e., using annual versus daily increment counts). With fish aging underpinning estimates of age composition, growth, and natural mortality in stock assessments, it is particularly important that precise and unbiased aging protocols be used across all stocks.

Age validation and comparison studies for tuna species are limited in the Atlantic Ocean. Our goals in this study were to provide additional evidence for the periodicity of daily and annual increment formation in yellowfin and bigeye tuna in the Atlantic Ocean and to provide guidance regarding the utility of daily and annual increment counts for studies of the age and growth of tropical tuna. We analyzed a subset of otoliths sourced from a large-scale tropical tuna tagging campaign that was carried out from 26 June 2015 through 28 February 2021. As part of the Atlantic Ocean Tropical tuna Tagging Program (AOTTP) of the International Commission for the Conservation of Atlantic Tunas (ICCAT) (AOTTP Coordination Team[5]), over 9000 tropical tuna were injected with oxytetracycline (OTC), a chemical marker commonly used to validate the rate of deposition of daily and annual increments in otoliths (Campana, 2001).

Once a fish is injected with OTC, the chemical is quickly incorporated into the otolith structure and leaves a permanent mark on the increment that formed at the time of tagging. Upon recovery, the mark can be detected by using fluorescence microscopy. Comparing the number of increments present beyond the OTC mark with the known time at liberty of a fish allows one to validate the rate of deposition of individual increments or growth bands. Our specific objectives therefore were as follows: 1) to test the frequency of deposition of daily and annual increments in the sagittal otoliths of yellowfin and bigeye tuna marked with OTC, 2) to compare age estimates based on daily versus annual increment counts for otolith thin sections taken from the same fish that were OTC marked and not, and 3) to test whether the sectioning plane used influenced total counts of daily increments and counts of increments after the OTC mark.

Material and methods

Otolith sampling

As part of the AOTTP, 3146 yellowfin tuna and 1967 bigeye tuna were injected with OTC. Of those injected fish, 498 yellowfin tuna and 384 bigeye tuna have been physically recovered to date (Suppl. Fig. 1) (online only). The OTC-marked fish were measured and dissected to obtain biological data (e.g., length, weight, and sex), and hard parts were extracted, cleaned, and stored for further analysis. A subsample of fish that included the most valuable samples (i.e., the largest fish and fish with times at liberty sufficient for increments to be detected beyond the OTC mark) were selected for the age analyses (Fig. 1). The subsample comprised 31 bigeye tuna and 38 yellowfin tuna marked or recaptured across the tropical and subtropical Atlantic Ocean, including waters off Brazil, Azores, Canary Islands, West Africa, St. Helena, and South Africa. Additional otoliths from large (127–172 cm SFL) yellowfin tuna not marked with OTC were donated to the project, 2 otoliths by the Centre for Environment Fisheries and Aquaculture Science (St. Helena, UK) and 11 otoliths by the University of Cape Town in South Africa (Fig. 1).

Otolith preparation

Otoliths were imaged prior to sectioning and weighed to the nearest milligram if unbroken. The most complete otolith from each pair was selected for preparation, and the core was marked prior to it being embedded in Polyplex Clear Ortho Casting Resin (Allnex, Frankfurt, Germany). Otoliths were then set in resin blocks, oriented to allow a transverse section to be cut from the center of the otolith (Suppl. Fig. 2A) (online only). Sectioning otoliths on the transverse plane allowed results and methods to be directly compared to those of previous studies on yellowfin tuna in the Atlantic Ocean (Stéquert et al., 1996; Shuford et al., 2007) and the western and central Pacific Ocean (Farley et al.[2]) and on yellowfin and bigeye tuna in the Indian Ocean (Stéquert and Conand, 2000; Sardenne et al., 2015). It also enabled us to conduct annual and daily aging on the same otolith because, once annual increment counts and OTC-mark examination were completed, the otolith could be ground thinner for daily increment analysis, leaving the remaining otolith to be retained for other purposes.

[4] Farley, J., K. Krusic-Golub, P. Eveson, N. Clear, P. L. Luque, I. Artetxe-Arrate, I. Fraile, I. Zudaire, A. Vidot, R. Govinden, et al. 2021. Estimating the age and growth of bigeye tuna (*Thunnus obesus*) in the Indian Ocean from counts of daily and annual increments in otoliths. Indian Ocean Tuna Comm. IOTC-2021-WPTT23-18_Rev1, 28 p. [Available from website.]

[5] AOTTP Coordination Team. 2021. ICCAT Atlantic Ocean Tropical tuna Tagging Programme (AOTTP)—final narrative report, 57 p. Int. Comm. Conserv. Atl. Tunas Secr., Madrid, Spain. [Available from website.]

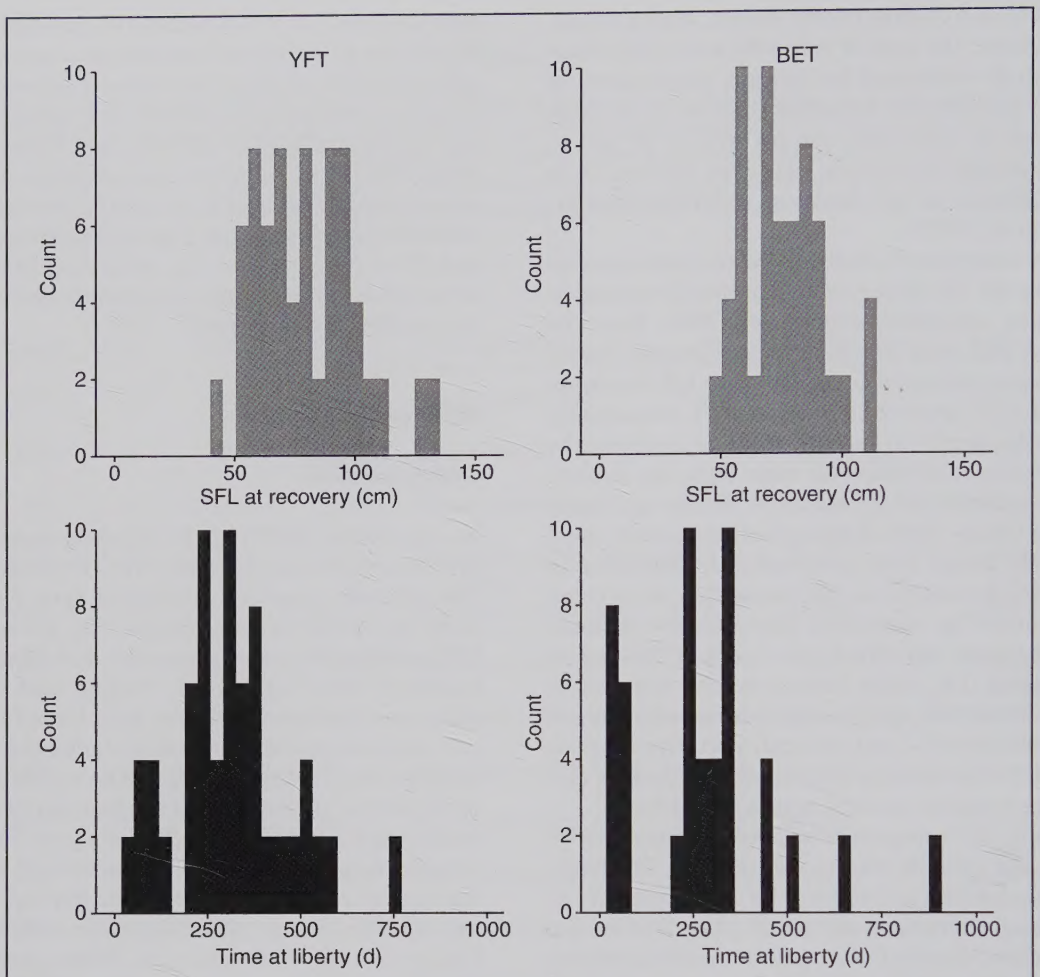

Figure 1

Frequency distributions for straight fork lengths (SFLs) at time of recovery and for times at liberty of yellowfin tuna (YFT) (*Thunnus albacares*) and bigeye tuna (BET) (*T. obesus*) sampled in the tropical and subtropical Atlantic Ocean from 2015 through 2021. Most fish (31 bigeye tuna and 38 yellowfin tuna) were injected with oxytetracycline (OTC) and recovered as part of the Atlantic Ocean Tropical tuna Tagging Program. An additional 11 otoliths from bigeye tuna and 2 otoliths from yellowfin tuna (127–172 cm SFL) were not marked with OTC.

One section approximately 500 µm thick was cut through the center of each embedded otolith, ensuring that the primordia and core area remained within the otolith section. Cuts were made by using an IsoMet 1000 precision cutting machine (Buehler Ltd., Lake Bluff, IL) and a single diamond wafering blade (102 × 0.3 mm) set to a cutting speed of 7.5 Hz (450 rpm). To allow detection of OTC marks and annual aging, sections were mounted on microscope slides (76.2 × 25.4 mm) by using thermoplastic resin (Cystalbond 509, Electron Microscopy Sciences, Hatfield, PA), with the side of the section farthest away from the core facing up. Each section was ground to a thickness between 320 and 350 µm with wet-and-dry sandpaper (800 and 1200 grit), lubricated with distilled water. Once annual increment counts and the OTC-mark examination were completed, the transverse sections were further ground down, by using 1200-grit wet-and-dry sandpaper, to a thickness of approximately 60–90 µm to reveal the daily increment structure. The sections were polished with 2-µm aluminum oxide slurry against a felt pad, rinsed, and dried.

For the donated otoliths sampled from large fish, slides were prepared only for use in annual aging for the following reasons: the discrepancy between annual and daily increment counts already reported for otoliths from large specimens caught in the Pacific Ocean (Williams et al., 2013); the value of preserving prepared slides for annual age estimation training purposes, especially considering that otoliths from very large fish are difficult to source; and the need to ensure that the otoliths remaining from each pair are still available for future analyses or validation work (e.g., age estimation through near-infrared spectroscopy or age validation through the use of bomb radiocarbon dating).

Age estimation with otoliths

Annual increment counts The methods used for the annual aging of bigeye tuna and yellowfin tuna follow those developed for other tuna species that are routinely aged at Fish Ageing Services, in Queenscliff, Australia (Farley et al., 2006; Gunn et al., 2008; Farley et al., 2013), and those in information available in the literature at the time (i.e., Lang et al., 2017). Information on aging bluefin tuna sampled in the Atlantic Ocean was also used as a basis to aid interpretation of what may constitute an annual growth zone in bigeye tuna and yellowfin tuna from the Atlantic Ocean (Rodríguez-Marín et al., 2007; Neilson and Campana, 2008; Rodríguez-Marín et al., 2014; Secor et al., 2014). Before reading each section, the ground surface of the otolith was covered in a thin layer of low-viscosity immersion oil (Type A, Cargille-Sacher Laboratories Inc., Cedar Grove, NJ) to fill in any residual scratches and aid in the imaging process. Sections were examined at 25× magnification under transmitted light with a Leica M125 C routine laboratory stereo microscope (Leica Microsystems, Wetzlar, Germany).

The annual age of each section was estimated by counting opaque growth zones (which appear dark under transmitted light). The last fully completed opaque zone before the otolith edge was counted only if translucent otolith material was detected between the outer edge of the last opaque zone and the otolith edge. All age readings were made without knowledge of fish size, otolith weight, sex, location of capture, or time at liberty. A single TIFF image was captured, and the distances between the primordium and the outer edge of each opaque zone was measured. For each section, a readability score of 1–5 was assigned, with 1 meaning a zone pattern could not be interpreted and 5 meaning there was a clear pattern of alternating opaque and translucent zones. Also recorded were any relevant comments related to the otolith structure or interpretation of the zones.

Daily increment counts Daily increments were counted by using a Leitz Diaplan compound microscope (Leica Microsystems) with transmitted light at various magnifications ranging between 400× and 1000×, depending on the area of the otolith being interpreted. The interpretation of the otolith microstructure in tuna can be subjective, and it can often be difficult to distinguish sub-daily increments from the assumed daily increments. These difficulties were recognized by Shuford et al. (2007) and Sardenne et al. (2015), and, as per their methods, the sub-daily increments were characterized by faint and incomplete rings. Further complicating the daily increment count was the presence of subsections within some otoliths for which little or no increment pattern could be detected. Because daily increment widths tend to be autocorrelated (Campana, 1992), the counts of micro-increments within these subsections were interpolated from the surrounding areas. The method used for the interpretation of daily increments is consistent with those methods published for reading transverse sections (Lehodey and Leroy[6]; Shuford et al., 2007; Sardenne et al., 2015) and frontal sections (Schaefer and Fuller, 2006). The otolith sections were read at least 2 times by the single reader before a final count was completed and the number of daily increments was recorded.

Validation of increment deposition rate: oxytetracycline-mark detection

Each otolith section from a fish that was injected with OTC was examined for the presence and position of the OTC mark by using a Leitz Diaplan compound microscope fitted with a 100-W incident ultraviolet light source and a Leitz D filter block (Leica Microsystems, with excitation filter of 450–520 nm) to suit the fluorescent properties of the OTC. Images were taken at magnifications of 25× and 40×, and, if the OTC mark was very faint, at 100× magnification with a DFK 31AU03 digital camera (The Imaging Source, Charlotte, NC) attached to the microscope and the camera's corresponding image analysis software (IC Measure, vers. 2.0.0.245; The Imaging Source). Scale bars appropriate to the magnification were included on each of the images. Images were collected for 2 reasons: 1) to capture an image of the section when the OTC mark was at its brightest, given that continual exposure to UV and the further processing of sections for daily increment counts can result in the OTC mark becoming very faint or even disappearing within the section, and 2) to detect, through the use of measured distances, the approximate position of the OTC mark in the otolith section, when not viewing the section under ultraviolet light. To make this detection, the distances between the OTC mark and the otolith margin on both the inside and outside of the ventral arm were measured by using the image capture software.

The number of annual increments observed between the position of the OTC mark (based on the measured distances taken in the previous step) and the otolith edge were recorded following the annual aging protocols detailed in the previous section. With annual aging, the direct comparison between the count of annual increments after the OTC mark and the time at liberty can be misleading because, unlike with daily increment counts, age estimates based on counts of opaque zones do not provide a fractional age (e.g., a fish at liberty for only 4 months could have an opaque zone between the OTC mark and the edge if the opaque zone completed formation shortly after tagging). It is possible to estimate a fractional age if the timing of annual zone formation is well known. However, for yellowfin and bigeye tuna sampled in the Atlantic Ocean, annual aging is only in its infancy, and the timing of zone formation for fish caught in the equatorial and southeast Atlantic Ocean is currently unknown. Therefore, to

[6] Lehodey, P., and B. Leroy. 1999. Age and growth of yellowfin tuna (*Thunnus albacares*) from the western and central Pacific Ocean as indicated by daily growth increments and tagging data. Standing Comm. Tuna Billfish 12, Work. Pap. YFT-2, 21 p. Ocean. Fish. Progr., Secr. Pac. Community, Noumea, New Caledonia. [Available from website.]

provide an alternative, yet practical, comparison between estimated time at liberty based on annual aging and the true time at liberty, we calculated an adjusted estimate (in fractional years) for each of the OTC-marked sections using methods modified from those used by Cappo et al. (2000). This adjusted count was based on the following: 1) the position of the first opaque zone after the OTC mark, relative to the OTC mark, 2) the number of annual zones observed after the mark, and 3) the relative distance between the last assumed annual opaque zone and the otolith edge—assuming that one translucent and one opaque zone are formed each year.

The sections prepared for daily increment counts were reexamined, and increment counts were made from the OTC mark to the otolith edge along a count path similar to that used for the total daily increment counts. For the sections in which the OTC mark had become undetectable because of additional otolith processing, the positions of the OTC marks were determined from the measurements taken on each of the otolith sections during the imaging procedure.

Longitudinal sections

To examine whether the sectioning plane that was used influenced increment counts, longitudinal (frontal) sections of the remaining otolith for a subset of fish (6 bigeye tuna and 5 yellowfin tuna) were prepared following methods used by Schaefer and Fuller (2006) (Suppl. Fig. 2B) (online only). These longitudinal sections were used to age the subset of fish following methods used by Williams et al. (2013), in which opaque zones were counted from the primordia to the otolith margin along the clearest count path in the area of the section adjacent to the proximal edge. The total count of daily increments and the number of daily increments between the OTC mark and the edge were recorded.

Analytical methods

For the comparison of age estimates, daily and annual increment counts from the same individuals were plotted against each other to help visualize differences. For the exercise of validating the increment deposition rate, daily increment, annual increment, and adjusted annual increment counts after the OTC mark were plotted against time at liberty to aid visualization of differences between estimated and true times at liberty. Age-agreement tables and age-bias plots (Ogle, 2016) were constructed, and an Evans–Hoenig test of symmetry (Evans and Hoenig, 1998) was applied to evaluate bias in the times at liberty estimated by using daily increment and adjusted annual increment counts. The Evans–Hoenig test is designed to detect bias in paired-age data and, in our study, was applied to paired data for estimated and true times at liberty. A significant P-value (≤ 0.05) indicates that differences between estimated times at liberty and true times at liberty were due to bias and not random error, implying that daily and annual increments were not strictly deposited on a daily and annual basis. For these calculations, times at liberty were converted to integer month to reduce the number of categories being compared.

To determine whether the sectioning plane that was used influenced total and post-OTC-mark counts of daily increments, the increment counts from transversely sectioned otoliths were compared with counts from frontal sections of otoliths. A Bland–Altman plot (Bland and Altman, 1999) was used to evaluate bias and define the interval of agreement between reads (total counts) from otoliths sections made with the 2 cutting planes.

Results

Age estimation: daily versus annual increment counts

Detailed results pertaining to each otolith analyzed for daily and annual increment counts are presented in Supplementary Tables 1 and 2 (online only). The annual increments in the form of one opaque and one translucent zone, although often difficult to interpret from sub-annual marks (also known as *check marks* or *split zones*), were apparent in all transverse sections examined, except in sections of otoliths from certain young-of-the-year samples for which the first zone had not yet formed. Zone structure was observed on both the dorsal and ventral side of otolith sections, although our experience in aging otoliths from samples of other tuna species indicates that the zone structure within the ventral arm is generally easier to interpret in comparison to that within the dorsal arm and that counts of assumed annual increments on the ventral side are likely to provide for more accurate age estimates. Annual increment counts ranged from 0 to 3 for bigeye tuna and from 0 to 10 for yellowfin tuna. A transverse section of an otolith from one of the oldest yellowfin tuna examined in this study (not OTC marked) appears in Figure 2, which shows the positions of each of the opaque zones used to assign age based on counts of annual increments.

Clear daily increments, consisting of alternating opaque and translucent zones, were observed throughout most of the ventral arms of the otolith sections examined. However, for some areas in many of the otolith sections examined, interpretation of the daily increment pattern was subjective. Overlapping and split increments often made interpretation difficult, and no increments were visible in some regions within the otolith sections. The number of regions that were difficult to interpret within an otolith generally increased with an increase in relative otolith size. Similar to that observed in otoliths from yellowfin tuna caught in the Pacific Ocean (Lehodey and Leroy[6]), the core area in otoliths examined in this study consisted of a primordium and approximately 8–10 fine daily increments (with widths of ≈2 μm) followed by a check mark. Increment widths became progressively wider, and at approximately the fifteenth increment, growth increments became very optically dense and their thickness increased up to 20 μm at their maximum concavity. Counts from the first obvious zone to the first apex averaged between 30–35 increments for both species. The internal zones closer to

Figure 2

Image of a section of an otolith from the oldest individual aged in this study: an Atlantic Ocean yellowfin tuna (*Thunnus albacares*) captured on 18 October 2018, measuring 161 cm straight fork length and weighing 80.3 kg. The white circles indicate the positions of the opaque zones used to assign age based on counting of annual increments. The letter *N* indicates the position of the nucleus. The opaque zone on the otolith margin (black arrow) is incomplete and was not included in estimation of integer age. This otolith was donated to the study by the Centre for Environment Fisheries and Aquaculture Science and was not marked with oxytetracycline.

the sulcus were more regularly spaced and did not have as much overlapping, splitting, or merging of zones compared with the zones close to the distal and ventral edges. Given these observations, it is our recommendation that the initial count path should include the clearer internal increments rather than run close to the distal and ventral edges of the otolith.

Unfortunately, for bigeye and yellowfin tuna, after approximately 150–180 daily increments, the internal structure of otoliths becomes difficult to interpret and a count path closer to the outer edge of the ventral arm needs to be used. As per the method of Lehodey and Leroy[6], the reading of the outer increments was directed along the axis of maximum concavity of increments. In many of the otoliths examined, subsections along the preferred reading path had a zone structure that was either difficult to interpret or not present. These areas were relatively common in otoliths from individuals of both species and often occurred with a change in the otolith growth plane, and in visual comparisons made with the otolith images captured during preparation for aging, the positions of these areas often corresponded to the positions of the opaque zones marked on images. In these cases, the zone structure adjacent to these areas usually had a clearer pattern of alternating opaque and translucent zones. For these cases, daily increments were counted in the adjacent area until increments could again be interpreted clearly along the preferred aging path. If the adjacent area was also unclear, interpolation was used (Suppl. Fig. 3) (online only). Daily increments were detectable close to the outer edge even in the largest otoliths from individuals of both species (114 and 159 cm SFL for bigeye and yellowfin tuna, respectively). These increments were at least 1.5–2 µm wide and well above the minimum resolution of light microscopy.

Age estimates, both daily increment counts and raw annual increment counts, are presented in Figure 3 and in Supplementary Tables 1 and 2 (online only). In the count comparison exercise, sizes of yellowfin tuna at recapture ranged from 45 to 159 cm SFL, daily increment counts ranged from 247 to 1168, and annual increment counts ranged from 0 to 8. For bigeye tuna, recapture sizes ranged from 50 to 114 cm SFL, daily increment counts ranged from 248 to 642, and annual increment counts ranged from 0 to 3. Age estimates of bigeye tuna with no annual zones were strongly negatively biased compared with the corresponding daily increment counts (Fig. 3). However, the edge type for all 6 otolith sections with no annual increments was classified as opaque, indicating that the fish was likely closer to age 1 than to age 0. Although it is difficult to objectively compare raw annual increment counts to fractional ages obtained from daily increment counts, for fish at sizes beyond 55 cm SFL (~age 1), age estimates based on annual aging tended to be higher than estimates based on daily aging for both species, with differences generally more pronounced in fish greater than 100 cm SFL for which age estimates from annual aging were consistently higher than estimates from daily aging (Fig. 3). The most drastic difference between age estimates was observed for a yellowfin tuna of 159 cm SFL: it had a daily increment count of 753 and an annual increment count of 8.

Validation with oxytetracycline marking

Oxytetracycline marks were detected in 32 of the 38 otoliths from yellowfin tuna and 20 of the 31 otoliths from bigeye tuna that were injected as part of the AOTTP and included in this study. For most examined otoliths, the OTC mark was clear and easy to detect from the background fluorescence of the otolith section (Fig. 4). Lengths at recapture of the fish successfully marked with OTC ranged from 45 to 159 cm SFL for yellowfin tuna and from 50 to 114 cm SFL for bigeye tuna (although the length ranges for fish with OTC marks on their otoliths are the same as those for all recaptured fish, not all recaptured fish had an OTC mark on their otolith). Known times at liberty ranged from 7 to 995 d for yellowfin tuna and from 18 to 879 d for bigeye tuna.

The estimated times at liberty (i.e., counts of increments after the OTC mark) were plotted against the known

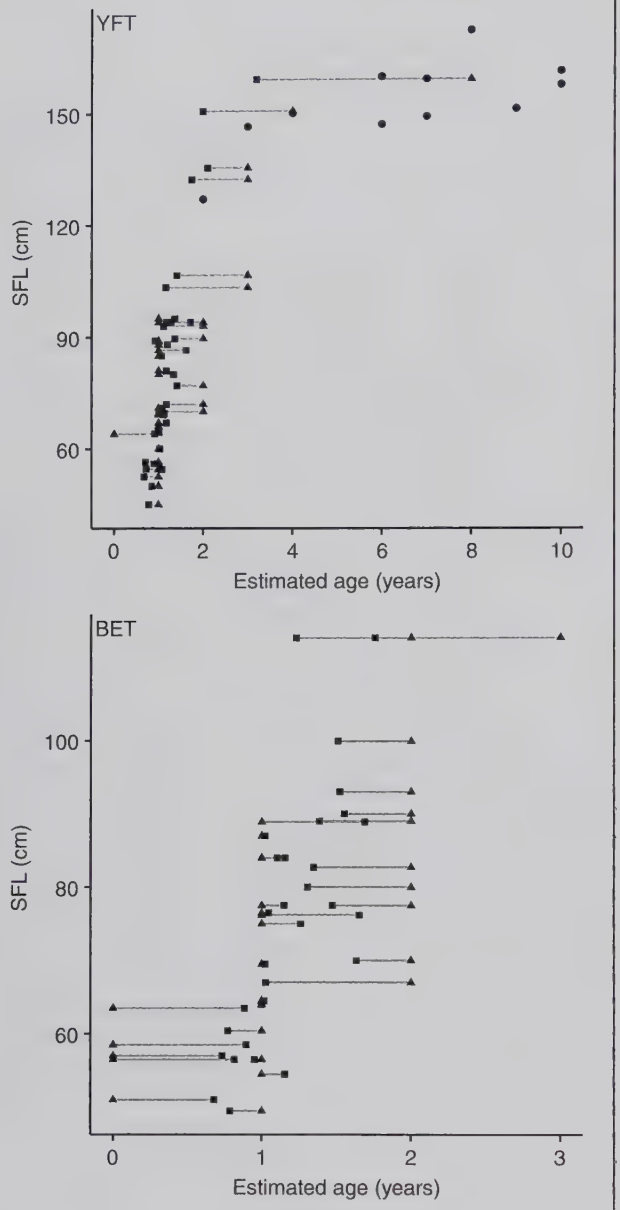

Figure 3

Comparison of age estimates based on daily (squares) and raw annual (triangles) increment counts on the same otolith, plotted by straight fork length (SFL), for yellowfin tuna (YFT) (*Thunnus albacares*) and bigeye tuna (BET) (*T. obesus*) sampled in the tropical and subtropical Atlantic Ocean between 2015 and 2021. Circles in the top panel indicate the increment counts for the 11 YFT for which only annual increment counts were taken.

times at liberty (Figs. 5 and 6). If the increments were truly deposited on a daily basis, and assuming there was no interpretation error, the points in each plot should fall directly on the solid black line that represents the 1:1 ratio of increment counts to times at liberty (Figs. 5A and 6A). Except for the readings of otoliths from one bigeye tuna and one yellowfin tuna, the daily increment counts fell below the 1:1 line, indicating that counts were lower than the true times at liberty. Results also indicate that the larger the fish size, the greater the discrepancy between the age assumed based on daily increment count and the true time at liberty. The raw counts of annual increments indicate a high level of correspondence between the number of opaque zones observed after the OTC mark and the actual time at liberty (Figs. 5B and 6B). The otolith from one yellowfin tuna at liberty for just over 2 years had only one visible opaque zone after the OTC mark, but the otolith had a wide translucent edge, indicating that a second opaque zone was due for deposition on the margin (Fig. 6). When the reader estimated times at liberty on the basis of the position of the OTC mark, the number of annual zones observed after the mark, and the relative distance between the last assumed annual opaque zone and the otolith margin, the estimated time at liberty agreed with the 1:1 line more closely and no directional bias was apparent (Figs. 5C and 6C).

Age-bias plots (Figs. 7 and 8) and results of the Evans–Hoenig test confirm our observation that daily increment counts are biased in that they are low in comparison to true times at liberty (Suppl. Tables 3–6) (online only). With the test, we detected a significant difference between the daily increment counts and the known time at liberty in both yellowfin tuna (χ^2=32, df=11, P=0.0008) and bigeye tuna (χ^2=18, df=10, P=0.05), indicating that increments were not systematically deposited on a daily basis for either species. The results from the Evans–Hoenig test of symmetry between the times at liberty estimated from annual increment counts and the actual times at liberty indicate that there was no systematic bias in times at liberty estimated from annual increment counts for both yellowfin tuna (χ^2=3.33, df=6, P=0.77) and bigeye tuna (χ^2=5.81, df=5, P=0.33).

Transverse versus longitudinal sections

When directly compared, the counts of increments in transverse versus longitudinal sections of otoliths did not differ greatly, nor did they indicate an obvious bias due to the preparation method. The Bland–Altman plot indicates a high degree of agreement between the counts made with the 2 reading methods, and there was no systematic difference between the paired counts (Fig. 9). There was a small negative bias in mean difference in counts with the 2 methods (−13 increments), a difference that is negligible in the context of age estimation (Fig. 9). All data points that were plotted fell within the 95% limits of agreement (−83, +57). This range indicates how far apart paired counts were most likely to be for most individuals, and the range is considered acceptable given the inter- and intra-reader variability typically observed in aging of tropical tuna. We did note, however, that daily increments within the longitudinal sections were easier to interpret than those within the transverse sections and that this difference in readability was particularly true for sections of otoliths from bigeye tuna.

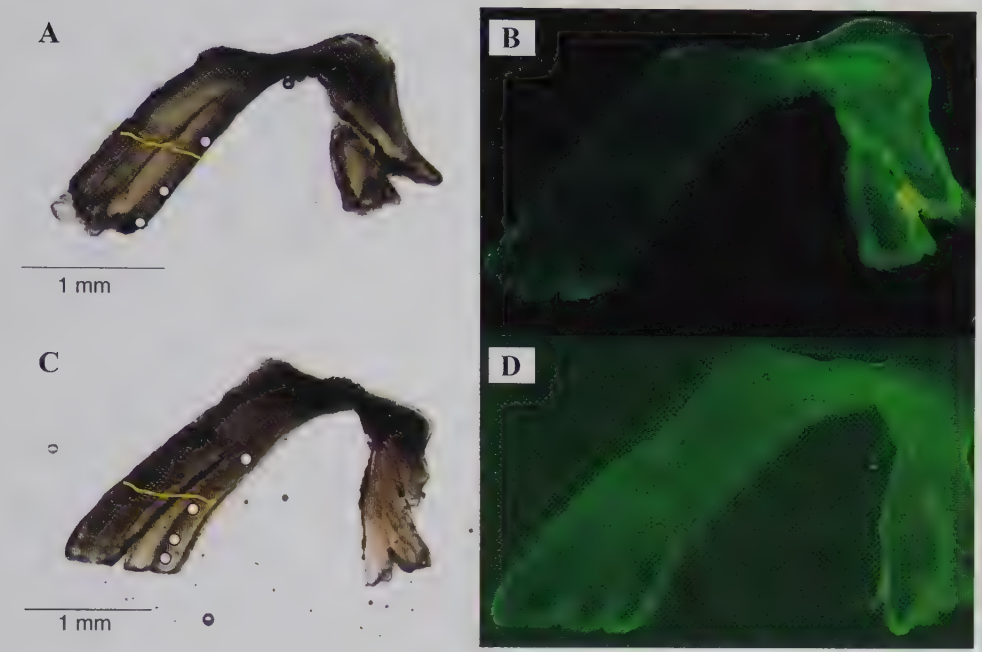

Figure 4

Examples of otolith sections from (**A** and **B**) a bigeye tuna (*Thunnus obesus*) and (**C** and **D**) a yellowfin tuna (*T. albacares*) sampled in the Atlantic Ocean. The images in panels A and C were illuminated with transmitted light, and the yellow line indicates the approximate position of the oxytetracycline (OTC) mark on each section. In panels B and D, the OTC marks are clearly visible in the corresponding sections illuminated with ultraviolet light. The white circles indicate the positions of the annual opaque zones used for aging. The bigeye tuna was recaptured on 29 April 2000 after 879 d at liberty, and its lengths at release and recapture were 45 and 114 cm straight fork length (SFL), respectively. The times at liberty estimated for this fish from daily and annual increment counts were 494 and 821 d, respectively. The yellowfin tuna was recaptured on 2 February 2020 after 995 d at liberty, and its lengths at release and recapture were 77 and 154 cm SFL, respectively. The times at liberty estimated for this fish from daily and annual increment counts were 357 and 912 d, respectively.

Discussion

In this study, reading otolith thin sections with transmitted light proved to be an appropriate method for obtaining age estimates based on annual increment counts for bigeye and yellowfin tuna sampled in the Atlantic Ocean. The age-at-length data presented in Figure 3 are similar to those data reported from other studies of tropical tunas that also are based on counts of annual increments over the age range examined, namely studies on yellowfin tuna in the Atlantic Ocean (Lang et al., 2017; Pacicco et al., 2021) and on both bigeye tuna and yellowfin tuna in the western Pacific Ocean (Farley et al., 2006; Farley et al.[2]). The strong relationship between the estimated time at liberty and the true time at liberty and the lack of systematic bias confirm that counting annual growth zones on otoliths from individuals of these 2 species is a valid method for age estimation. Furthermore, there were no instances of multiple annual rings being detected in a single year, as have been detected for little tunny (*Euthynnus alletteratus*), skipjack tuna (*Katsuwonus pelamis*), and blackfin tuna (*T. atlanticus*) from the Atlantic Ocean (Adams and Kerstetter, 2014).

Further work is needed to convert zone counts to decimal age estimates for both bigeye tuna and yellowfin tuna from the Atlantic Ocean and to increase the accuracy of age estimates for our geographically disparate fish samples. Multiple methods are currently used for assigning fractional ages for fish species. A common approach is to adjust the raw count on the basis of knowledge of the timing of band deposition and the birth date of the fish. However, neither the timing of band deposition nor the natal origin of the fish sampled were known for the otoliths used in this analysis; therefore, this approach could not be used reliably. An alternative and arguably preferable approach developed by Farley et al.[2] does not require information on spawning and timing of band formation. Instead, this approach involves developing a relationship between the age based on daily increment counts and the length of the ventral otolith arm for age 0+ fish and determining estimates of average annual increment width for each age class. Still, this approach requires large numbers of fish to

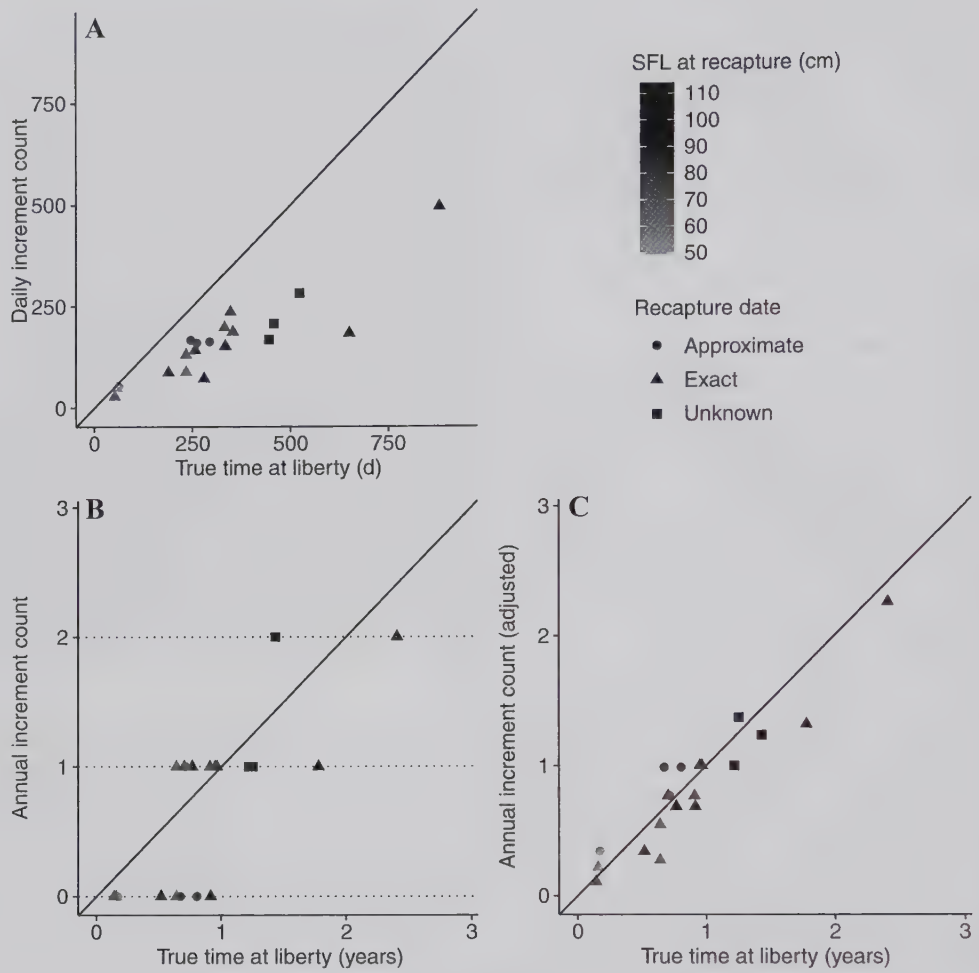

Figure 5

Comparison of (**A**) daily, (**B**) annual, and (**C**) adjusted annual increment counts, plotted with true times at liberty, for bigeye tuna (*Thunnus obesus*) marked and recaptured in the tropical and subtropical Atlantic Ocean during 2015–2021. Points that appear below the solid black line that represents the 1:1 ratio of increment counts to times at liberty indicate that the increment count is an underestimation of the true time at liberty, and points that appear above the line indicate that the increment count is an overestimation of the true time at liberty. Adjusted annual increment counts were determined on the basis of the position of the oxytetracycline mark, the number of annual zones observed after the mark, and the relative distance between the last assumed annual opaque zone and the otolith edge. Symbols relate to the quality of the recovery date: date is known only approximately and could be off by a few days, date is known exactly, and the quality of the date is unknown. Shades of gray used for symbols correspond to straight fork lengths (SFLs) of the fish at recapture according to the scale provided, with darker shades indicating longer lengths.

be sampled and to be analyzed a priori, something that could not be accomplished within the scope of our study but that could certainly be attempted in the future by using the remaining sampled fish from the AOTTP.

In the otoliths prepared for daily aging, areas with readily identifiable daily increments were observed throughout the otolith section in both transverse and longitudinal sections, albeit they were separated by areas in which the increment structure was difficult to interpret or was not present at all. Although the theory that the otoliths of older fish contain daily increments that are below the resolution limits of light microscopy is commonly held, in our study, daily increments were still detected close to the outer edge of otoliths even in the sections of the largest otoliths of both species examined. Schaefer and Fuller (2006) made the same observation for otoliths from bigeye tuna that were up to 145 cm SFL and were sampled from the eastern Pacific Ocean, although they used longitudinal sections. Similarly, Williams et al. (2013), comparing both longitudinal and transverse sections, detected daily

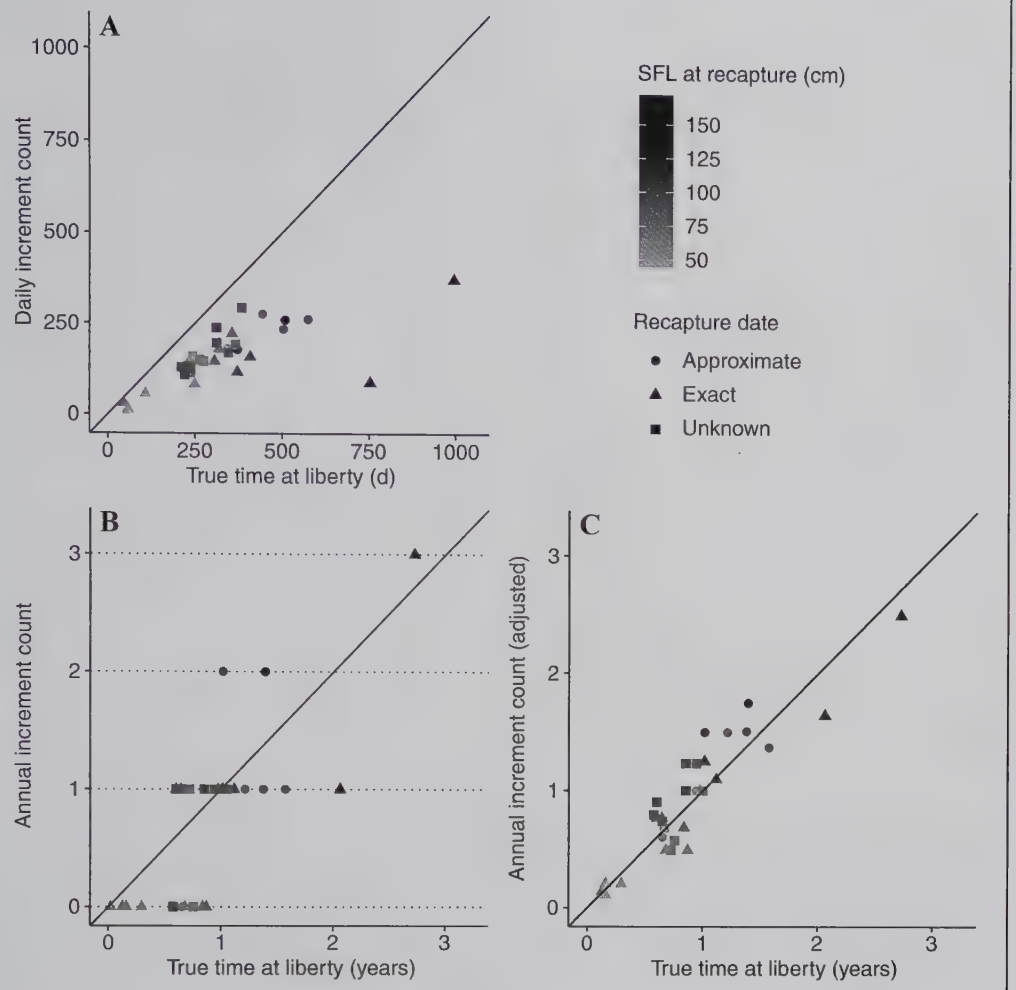

Figure 6

Comparison of (**A**) daily, (**B**) annual, and (**C**) adjusted annual increment counts, plotted with true times at liberty, for yellowfin tuna (*Thunnus albacares*) marked and recaptured in the tropical and subtropical Atlantic Ocean during 2015–2021. Points that appear below the solid black line that represents the 1:1 ratio of increment counts to times at liberty indicate that the increment count is an underestimation of the true time at liberty, and points that appear above the line indicate that the increment count is an overestimation of the true time at liberty. Adjusted annual increment counts were determined on the basis of the position of the oxytetracycline mark, the number of annual zones observed after the mark, and the relative distance between the last assumed annual opaque zone and the otolith edge. Symbols relate to the quality of the recovery date: date is known only approximately and could be off by a few days, date is known exactly, and the quality of the date is unknown. Shades of gray used for symbols correspond to straight fork lengths (SFLs) of the fish at recapture according to the scale provided, with darker shades indicating longer lengths.

increments in the outer part of the otolith section of the largest (175 cm SFL) southern bluefin tuna (*T. maccoyii*) examined in their study (senior author, personal observ.), despite the considerable divergence of the age estimates based on total annual (29 years) and daily (4 years) increment counts.

The advantage of using longitudinal sections is that this sectioning plane provides the longest axis for counting daily increments, with increment spacing that is usually wider than that in corresponding transverse sections. This wider spacing can lead to fewer areas within the otolith section having daily increments that are hard to interpret or requiring interpolation. Although a detailed comparison of sectioning methods was not an objective of this study, we did compare the results between a small number of otoliths prepared by using the 2 different sectioning planes. This comparison was important to avoid potential bias in the results from using either of the otolith preparation methods and to provide insight into which sectioning method should be preferred for use in future aging work

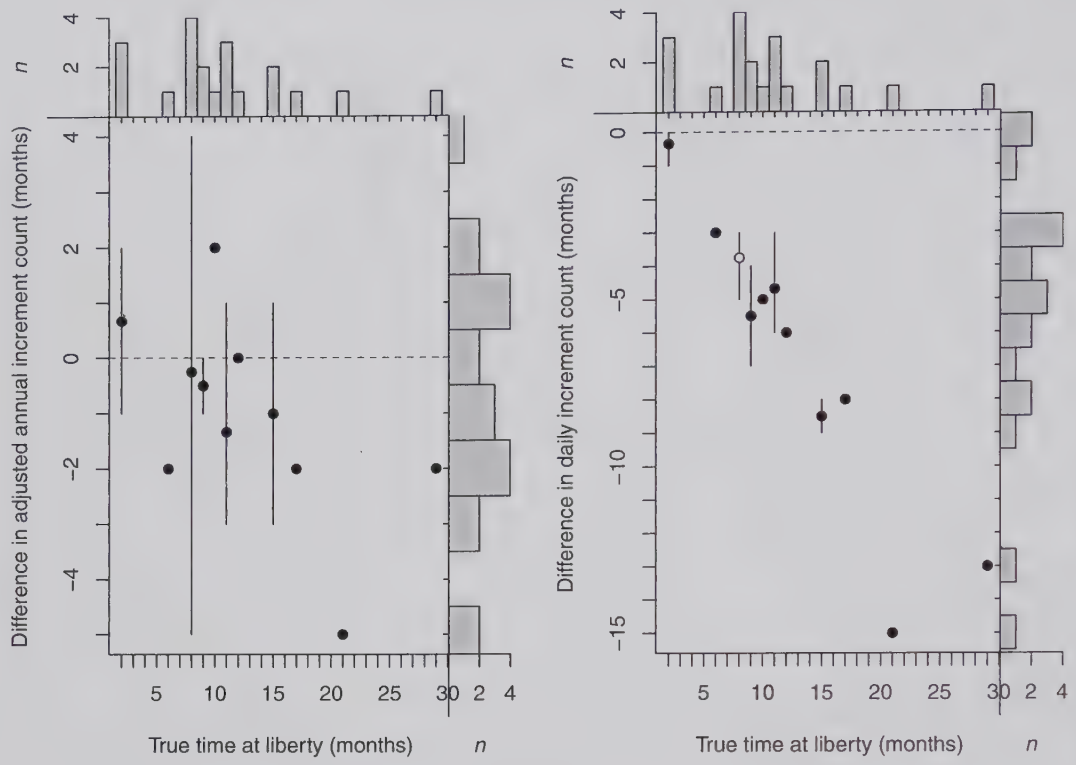

Figure 7

Age-bias plots showing the differences between annual and daily increment counts, or estimated times at liberty, against the true times at liberty for bigeye tuna (*Thunnus obesus*) marked and recaptured in the tropical and subtropical Atlantic Ocean from 2015 through 2021. In each panel, a histogram of the differences between the estimated and true times at liberty are provided in the right margin. The number of samples (n) for each time at liberty (in months) is provided in a histogram in the top margin. Circles indicate mean differences between the estimated and true times at liberty at each true month at liberty, and the bars stretch from the minimum to the maximum difference observed. The open circle indicates that the mean is significantly different from zero.

based on counts of daily increments for these 2 species. Preliminary results indicate no clear bias in the daily increment counts between the preparation methods used and are consistent with those of an earlier study on yellowfin tuna in the Indian Ocean for which preparation method also did not influence the age estimates (Stéquert et al., 1996). We note, however, that daily increments within the longitudinal sections in our study were easier to interpret than those within the transverse sections, and this difference in ease of detecting increments was particularly true for bigeye tuna. We therefore recommend that a more thorough comparison of the 2 methods be completed.

Results from both the comparison of annual versus daily increment counts and the validation of deposition rates of daily increments in otoliths based on examination of OTC-marked fish indicate that counting daily increments in otoliths of yellowfin and bigeye tuna may lead to underestimating age for fish larger than 55 cm SFL (greater than ~age 1). The difference between age estimates based on the 2 methods of counting can become quite large as fish grow older, as was observed for one of the yellowfin tuna examined in our study, with a difference in age of 6 years. Williams et al. (2013) counted both daily and annual increments on their largest southern bluefin tuna and found an overall difference of 20 years between the age estimates from the 2 counts. Sardenne et al. (2015) similarly found that daily increment counts in otoliths of large (>100 cm FL) bigeye tuna from the Indian Ocean resulted in underestimates of age.

One explanation for this underestimation could be that daily increments are not systematically deposited at a daily rate. It has been hypothesized that increment deposition may cease to be daily after a certain age or life history stage and that changes in environmental conditions might disrupt the regular pattern of daily increment deposition (e.g., Francis et al. 1992). Another potential explanation relates to the fact that there are areas within otoliths (even in those from relatively small fish, <75 cm SFL) where daily increments are either extremely difficult to interpret or do not appear to form at all; such areas also have been found in other studies (Shuford et al., 2007; Sardenne et al., 2015). Daily increments tend to have a merging or splitting structure in some areas, making it difficult to distinguish individual increments, and other

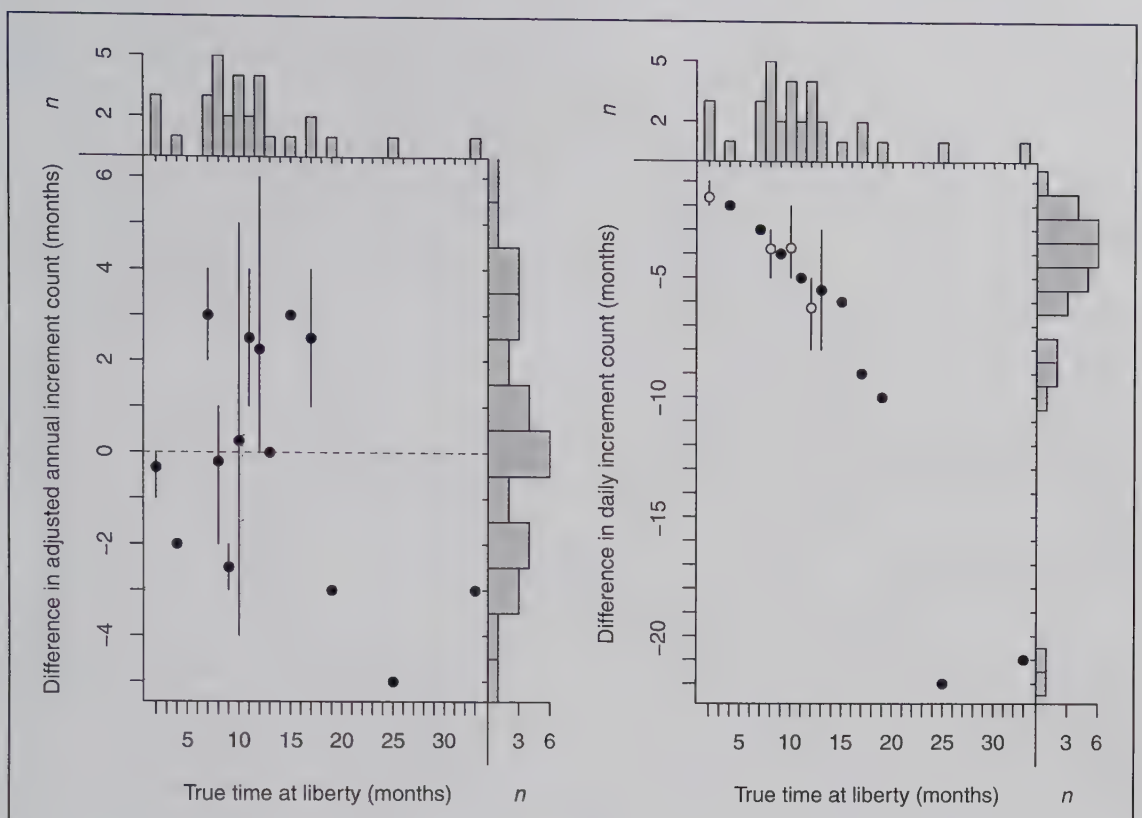

Figure 8

Age-bias plots showing the differences between the annual and daily increment counts, or estimated times at liberty, against the true times at liberty for yellowfin tuna (*Thunnus albacares*) marked and recaptured in the tropical and subtropical Atlantic Ocean from 2015 through 2021. In each panel, a histogram of the differences between the estimated and true times at liberty are provided in the right margin. The number of samples (n) for each time at liberty (in months) is provided in a histogram in the top margin. Circles indicate mean differences between the estimated and true times at liberty at each true month at liberty, and the bars stretch from the minimum to the maximum difference observed. Open circles indicate that the means are significantly different from zero.

areas are devoid of increments, forcing analysts to resort to interpolation to fill the missing patterns. Campana (1992) suggested that the use of interpolation is considered reasonable in cases in which the number of interpolated daily increments is relatively small in comparison to the total increment count. Unfortunately, for the otoliths of bigeye and yellowfin tuna examined in this study, these areas were relatively common and likely the main contributing factor in age underestimation.

Despite these limitations to the use of daily increment counts for aging yellowfin and bigeye tuna, daily increments do hold considerable value in the overall aging process. Daily increment counts are still important for confirming the location of the first annual increment in sectioned otoliths, as has been reported for yellowfin tuna in the Atlantic Ocean (Lang et al., 2017) and both bigeye and yellowfin tuna in the Pacific Ocean (Farley et al., 2006; Farley et al.[2]), and for providing length-at-age data during the first year of life. More recently, aging through the use of daily increments counts, particularly out to a count of 365 d, has proven to be a valuable tool in refining counts of annual zones and, therefore, in providing more accurate fractional ages and has also allowed improvement in the growth curves of yellowfin and bigeye tuna from the western and central Pacific Ocean (Farley et al.[2]). With this in mind, the challenge is determining the point at which age estimation based on daily increment counts provides a larger source of error than the use of annual zone counts. Finding that point should be considered a vital step in developing suitable aging methods for any species, let alone for tropical tunas, and the need to obtain that knowledge highlights the value of conducting a large-scale tag-recapture program such as the AOTTP.

Conclusions

On the basis of our findings, the use of annual increment counts is the best method for aging yellowfin and bigeye tuna sampled in the Atlantic Ocean, and the use of daily increment counts should be limited to aging young of the year. Additional work is needed to resolve the timing of opaque zone formation in otoliths from fish from different parts of the Atlantic Ocean and to derive fractional

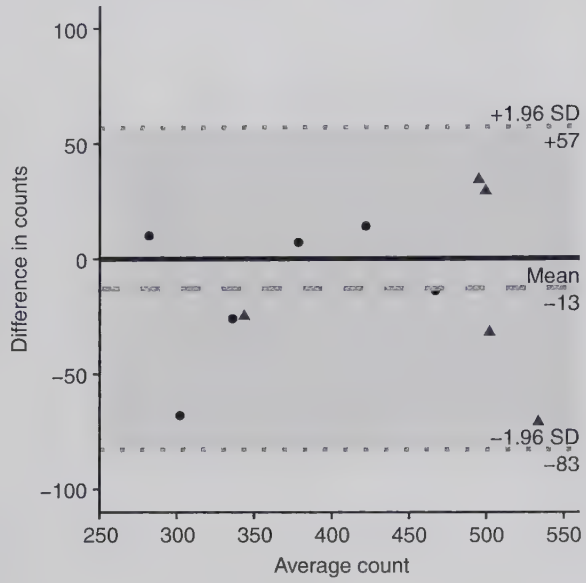

Figure 9

Bland–Altman plot of the paired readings of total daily increment counts for otoliths from bigeye tuna (*Thunnus obesus*) (circles) and yellowfin tuna (*T. albacares*) (triangles) marked and recaptured in the tropical and subtropical Atlantic Ocean between 2015 and 2021. The horizontal dashed line indicates the mean bias in the difference in counts between the transverse and longitudinal sections. The horizontal dotted lines indicate the 95% limits of agreement, calculated as the mean plus and minus 1.96 standard deviations (SDs).

ages, and we believe the AOTTP otolith collection could serve that purpose. Although the AOTTP has now ended, networks across the Atlantic Ocean are being maintained to ensure that there is a continued effort to recover OTC-marked fish and to analyze hard parts. As this effort continues, more valuable and informative samples (i.e., larger fish, with longer times at liberty) will become available, and analysis of their otoliths is likely to confirm our findings and recommendations for these 2 key tuna species.

Validating age estimation methods is particularly valuable for improving stock assessments; the importance of obtaining correct age and growth information in assessing stock status has been well documented (Maunder and Punt, 2013). Lang et al. (2017) and Pacicco et al. (2021) have suggested that yellowfin and bigeye tuna from the Atlantic Ocean can be aged by using counts of annual increments and that the maximum longevity for both species was far greater than originally determined. More importantly, the aging protocols used in those recent studies have been verified by the use of bomb radiocarbon analysis (Andrews et al., 2020). The results of that recent work, along with the results from our analysis of otoliths from OTC-marked fish in our study, support the use of annual increments for aging yellowfin and bigeye tuna sampled in the Atlantic Ocean.

The findings of our study are particularly important because the recent shift to base age estimates on annual increment counts has led to raising the estimated maximum age in the latest assessment of the Atlantic stock of yellowfin tuna from 11 to 18 years (ICCAT, 2020), which in turn has caused substantial changes in stock status (ICCAT, 2019). The ICCAT has assessed the Atlantic stocks of both the bigeye tuna and yellowfin tuna with modeling approaches of varying complexities, from simple production models to integrated statistical assessment models, and the capacity to accommodate age data in several different ways. Although age data have not yet been used to their full extent for tuna stocks in the Atlantic Ocean, we anticipate that that will change in the future, given the recent advances in the study of age and growth of tropical tuna species.

Resumen

Un experimento reciente de marcado-recaptura en todo el Atlántico llevado a cabo por la Comisión Internacional para la Conservación del Atún del Atlántico fue una oportunidad para validar directamente las tasas de incrementos de otolitos para el patudo (*Thunnus obesus*) y el atún de aleta amarilla (*T. albacares*) en la región. Se estimaron la edad y el tiempo en libertad utilizando conteos de incrementos anuales y diarios de otolitos seccionados de peces muestreados previamente inyectados con oxitetraciclina y recapturados posteriormente. Los conteos de incrementos anuales dieron lugar a mayores estimaciones de edad que las realizadas con conteos diarios, para los peces mayores de 55 cm de longitud furcal recta (SFL). El conteo de incrementos diarios condujo a una subestimación del tiempo en libertad para los peces mayores de 55 cm de SFL al ser recapturados, en comparación con los tiempos en libertad conocidos. Por el contrario, las predicciones basadas en los recuentos de incrementos anuales son precisas en todo el rango de tallas de los peces muestreados, validando así, que los incrementos se depositan anualmente. Por lo tanto, recomendamos que el conteo de incrementos anuales sea el método preferido para determinar la edad del atún de aleta amarilla y el patudo del Océano Atlántico y que el uso de incrementos diarios para determinar la edad se limite a los juveniles del año. La determinación precisa de la edad en peces es importante para la evaluación de poblaciones, en las que los datos sobre edad y crecimiento desempeñan un papel cada vez más esencial en el estudio de dinámica de poblaciones. Es crucial que las prácticas de lectura de otolitos y los análisis basados en los datos de edad reflejen las recomendaciones más actualizadas para la estimación de la edad.

Acknowledgments

We thank members of the AOTTP tag and recovery teams, including biological samplers, for doing the meticulous work of otolith extraction from recovered fish. We thank

D. Fuller (Inter-American Atlantic Tropical Tuna Commission) for providing his expertise and for aging one of the AOTTP samples. We thank J. Farley and B. Barnett for valuable input and reviews of the draft manuscript. This work was supported by the European Union (grant no. DCI-FOOD/2015/361-161). We gratefully acknowledge the additional financial support from ICCAT contracting parties and cooperating non-contracting parties.

Literature cited

Adams, J. L., and D. W. Kerstetter.
2014. Age and growth of three coastal-pelagic tunas (Actinopterygii: Perciformes: Scombridae) in the Florida Straits, USA: blackfin tuna, *Thunnus atlanticus*, little tunny, *Euthynnus alletteratus*, and skipjack tuna, *Katsuwonus pelamis*. Acta Ichthyol. Piscat. 44:201–211.

Allman, R., L. Ailloud, R. Austin, B. Falterman, J. Farley, K. Krusic-Golub, E. Lang, A. Pacicco, and K. Satoh.
2020. Report of the international workshop on the ageing of yellowfin and bigeye tuna. Collect. Vol. Sci. Pap. ICCAT 77(8):32–46.

Andrews, A. H., A. Pacicco, R. Allman, B. J. Falterman, E. T. Lang, and W. Golet.
2020. Age validation of yellowfin (*Thunnus albacares*) and bigeye (*Thunnus obesus*) tuna of the northwestern Atlantic Ocean. Can. J. Fish. Aquat. Sci. 77:637–643.

Bland, J. M., and D. G. Altman.
1999. Measuring agreement in method comparison studies. Stat. Methods Med. Res. 8:135–160.

Campana, S. E.
1992. Measurement and interpretation of the microstructure of fish otoliths. *In* Otolith microstructure examination and analysis (D. K. Stevenson and S. E. Campana, eds.), p. 59–71. Can. Spec. Publ. Fish. Aquat. Sci. 117.
2001. Accuracy, precision and quality control in age determination, including a review of the use and abuse of age validation methods. J. Fish Biol. 59:197–242.

Cappo, M., P. Eden, S. J. Newman, and S. Robertson.
2000. A new approach to validation of periodicity and timing of opaque zone formation in the otoliths of eleven species of *Lutjanus* from the central Great Barrier Reef. Fish. Bull. 98:474–488.

Casselman, J. M.
1983. Age and growth assessment of fish from their calcified structures—techniques and tools. *In* Proceedings of the international workshop on age determination of oceanic pelagic fishes: tunas, billfishes, and sharks; Miami, 15–18 February 1982 (E. D. Prince and L. M. Pulos, eds.), p. 1–17. NOAA Tech. Rep. NMFS 8.

Evans, G. T., and J. M. Hoenig.
1998. Testing and viewing symmetry in contingency table, with applications to readers of fish ages. Biometrics 54:620–629.

Farley, J. H., N. P. Clear, B. Leroy, T. L. O. Davis, and G. McPherson.
2006. Age, growth and preliminary estimates of maturity of bigeye tuna, *Thunnus obesus*, in the Australian region. Mar. Freshw. Res. 57:713–724.

Farley, J. H., A. J. Williams, N. P. Clear, C. R. Davies, and S. J. Nicol.
2013. Age estimation and validation for South Pacific albacore *Thunnus alalunga*. J. Fish Biol. 82:1523–1544.

Fowler, A. J.
2009. Age in years from otoliths of adult tropical fish. *In* Tropical fish otoliths: information for assessment, management and ecology. Reviews: methods and technologies in fish biology and fisheries, vol. 11 (B. S. Green, B. D. Mapstone, G. Carlos, and G. A. Begg, eds.), p. 55–92. Springer, Dordrecht, Netherlands.

Francis, R. I. C. C., L. J. Paul, and K. P. Mulligan.
1992. Ageing of adult snapper (*Pagrus auratus*) from otolith annual ring counts: validation by tagging and oxytetracycline injection. Aust. J. Mar. Freshw. Res. 43:1069–1089.

Griffiths, S. P., G. C. Fry, F. J. Manson, and D. C. Lou.
2010. Age and growth of longtail tuna (*Thunnus tonggol*) in tropical and temperate waters of the central Indo-Pacific. ICES J. Mar. Sci. 67:125–134.

Gunn, J. S., N. P. Clear, T. I. Carter, A. J. Rees, C. A. Stanley, J. H. Farley, and J. M. Kalish.
2008. Age and growth in southern bluefin tuna, *Thunnus maccoyii* (Castelnau): direct estimation from otoliths, scales and vertebrae. Fish. Res. 92:207–220.

Hallier, J. P., B. Stequert, O. Maury, and F.-X. Bard.
2005. Growth of bigeye tuna (*Thunnus obesus*) in the eastern Atlantic Ocean from tagging-recapture data and otolith readings. Col. Vol. Sci. Pap. ICCAT 57(1):181–194.

ICCAT (International Commission for the Conservation of Atlantic Tunas).
2019. YFT—yellowfin tuna. *In* Report of the Standing Committee on Research and Statistics (SCRS) (Madrid, Spain, 30 September to 4 October 2019), p. 24–43. ICCAT, Madrid, Spain. [Available from website.]
2020. Report of the 2019 ICCAT yellowfin tuna stock assessment meeting. Collect. Vol. Sci. Pap. ICCAT 76(6):344–515.

Jones, C.
1992. Development and application of the otolith increment technique. *In* Otolith microstructure examination and analysis (D. K. Stevenson and S. E. Campana, eds.), p. 1–11. Can. Spec. Publ. Fish. Aquat. Sci. 117.

Lang, E. T., B. J. Falterman, L. L. Kitchens, and C. D. Marshall.
2017. Age and growth of yellowfin tuna (*Thunnus albacares*) in the northern Gulf of Mexico. Collect. Vol. Sci. Pap. ICCAT 73(1):423–433.

Langley, A., J. Hampton, P. Kleiber, and S. Hoyle.
2008. Stock assessment of bigeye tuna in the western and central Pacific Ocean, including an analysis of management options. West. Cent. Pac. Fish. Comm. WCPFC-SC4-2008/SA-WP-1 Rev 1, 111 p. [Available from website.]

Maunder, M. N., and A. E. Punt.
2013. A review of integrated analysis in fisheries stock assessment. Fish. Res. 142:61–74.

Minte-Vera, C., M. N. Maunder, H. Xu, J. L. Valero, C. E. Lennert-Cody, and A. Aires-da-Silva.
2020. Yellowfin tuna in the eastern Pacific Ocean, 2019: benchmark assessment. Inter-Am. Trop. Tuna Comm. Doc. SAC-11-07 REV, 60 p. [Available from website.]

Morales-Nin, B.
2000. Review of the growth regulation processes of otolith daily increment formation. Fish. Res. 46:53–67.

Morales-Nin, B., and J. Panfili.
2005. Seasonality in the deep sea and tropics revisited: what can otoliths tell us? Mar. Freshw. Res. 56:585–598.

Murua, H., E. Rodriguez-Marin, J. D. Neilson, J. H. Farley, and M. J. Juan-Jordá.
2017. Fast versus slow growing tuna species: age, growth, and implications for population dynamics and fisheries management. Rev. Fish Biol. Fish. 27:733–773.

Neilson, J. D., and S. E. Campana.
2008. A validated description of age and growth of western Atlantic bluefin tuna (*Thunnus thynnus*). Can. J. Fish. Aquat. Sci. 65:1523–1527.

Newman, S. J., D. M. Williams, and G. R. Russ.
1996. Age validation, growth and mortality rates of the tropical snappers (Pisces: Lutjanidae) *Lutjanus adetii* (Castelnau, 1873) and *L. quinquelineatus* (Bloch, 1790) from the central Great Barrier Reef, Australia. Mar. Freshw. Res. 47:575–584.

Ogle, D. H.
2016. Introductory fisheries analyses with R, 337 p. CRC Press, Boca Raton, FL.

Pacicco, A. E., R. J. Allman, E. T. Lang, D. J. Murie, B. J. Falterman, R. Ahrens, and J. F. Walter III.
2021. Age and growth of yellowfin tuna in the U.S. Gulf of Mexico and western Atlantic. Mar. Coast. Fish. 13:345–361.

Pilling, G. M., R. S. Millner, M. W. Easey, C. C. Mees, S. Rathacharen, and R. Azemia.
2000. Validation of annual growth increments in the otoliths of the lethrinid *Lethrinus mahsena* and the lutjanid *Aprion virescens* from sites in the tropical Indian Ocean, with notes on the nature of growth increments in *Pristipomoides filamentosus*. Fish. Bull. 98:600–611.

Rodríguez-Marín, E., N. Clear, J. L. Cort, P. Megalofonou, J. D. Neilson, M. Neves dos Santos, D. Olafsdottir, C. Rodríguez-Cabello, M. Ruiz, and J. Valeiras.
2007. Report of the 2006 ICCAT workshop for bluefin tuna direct ageing. Collect. Vol. Sci. Pap. ICCAT 60(4):1349–1392.

Rodríguez-Marín, E., P. L. Luque, P. Quelle, M. Ruiz, B. Perez, D. Macias, and S. Karakulak.
2014. Age determination analyses of Atlantic bluefin tuna (*Thunnus thynnus*) within the biological and genetic sampling and analysis contract (GBYP). Collect. Vol. Sci. Pap. ICCAT 70(2):321–331.

Sardenne, F., E. Dortel, G. Le Croizier, J. Million, M. Labonne, B. Leroy, N. Bodin, and E. Chassot.
2015. Determining the age of tropical tunas in the Indian Ocean from otolith microstructures. Fish. Res. 163:44–57.

Schaefer, K. M., and D. W. Fuller.
2006. Estimates of age and growth of bigeye tuna (*Thunnus obesus*) in the eastern Pacific Ocean, based on otolith increments and tagging data. Inter-Am. Trop. Tuna Comm., Bull. 23:35–59.

Secor, D. H., R. Allman, D. Busawon, B. Gahagan, W. Golet, E. Koob, P. L. Luque, and M. Siskey.
2014. Standardization of otolith-based ageing protocols for Atlantic bluefin tuna. Collect. Vol. Sci. Pap. ICCAT 70(2):357–363.

Shuford, R. L., J. M. Dean, B. Stéquert, and E. Morize.
2007. Age and growth of yellowfin tuna in the Atlantic Ocean. Collect. Vol. Sci. Pap. ICCAT 60(1):330–341.

Stéquert, B., and F. Conand.
2000. Preliminary studies of age and growth of bigeye tuna (*Thunnus obesus*) in the Western Indian Ocean. *In* Proceedings of the 7th Expert Consultation on Indian Ocean Tunas; Victoria, 9–14 November 1998, p. 249–255. Indian Ocean Tuna Commission, Victoria, Seychelles. [Available from website.]

Stéquert, B., J. Panfili, and J. M. Dean.
1996. Age and growth of yellowfin tuna, *Thunnus albacares*, from the western Indian Ocean, based on otolith microstructure. Fish. Bull. 94:124–134.

Uchiyama, J. H., and P. Struhsaker.
1981. Age and growth of skipjack tuna, *Katsuwonus pelamis*, and yellowfin tuna, *Thunnus albacares*, as indicated by daily growth increments of sagittae. Fish. Bull. 79:151–162.

Wells, R. J. D., S. Kohin, S. L. H. Teo, O. E. Snodgrass, and K. Uosaki.
2013. Age and growth of North Pacific albacore (*Thunnus alalunga*): implications for stock assessment. Fish. Res. 147:55–62.

Wild, A.
1986. Growth of yellowfin tuna, *Thunnus albacares*, in the eastern Pacific Ocean based on otolith increments. Inter-Am. Trop. Tuna Comm., Bull. 18:423–482.

Wild, A., and T. J. Foreman.
1980. The relationship between otolith increments and time for yellowfin and skipjack tuna marked with tetracycline. Inter-Am. Trop. Tuna Comm., Bull. 17:509–560.

Wild, A., J. B. Wexler, and T. J. Foreman.
1995. Extended studies of increment deposition rates in otoliths of yellowfin and skipjack tunas. Bull. Mar. Sci. 57:555–562.

Williams, A. J., B. M. Leroy, S. J. Nicol, J. H. Farley, N. P. Clear, K. Krusic-Golub, and C. R. Davies.
2013. Comparison of daily- and annual- increment counts in otoliths of bigeye (*Thunnus obesus*), yellowfin (*T. albacares*), southern bluefin (*T. maccoyii*) and albacore (*T. alalunga*) tuna. ICES J. Mar. Sci. 70:1439–1450.

Xu, H., M. N. Maunder, C. Minte-Vera, J. L. Valero, C. E. Lennert-Cody, and A. Aires-da-Silva.
2020. Bigeye tuna in the eastern Pacific Ocean, 2019: benchmark assessment. Inter-Am. Trop. Tuna Comm. Doc. SAC-11-06 REV, 51 p. [Available from website.]

National Marine
Fisheries Service
NOAA

Fishery Bulletin
established in 1881

Spencer F. Baird
First U.S. Commissioner
of Fisheries and founder
of *Fishery Bulletin*

Juvenile yield and adult abundance, genetic diversity and structure, and linkages among marine habitats for goldlined spinefoot (*Siganus guttatus*) in the coastal waters of Vietnam

Long V. Nguyen (contact author)[1,2]
Dat X. Mai[1]
Quang M. Thai[1]
Tuan S. Vo[1]

Email address for contact author: longhdh@gmail.com

[1] Institute of Oceanography
Vietnam Academy of Science and Technology
01 Cau Da Street
Nha Trang 650000, Vietnam

[2] Graduate University of Science and Technology
Vietnam Academy of Science and Technology
18 Hoang Quoc Viet
Cau Giay, Ha Noi 100000, Vietnam

Abstract—Assessments of the status and ecological linkages of target fish species related to marine habitats are playing important roles in enhancing the effectiveness of marine protected areas (MPAs) and of management in other coastal areas. In this study, we assessed juvenile yield and the abundance of goldlined spinefoot (*Siganus guttatus*) by using local knowledge and visual census in coastal waters of Vietnam. Genetic structure was examined by using DNA analysis of juveniles, collected in seagrass beds and mangroves at major lagoons and estuaries, and of adults, collected from coral reefs. More than 38.6 million juveniles were collected from 8 coastal lagoons and estuaries. The coastal lagoons and estuaries with seagrass beds supported high yield of juveniles, and the nearby MPAs had higher densities of adults. Three distinct genetic groups were identified, with one group found off the central part of the eastern coast from Con Co Island to Quy Nhon Bay, a second group found off the southeastern coast from Nha Trang Bay to the Con Dao Islands, which are located off the southern tip of Vietnam, and a third group found off the southwestern coast at the Phu Quoc Islands in the Gulf of Thailand.

Manuscript submitted 12 July 2022.
Manuscript accepted 20 January 2023.
Fish. Bull. 121:17–29 (2023).
Online publication date: 14 February 2023.
doi: 10.7755/FB.121.1-2.2

The views and opinions expressed or implied in this article are those of the author (or authors) and do not necessarily reflect the position of the National Marine Fisheries Service, NOAA.

Results from previous research indicate that more than 210 species of 34 reef fish families have pelagic stages, that larvae disperse away from their spawning area (Green et al., 2015), and that many of them migrate from their settlement habitats of mangroves and seagrass beds in coastal lagoons and estuaries (nursery grounds) to adjacent coral reefs for feeding or shelter (Luo et al., 2009; Honda et al., 2013; Le et al., 2019; Vrdoljak et al., 2021). In an increasing number of studies of marine fish species, strong genetic differentiation among populations from different regions, separated by distances from tens to a few hundred kilometers, has been observed (Hellberg et al., 2002; Jones et al., 2005; Laikre et al., 2005; Planes et al., 2009). These patterns may be influenced by several ecological and behavioral factors, such as the timing of reproduction (Selkoe et al., 2006), larval dispersal ability (Kinlan and Gaines, 2003), homing behavior (Almany et al., 2007), oceanographic patterns (White et al., 2010), biogeographic barriers (McMillan and Palumbi, 1995), local adaptation (Conover et al., 2006), habitat specialization (Knudsen et al., 2006), and the ecological requirements of each species (Rocha et al., 2002).

Reports from several studies indicate that many reef fish families (Lutjanidae, Haemulidae, Lethrinidae, Scaridae, Siganidae, and others) utilize seagrass beds and mangroves in nearshore and estuarine regions as their nursery grounds (Verweij et al., 2008). Therefore, understanding the degree of connectivity between populations in different geographic areas, or the specific location of genetic breaks, sets the scale at which management strategies for species need to be applied. This information is important in the management of reef fish resources in many coastal areas, especially in marine protected areas (MPAs) (Cowen and Sponaugle, 2009).

Results of studies on the genetic structure of several species of siganids indicate that there are differences in

connectivity among species. In waters of Japan, Iwamoto et al. (2009) reported a higher degree of interpopulation gene flow for bluntnosed spinefish (*Siganus spinus*) than for goldlined spinefoot (*S. guttatus*) between Okinawa Island, Miyako Island, and Ishigaki Island. Magsino and Juinio-Meñez (2008) found higher genetic structuring in dusky spinefoot (*S. fuscescens*) than in streamlined spinefoot (*S. argenteus*) along the eastern coasts of the Philippines, and they also observed genetic structure for the these 2 species in the South China Sea and South Philippine Sea but no structure for them in the Sulu Sea and Inland Sea. In the South China Sea, high connectivity between populations of reef fish species, including the false pennant bullfish (*Heniochus acuminatus*), the six-barred wrasse (*Thalassoma hardwicke*), and the threespot dascyllus (*Dascyllus trimaculatus*), has been reported from genetic studies, indicating population differences in some areas (Ablan et al., 2002; Chen et al., 2004).

In the coastal waters of Vietnam, results of a genetic study indicate broad connectivity of the goldstripe sardinella (*Sardinella gibbosa*), the giant tiger prawn (*Penaeus monodon*), the threespot dascyllus, the cupped oyster *Crassostrea rivularis*, and the giant clams *Tridacna crocea* and *T. squamosa* between a northern region (from the Cat Ba Islands to Da Nang Bay), a central section (from Quy Nhon Bay to Nha Trang Bay), an area in and around the Con Dao Islands, located off the southern tip of Vietnam, and a region in and around the Phu Quoc Islands, located off the southwestern coast in the Gulf of Thailand, although a weak separation of populations has been found between the Con Dao Islands and Phu Quoc Islands (Dang et al., 2014). Similar patterns have been reported for the ornate spiny lobster (*Panulirus ornatus*) in Southeast Asia (Dao et al., 2015) and for a complex of mullet species, *Mugil cephalus*, in Vietnam (Tran et al., 2017).

The goldlined spinefoot, also known as the *orange-spotted spinefoot* and the *golden rabbitfish*, is 1 of 28 species in the Indo-Pacific family Siganidae. It is widely distributed in shallow-water habitats (including lagoons and river mouths, mangrove swamps, seagrass beds, coral reefs, and sandy and rocky bottoms) to a depth of 6 m in the eastern Indian Ocean and the Indo-West Pacific Ocean (Woodland, 1990; Duray, 1998; Froese and Pauly, 2021). This species is one of the most economically important commercial fishes in tropical and subtropical regions. It has attracted attention from the aquaculture industry in the Indo-Pacific and in the Indian Ocean (Lam, 1974; Randall et al., 1990). Juveniles settle in seagrass beds in lagoons and estuaries during certain periods of the year (Kami and Ikehara, 1976), whereas adults are found in coral reefs (Froese and Pauly, 2021). Because this species has a complex life cycle with linkages to different habitats at different stages, understanding the genetic structure of populations of the goldlined spinefoot is important for developing effective strategies for its proper and sustainable management.

On the western side of the South China Sea, the coastline of Vietnam spans 14° of latitude and extends for 3260 km. The coastal waters support more than 156,000 ha of mangroves (Do et al., 2005) and 17,000 ha of seagrass beds (Luong et al., 2012), and coral reefs are mainly distributed along the coast and around the adjacent islands over a total area of about 13,400 ha (Nguyen and Vo, 2014; Nguyen et al., 2019). In Vietnam, juvenile goldlined spinefoot have been recruited to seagrass beds and mangrove swamps in the coastal lagoons and estuaries in the central part of the country from Thua Thien Hue Province (which includes Tam Giang–Cau Hai and Lap An Lagoons) to Binh Dinh Province (where Thi Nai Lagoon is located) (Le and Le, 2006). Large numbers have been observed settling during the dark phase of the moon in the summer months from May to August (from day 20 in one month to day 5 in the next month) and sometimes in to September (Le and Le, 2006; Nguyen and Mai, 2018). Adults have been found in the major coral reefs along the coast and around nearshore islands (Nguyen and Mai, 2020). Large schools of juvenile goldlined spinefoot have been caught by purse seine, lift net, stow net, and long trap cage along the coast of Vietnam, including in Thi Nai Lagoon (8.58 million juveniles in 2008) (Nguyen et al., 2010) and in Thu Bon estuary (780 kg, equivalent to 7.02 million juveniles, in 2015) (Nguyen and Mai, 2018). However, data at a larger spatial scale on the distribution of juveniles and broodstocks is lacking, and such information is needed for effective management of this resource in Vietnam.

The aims of this study were as follows: 1) to assess the juvenile yield and adult abundance (broodstock) of goldlined spinefoot; 2) to determine the genetic diversity, structure, and linkages of juvenile goldlined spinefoot collected in coastal estuaries and lagoons and of broodstock collected in coral reefs in coastal waters of Vietnam; and 3) to provide a baseline for future management decisions regarding this species in Vietnam.

Materials and methods

Sampling strategies

Assessments of juvenile yield Assessments of the yield of juvenile goldlined spinefoot were conducted through consultations with local communities. The word *juvenile* is used herein for the specimens of goldlined spinefoot, with total lengths (TLs) of 18–45 mm, collected by fishermen for the aquaculture industry. Although there are some limits to accuracy, information and data collected through local consultations, including local ecological knowledge, have been widely used in many countries around the world where accurate scientific data are insufficient (Begossi, 2015; Berkström et al., 2019). Data from local consultations have been considered *semi-quantitative data* for rapid assessments of the status of habitats and related resources that contribute to providing a comprehensive baseline for appropriate planning and sustainable utilization of resources in Latin American countries (Fischer et al., 2015). The local consultations were conducted at 8 fishing communities near major estuaries and lagoons along the coast of Vietnam in November and

December 2019 under a national project. The 8 locations where consultations were conducted are Cua Tung estuary, Cua Viet estuary, Tam Giang–Cau Hai Lagoon, Lap An Lagoon, Thu Bon estuary, Tra Bong estuary, Sa Ky estuary, and Nha Phu Lagoon (Fig. 1).

For each consultation, biological scientists from the Institute of Oceanography, Vietnam Academy of Science and Technology (VAST), together with local authorities selected 10–20 consultants, including experienced fishermen that use different fishing gears, local dealers, and

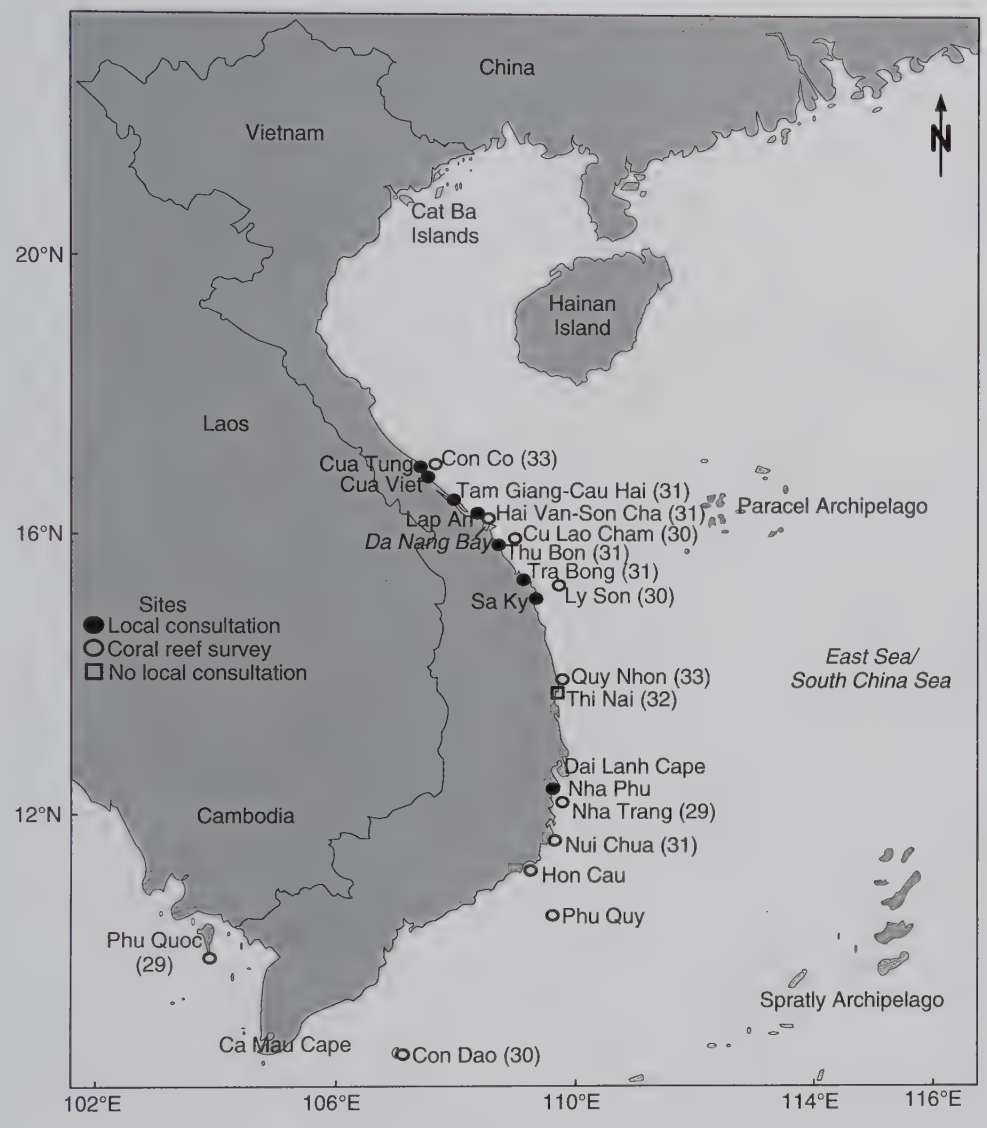

Figure 1

A map of the locations where local consultations regarding goldlined spinefoot (*Siganus guttatus*) (black circles) or coral reef surveys of reef fish taxa (open circles) were conducted along the coast of Vietnam. Yield of juveniles (18–45 mm total length [TL]) was assessed through local consultations at 8 fishing communities near major estuaries or lagoons in November and December 2019. Density of adult (>100 mm TL) goldlined spinefoot was assessed at 11 locations at coral reefs in established or proposed conservation areas during July–September 2020 as part of this study (Con Co Island, Hai Van–Son Cha, the Ly Son Islands, and Nha Trang Bay) or from 2017 through 2021 under support from other projects (the Cu Lao Cham Islands, Quy Nhon Bay, Nui Chua National Park, Hon Cau Island, the Phu Quy Islands, the Con Dao Islands, and the Phu Quoc Islands). For DNA analysis, goldlined spinefoot were sampled from 2017 through 2020: juveniles from 3 locations in an estuary or a lagoon where consultations occurred, as well as from Thi Nai Lagoon, and adults from 9 locations at coral reefs where surveys were conducted. The numerals in parentheses indicate the number of specimens that were collected at each of these 13 sites.

marine aquaculturists, to provide the needed information. Questions were focused on fishing activities for the juvenile yield of goldlined spinefoot and designed to gather the following information: fishing gear and seasons; number of fishing boats; number of fishermen per fishing boat; and catch per unit of effort (CPUE), defined as catch per boat per day or night.

Assessments of adult abundance The density of adult goldlined spinefoot was assessed together with those of other groups of reef fishes at 11 widely distributed locations at coral reefs that have been established as MPAs (Con Co Island, the Cu Lao Cham Islands, Ly Son the Islands, Nha Trang Bay, Nui Chua National Park, Hon Cau Island, the Con Dao Islands, and the Phu Quoc Islands) or are being proposed as MPAs (Hai Van–Son Cha and the Phu Quy Islands) or locally managed marine area (Quy Nhon Bay) in Vietnam. The recorded sizes of adult goldlined spinefoot collected on coral reefs were >100 mm TL. Census surveys were conducted at 4 locations—3 sites off the central part of the eastern coast, Con Co Island, Hai Van–Son Cha, and the Ly Son Islands, and 1 site farther south in Nha Trang Bay—during July–September 2020 within the framework of this project and at 7 other locations—2 sites off the central part of the eastern coast in 2017 at the Cu Lao Cham Islands and in Quy Nhon Bay, 3 sites farther south at Nui Chua National Park in 2018, Hon Cau Island in 2020, and the Phu Quy Islands in 2021, 1 site at the Con Dao Islands in 2018, and 1 site at the Phu Quoc Islands in 2019—under support from other projects (Table 1, Fig. 1). At each study site, 2 transects, each 100 m long, were placed haphazardly in 2 reef zones (1 transect on a reef flat and 1 transect on a reef slope) parallel to the shoreline. The depths below low tide level at transects were approximately 2–4 m at reef flats and 5–12 m at reef slopes. Each 100-m transect was divided into 4 replicates (each 20 m long by 5 m wide). Hence, 8 replicate transects were surveyed at each study site.

Along the transect line, the fish observer used scuba gear and swam slowly to count the number of individuals and to estimate the size (TL) of each individual fish from visual estimates using the methods proposed by English et al. (1997) and Hodgson et al. (2006). Fish were identified to species level by using Randall et al. (1990). The survey time at each site was about 50–60 min. The surveys were all carried out during daylight hours between 0900 and 1400 local time. To avoid disturbance from divers, fish surveys were conducted 15 min after the first transect was placed.

Assessments of genetic diversity and structure The sequence data used in this study are from fish specimens that were collected from 4 locations at estuaries and lagoons and from 9 locations at coral reefs in the coastal waters of Vietnam from 2017 through 2020 under support from different projects (Fig. 1). Three locations in an estuary or a lagoon, including Tam Giang–Cau Hai Lagoon, Tra Bong estuary, and Thi Nai Lagoon, and 4 locations at coral reefs, including Con Co Island, Hai Van–Son Cha, the Ly Son Islands, and Quy Nhon Bay, were sampled from 2019 through 2020 as part of this study. Thu Bon estuary and the Cu Lao Cham Islands were sampled in 2017 for a study supported by the VAST, and 4 other reef locations, including Nha Trang Bay, Nui Chua National Park, the Con Dao Islands, and the Phu Quoc Islands, were sampled from 2018 through 2019 as part of a study funded by the U.S. Agency for International Development. Because information on occurrence and distribution of juvenile goldlined spinefoot at Nha Phu Lagoon and other lagoons and estuaries off the southern coast was not yet available prior to the designing of sampling for this study, samples were not collected at these locations.

Fish samples were collected by using cast nets and by purchasing specimens at fish landing sites. At each location, 29–33 goldlined spinefoot were collected in estuaries or lagoons (29–105 mm TL) and at coral reefs (202–340 mm TL). A total of 401 individuals (125 juveniles and 276 adults) were sampled.

For each individual, a 1-cm^2 section of the right pectoral fin and a 1-cm^2 section of the upper caudal fin were cut out with fine scissors, washed with water, and immediately fixed in a solution of 95% alcohol in a 2-mL screw-cap tube labeled with species name, code, and preservation solution. Then, these fin samples were cooled and stored frozen at −20°C for further analysis in the laboratory.

Samples of DNA were extracted by using the cetyltrimethylammonium bromide method (Adamkewicz and Harasewych, 1996) and preserved in Tris-EDTA buffer solution (10 mM Tris-HCl, pH 7.2, 1 mM EDTA, pH 8.0) at −20°C. The concentration and purity of the extracted DNA were tested on 1.5% agarose gel and on a spectrophotometer (BioSpec-nano[1], Shimadzu Corp., Kyoto, Japan). The use of microsatellites or single sequence repeats was referenced from existing studies of molecular biology and population genetics for goldlined spinefoot. In this study, 5 microsatellites used for population genetic analyses of goldlined spinefoot and suggested by Mao et al. (2016) were applied: HLZY-3 (F: TAACGGTTCTATCAGGG and R: TGCTTCGGATTCAGG at 55°C), HLZY-5 (F: TTCATCACTGCCTGTCCTT and R: AGCGTGTCATTGTTGGGT at 62°C), HLZY-12 (F: CGGACCTGCTTGAGT and R: AACCTGTTTGGTGGAA at 47°C), HLZY-13 (F: TGGCAGTGATGAGGTG and R: CATTTGGAATCGCAGT at 57°C), and HLZY-21 (F: CTGACTCCCAACTTCC and R: CAGACCTGTTTCCAATC at 52°C).

Five forward and reverse primer pairs were run through the polymerase chain reaction (PCR) process, in which primers were marked by HEX or FAM fluorescence staining at the 5′ end. The PCR amplification was performed with a BOECO Thermal Cycler TC-PRO (Boeckel and Co. GmbH and Co., Hamburg, Germany). The PCR reaction was performed at a total volume of 50 µL, including 10 µL of buffer, 0.2 µL Bioline MyTaq HS Polymerase (Meridian Bioscience, Cincinnati, OH), 0.4 µM of each primer, and 5 ng of the template DNA. The PCR process for microsatellites

[1] Mention of trade names or commercial companies is for identification purposes only and does not imply endorsement by the National Marine Fisheries Service, NOAA.

Table 1

The number of sites at which visual census surveys for adult goldlined spinefoot (*Siganus guttatus*), among other reef fish species, were conducted at each of 11 locations at coral reefs along the coast of Vietnam during 2017–2021. At the time of this study, all locations either had been established or were being proposed as marine protected areas (MPAs) or locally managed marine area. An asterisk (*) indicates that the location was an established MPA.

Location	No. of sites surveyed	Time of surveys	Sources
Con Co*	10	August 2020	This study
Hai Van–Son Cha	10	July 2020	This study
Cu Lao Cham*	10	July 2017	Nguyen et al.[1]
Ly Son*	10	September 2020	This study
Quy Nhon Bay	24	April 2017	Nguyen[2]
Nha Trang Bay*	10	July 2020	This study
Nui Chua*	10	September 2018	Mai and Nguyen[3]
Hon Cau*	12	August 2020	Hoang et al.[4]
Phu Quy	11	April 2021	Nguyen et al.[5]
Con Dao*	9	June 2018	Mai and Nguyen[3]
Phu Quoc*	10	April 2019	Nguyen[6]

[1] Nguyen, V. L., T. H. Dao, X. D. Mai, T. K. H. Phan, and H. T. Nguyen. 2020. Studies on population connectivity of target fishes among marine habitats in the World Biosphere Reserve of Cu Lao Cham–Hoi An. Final report for the Vietnam Academy of Science and Technology project VAST06.02/17-18, 24 p. [In Vietnamese.] [Available from Inst. Oceanogr., Vietnam Acad. Sci. Tech., 01 Cau Da St., Nha Trang 650000, Vietnam.]

[2] Nguyen, V. L. 2017. Additional assessments and identification of locations with high marine biodiversity in the Quy Nhon Bay. Final report of the project CRSD/BD/3.d.4.1/2016 under the provincial project "Resources in coastal waters for sustainable development (CRSD) in Binh Dinh Province," 142 p. [In Vietnamese.] [Available from Inst. Oceanogr., Vietnam Acad. Sci. Tech., 01 Cau Da St., Nha Trang 650000, Vietnam.]

[3] Mai, X. D., and L. V. Nguyen. 2021. Status and trends of change of reef fish communities at some locations in the coastal waters of south Vietnam in the period of 2017–2019. Technical report of the project titled, "Study on coral reef resilience in comparative areas in south Vietnam for marine biodiversity conservation in a changing world" (project code: AID-OAA-A-11-0012), 60 p. [In Vietnamese.] [Available from Dep. Mar. Living Resour., Inst. Oceanogr., Vietnam Acad. Sci. Tech., 01 Cau Da St., Nha Trang 650000, Vietnam.]

[4] Hoang, X. B., T. K. H. Phan, K. H. Phan, X. D. Mai, and M. Q. Thai. 2020. Status and trends of change in marine biodiversity and related resources at key sites in the Hon Cau Marine Protected Area. Technical report of the project titled, "Advice on the planning of review, re-zoning, and boundary of Hon Cau Marine Protected Area, Binh Thuan Province," 57 p. [In Vietnamese.] [Available from Dep. Mar. Living Resour., Inst. Oceanogr., Vietnam Acad. Sci. Tech., 01 Cau Da St., Nha Trang 650000, Vietnam.]

[5] Nguyen, T. H., M. Q. Thai, X. D. Mai, and B. X. Hoang. 2022. Assessments of status of marine biodiversity and related resources in key marine habitats (coral reefs, seagrass beds) in the waters surrounding Phu Quy district. Technical report of the project titled "Advice on the development of the project for the establishment of Phu Quy Marine Protected Area, Binh Thuan Province" (project code: 01-DABTBPQ) 50 p. [In Vietnamese.] [Available from Dep. Mar. Living Resour., Inst. Oceanogr., Vietnam Acad. Sci. Tech., 01 Cau Da St., Nha Trang 650000, Vietnam.]

[6] Nguyen, V. L. 2019. Assessments of marine biodiversity and re-zoning for management of Phu Quoc Marine Protected Area. Final report of provincial project submitted to the Department of Agriculture and Rural Development of Kien Giang Province, 310 p. [In Vietnamese.] [Available from Inst. Oceanogr., Vietnam Acad. Sci. Tech., 01 Cau Da St., Nha Trang 650000, Vietnam.]

or single sequence repeats had six stages. The first stage was the initial denaturation at 95°C for 1 min, followed by 35 cycles of denaturation at 95°C for 15 s, an annealing phase at a suitable temperature for each primer for 15 s, and an extension phase at 72°C for 90 s. Then, the final extension phase began at 72°C for 10 s and ended at 20°C for 60 s. The PCR products were then run on 1.6% agarose gel/100 mL TBE buffer (0.5×) with 1.0 µL gelled and detected by ultraviolet transilluminator (UVP DigiDoc-It, Analytik Jena GmbH, Jena, Germany) prior to genotyping on an Applied Biosystems 3730XL DNA Analyzer (Thermo Fisher Scientific, Waltham, MA).

Data storage and analysis

Annual yield of juveniles was calculated as follows: number of boats multiplied by fishing time multiplied by average yield per time unit (CPUE).

The density of fish at each study site was calculated as the mean value of the 8 replicates from the 2 transects on the reef flat and reef slope. To improve the homogeneity of variances, raw data on abundance of adults was $\log_{10}(x+1)$ transformed prior to the analyses. When the analysis of variance detected significant differences, Tukey's honestly significant difference test was applied in order to separate differences between locations.

The software GeneMarker, vers. 2.7.4 (SoftGenetics, State College, PA), was used to determine the length of alleles. Null alleles were detected by using the software Micro-Checker, vers. 2.2.3 (Van Oosterhout et al., 2004). Genetic variability estimates for each locus, such as those made by using the Hardy–Weinberg equilibrium, number of alleles on each satellite, number of rare alleles, observed heterozygosity, and expected heterozygosity were calculated by using the software GenAlEx 6.1 (Peakall and Smouse, 2006). The statistical significance tests for these indices were revised on the basis of the Bonferroni correction (Rice, 1989).

Evaluation of differences between groups in genetic structure (fixation index [F_{ST}] and pairwise F_{ST}) was done through analysis of molecular variance with Arlequin, vers. 3.11 (Excoffier et al., 2005). We used the model-based clustering method in the software Structure, vers. 2.3.4 (Pritchard et al., 2000), to elucidate the group structure and visualized results in images by using the program Structure Harvester, vers.0.6.94 (Earl and vonHoldt, 2012). In the model of the software Structure, a Bayesian approach is applied to estimate the probability of correctly assigned genotypes in the data in the number of clusters (K). Each value of K (1–10 clusters) was run for 10 repetitions, and the average log probability of the data, L(K), was calculated. The L(K) plateaued (or continued to increase slightly) when K approached the true value, and high variance between runs also occurred (Rosenberg et al., 2001). The number of K groups was then evaluated by using ΔK, an ad hoc statistic based on the second order rate of change of L(K) (Evanno et al., 2005).

Results

Juvenile yield

Information for the local consultations at 8 locations in estuaries and lagoons indicates that juvenile goldlined spinefoot were collected only from Tam Giang–Cau Hai Lagoon (in Thua Thien Hue Province) to south-central Vietnam, with 38.61 million juveniles (equivalent to 4290 kg) collected in 2019. Among the 8 locations, the 3 most important locations, including Tam Giang Cau–Hai Lagoon, Thu Bon estuary, and Nha Phu Lagoon, supported high CPUE (215,000–826,000 juveniles per boat per day) and yield (9.77–13.01 million juveniles). The locations of Lap An Lagoon and Sa Ky estuary supported the lowest CPUE (0.03–0.04 juveniles per boat per day) and yield (<1 million juveniles at each location) (Fig. 2). In general, juvenile goldlined spinefoot were found in lagoons and estuaries that had seagrass beds, with an exception of Tra Bong estuary. However, there was no correlation between the area of seagrass beds and both CPUE and yield of juveniles of this species (Fig. 2). Information from local fishermen indicates that juvenile goldlined spinefoot were also found in the Cua Tung and Cua Viet estuaries (in Quang Tri Province). However, because they occurred in very low numbers, the local fishermen did not make an effort to collect them.

Abundance of adult stock

Results of an analysis of data from 138 sites at 11 reef locations in the coastal waters of Vietnam that were surveyed during 2017–2021 indicate that the overall mean density of goldlined spinefoot was 0.37 fish/100 m^2 (standard error of the mean [SE] 0.04), with the sites in MPAs supporting a significantly higher mean density (0.51 fish/100 m^2 [SE 0.06]) than that of the sites that were not in MPAs (0.09 fish/100 m^2 [SE 0.03]) (analysis of variance: $P<0.001$). Among the sites in MPAs, the mean densities in the Cu Lao Cham, Nha Trang Bay, and Phu Quoc MPAs were 3.3–51.2 times higher than and significantly different (analysis of variance: $P<0.001$) from those in other MPAs (the Con Co, Ly Son, and Nui Chua MPAs) and those in sites not in MPAs (Hai Van–Son Cha and Quy Nhon Bay) (Fig. 3). No goldlined spinefoot were recorded at the Hon Cau MPA, the Phu Quy Islands (proposed MPA),

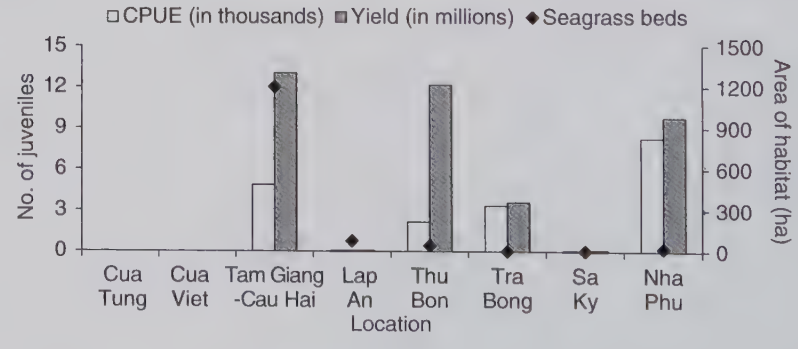

Figure 2

The relationship between catch per unit of effort (CPUE) and yield of juvenile goldlined spinefoot (*Siganus guttatus*) in major estuaries and lagoons along the coast of Vietnam, based on local consultations conducted in 8 fishing communities during November and December 2019. The black diamonds indicate the locations that had seagrass beds and the extent of these habitats.

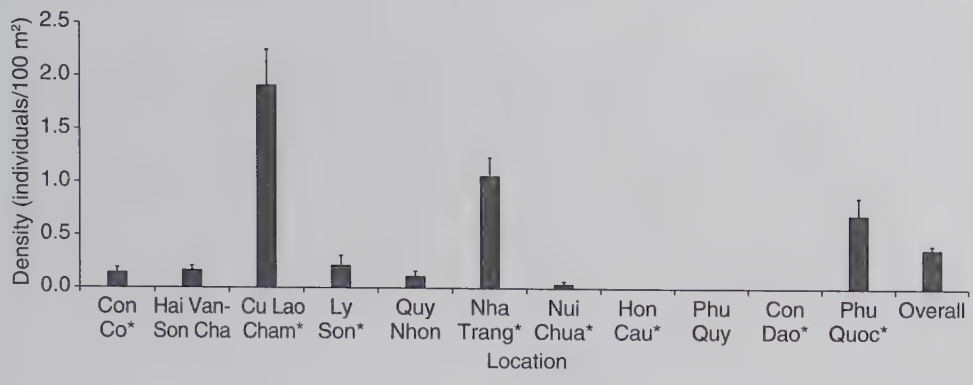

Figure 3

Mean density of adult goldlined spinefoot (*Siganus guttatus*) sampled at 11 locations at major coral reefs in the coastal waters of Vietnam between 2017 and 2021. An asterisk (*) indicates that a location was an established marine protected area at the time of this study. Error bars indicate standard errors of the means.

and the Con Dao MPA. The reef locations that supported higher densities of adult goldlined spinefoot (the Cu Lao Cham and Nha Trang Bay MPAs) than other reef locations are closer geographically to the lagoons and estuaries with higher juvenile yield (Thu Bon estuary and Nha Phu Lagoon). However, sites not in MPAs (Hai Van–Son Cha and Quy Nhon Bay) supported much lower densities than MPA sites despite their proximity to Tam Giang–Cau Hai and Thi Nai Lagoons, which had very high juvenile yield for collections made in this study (Fig. 3).

Genetic diversity and structure

Results of analysis of sequence data for 347 samples from 401 specimens collected from 13 locations indicate that the total number of alleles of 5 microsatellites was 110, of which 32 alleles were private (Table 2). Among the 5 microsatellites, HLZY-12 had the highest alleles per locus (36), followed by 25, 22, 18, and 9 alleles per locus for HLZY-13, HLZY-5, HLZY-21, and HLZY-3, respectively. The population of goldlined spinefoot in the Phu Quoc Islands appears to be the most diverse, given that samples from specimens caught at that location had the highest number of alleles (73) compared with the numbers of alleles for samples from specimens collected at the other locations (41–57). The samples from fish caught at Phu Quoc Islands also had the highest number of private alleles (20). The values of observed heterozygosity and expected heterozygosity of each single sequence repeat varied slightly between locations, ranging from 0.33 to 1.00 and from 0.49 to 0.92, respectively (Fig. 4). In general, there was no deviation from the Hardy–Weinberg equilibrium in sequence data for most locations, with some exceptions for microsatellite HLZY-3 (Thu Bon estuary, Thi Nai Lagoon, and the Phu Quoc Islands), HLZY-5 (Hai Van–Son Cha, the Cu Lao Cham Islands, Thi Nai Lagoon, Quy Nhon Bay, and Nha Trang Bay), HLZY-12 (the Cu Lao Cham Islands), HLZY-13 (Con Co Island, the Con Dao Islands, and the Phu Quoc Islands), and HLZY-21 (Hai Van–Son Cha, Tra Bong estuary, and Nui Chua National Park) (Table 3).

Genetic linkages among marine habitats

The results of the analyses of molecular variance indicate a significant difference in genetic structure (F_{ST}=0.015, P<0.05) among genetic groups, a central group (specimens from Con Co Island to Quy Nhon Bay), a southern group (specimens from Nha Trang Bay to the Con Dao Islands), and a southwestern group (specimens from the Phu Quoc Islands), at the sampling locations with a low percentage of genetic variation (1.5%; Table 4). Results from comparison of pairwise F_{ST} values indicate that genetic differentiation occurred at all locations (at levels of 1.2–6.5%) and that the difference was significant (P<0.05). Generally, results from analyses of molecular variance reveal that there were 2 distinct groups in the genetic structure of collected goldlined spinefoot among the 13 sampling locations: a central group that included specimens from Con Co Island to Quy Nhon Bay and a southern group that included fish caught from Nha Trang Bay south and all the way around to the Phu Quoc Islands on the southwestern coast, with the genetic similarity among locations within each group reaching 99–100%. This genetic similarity indicates that genetic linkages occurred only within each group.

The results from Bayesian analysis (done with the software Structure) indicate that ΔK ranged from 0.018305 to 0.774668 when K was set from 1 to 8. The clearest peak in ΔK occurred when K was set to 3, with a value of 0.774668, indicating that 3 distinct genetic clusters (assigned the colors of green, red and blue in visualizations) existed in goldlined spinefoot among the sampling locations (Fig. 5). The central group included specimens from Con Co Island to Quy Nhon Bay, with most fish having the majority of their genome assigned to the green cluster (Fig. 5). The southern

Table 2

Total number of alelles and private alleles for each microsatellite found in sequence data from goldlined spinefoot (*Siganus guttatus*) sampled from 2017 through 2020 in the coastal waters of Vietnam. Sites where fish were collected include the following locations at estuaries, lagoons, or coral reefs: Con Co Island (CCO), Tam Giang–Cau Hai Lagoon (TAG), Hai Van–Son Cha (HVS), Thu Bon estuary (THB), the Cu Lao Cham Islands (CLC), Tra Bong estuary (TBO), the Ly Son Islands (LSO), Thi Nai Lagoon (TNA), Quy Nhon Bay (QNH), Nha Trang Bay (NTR), Nui Chua National Park (NCH), the Con Dao Islands (CDA), and the Phu Quoc Islands (PQU).

Sampling location	Microsatellite					Total
	HLZY-3	HLZY-5	HLZY-12	HLZY-13	HLZY-21	
Alleles						
CCO	4	5	12	12	8	41
TAG	6	7	15	14	6	48
HVS	4	6	14	17	8	49
THB	5	9	12	15	8	49
CLC	4	7	14	16	10	51
TBO	4	7	11	16	9	47
LSO	4	7	13	16	10	50
TNA	5	8	16	14	9	52
QNH	5	11	15	15	11	57
NTR	3	7	14	15	9	48
NCH	5	6	11	15	11	48
CDA	5	6	11	16	9	47
PQU	7	14	22	16	14	73
Total	9	22	36	25	18	110
Private alleles						
THB			1			1
CLC		2				2
LSO					1	1
QNH	1	4	3			8
PQU	2	3	6	6	3	20
Total	3	9	10	6	4	32

group was composed of individuals caught at locations from Nha Trang Bay to the Con Dao Islands, forming the red cluster (Fig. 5). The southwestern group, consisting of specimens caught off the Phu Quoc Islands, formed the blue cluster (Fig. 5).

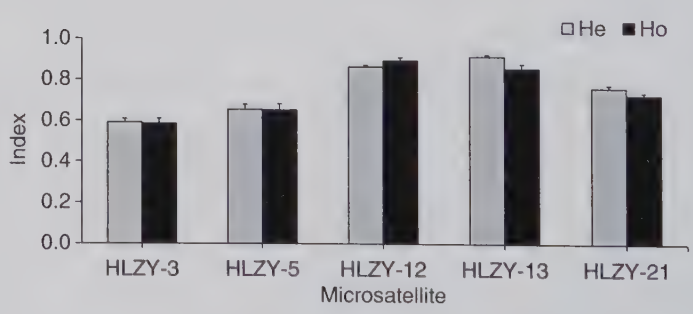

Figure 4

Mean values of observed heterozygosity (Ho) and expected heterozygosity (He) for each microsatellite used in genetic analysis of goldlined spinefoot (*Siganus guttatus*) sampled from 2017 through 2020 in the coastal waters of Vietnam. Error bars indicate standard errors of the means.

Discussion

The results of this study indicate that the central coast of Vietnam supported the highest yield of juvenile goldlined spinefoot in 2019, with higher yield recorded at Tam Giang–Cau Hai Lagoon, Thu Bon estuary, Thi Nai Lagoon, and Nha Phu Lagoon compared to that at the other estuaries and lagoons. This greater level of yield may be related to the presence and structure of seagrass beds (Nagelkerken, 2009; Nguyen et al., 2015). In this study, CPUE had no correlation with areas of seagrass beds; therefore, differences in the composition of seagrass species may contribute to marked differences in the total yield of juvenile goldlined spinefoot among the lagoons and estuaries.

Higher densities of adult goldlined spinefoot were mainly found during coral reef surveys at the locations that have been established as MPAs rather than at locations where MPAs do not exist. This finding is consistent with those of other studies in which higher densities or

Table 3

P-values from tests for deviation from the Hardy–Weinberg equilibrium (HWE), by location for each microsatellite found in sequence data from goldlined spinefoot (*Siganus guttatus*) sampled from 2017 through 2020 in the coastal waters of Vietnam. An asterisk (*) indicates a significant difference ($P<0.05$) from HWE. Sites where fish were collected include the following locations at estuaries, lagoons, or coral reefs: Con Co Island (CCO), Tam Giang–Cau Hai Lagoon (TAG), Hai Van–Son Cha (HVS), Thu Bon estuary (THB), the Cu Lao Cham Islands (CLC), Tra Bong estuary (TBO), the Ly Son Islands (LSO), Thi Nai Lagoon (TNA), Quy Nhon Bay (QNH), Nha Trang Bay (NTR), Nui Chua National Park (NCH), the Con Dao Islands (CDA), and the Phu Quoc Islands (PQU).

Sampling location	Microsatellite				
	HLZY-3	HLZY-5	HLZY-12	HLZY-13	HLZY-21
CCO	0.45	0.81	0.82	0.02*	0.36
TAG	0.59	0.63	0.89	0.22	0.26
HVS	0.91	0.03*	0.60	0.79	0.02*
THB	0.02*	1.00	0.74	0.16	0.21
CLC	0.27	0.00*	0.00*	1.00	0.56
TBO	0.95	0.48	0.49	0.14	0.00*
LSO	0.95	1.00	0.68	0.33	0.33
TNA	0.01*	0.01*	0.53	0.72	1.00
QNH	0.99	0.00*	0.30	0.96	0.61
NTR	0.99	0.00*	0.45	0.24	0.23
NCH	0.62	0.99	0.35	0.11	0.02*
CDA	0.99	0.73	0.54	0.01*	0.09
PQU	0.00*	0.84	0.74	0.00*	0.55

Table 4

Summary of results from analyses of molecular variance that indicate differences in genetic variation among and within distinct genetic groups of goldlined spinefoot (*Siganus guttatus*). Sequence data used in analyses are from specimens collected in the coastal waters of Vietnam during 2017–2020. The fixation index was 0.015.

Source of variation	df	Sum of squares	Mean of squares	Estimate of variation	Percentage of variation (%)
Among populations	2	23.756	11.878	0.060	1.5
Within populations	344	705.852	2.051	0.114	98.5
Total	693	1362.108		1.997	100.0

abundances and higher levels of biomass of target species were recorded inside MPAs as opposed to outside MPAs (Russ and Alcala, 2003; Maliao et al., 2009). However, the overall densities of goldlined spinefoot in MPAs were very low (with a mean of 0.51 fish/100 m^2), and these populations may take a long time to recover to a high level of abundance. An effort to protect and conserve broodstocks at some MPAs with higher densities of goldlined spinefoot, especially at the Cu Lao Cham, Nha Trang Bay, and Phu Quoc MPAs, is an important measure that can be used by resource managers in the short term, and conservation at other MPAs can be useful in the longer term as well, because MPAs play an key role in enhancing local fisheries outside MPAs through either net movement or net export of larvae from MPAs (Russ, 2002).

The differentiation in population genetics of goldlined spinefoot between the central and southern groups is consistent with results of some previous studies, indicating that an oceanographic boundary limits the genetic dispersal between the areas where these groups were found. Ablan et al. (2002) studied the genetic structure of threespot dascyllus and suggested that the South China Sea may be divided into 2 distinct parts on the basis of the differentiation in population genetics with geographical

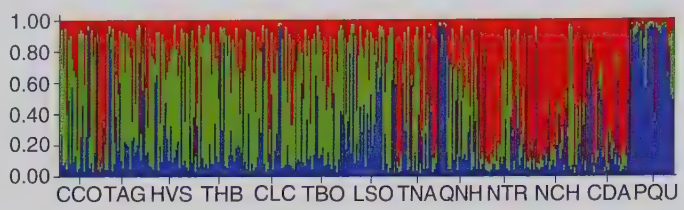

Figure 5

Visualization of the results from Bayesian analysis of the genetic structure of goldlined spinefoot (*Siganus guttatus*) collected from 13 locations in the coastal waters of Vietnam during 2017–2020. Three distinct genetic groups were found in the sequence data from sampled fish. Bars represent the proportion of an individual fish's genome that was assigned to the green, red, or blue genetic cluster. Specimens were collected from Con Co Island (CCO), Tam Giang–Cau Hai Lagoon (TAG), Hai Van–Son Cha (HVS), Thu Bon estuary (THB), the Cu Lao Cham Islands (CLC), Tra Bong estuary (TBO), the Ly Son Islands (LSO), Thi Nai Lagoon (TNA), Quy Nhon Bay (QNH), Nha Trang Bay (NTR), Nui Chua National Park (NCH), the Con Dao Islands (CDA), and the Phu Quoc Islands (PQU).

boundaries located in south-central Vietnam close to Nha Trang Bay. A notable division in the genetic structure of goldlined spinefoot found in this study at the Phu Quoc Islands is in accordance with findings of the previously mentioned studies (Ablan et al., 2002; Dang et al., 2014). In addition, the results from recent studies based on analyses of communities of reef-building corals also indicate a separation in the distribution between the central and the southern groups, with a geographical boundary located at Dai Lanh Cape (at about 13°N) near the city of Tuy Hoa, and between the southern and southwestern groups at Ca Mau Cape (at about 8°N) at the southernmost tip of Vietnam (Vo, 2014; Vo and Nguyen, 2022).

The discharge of the Mekong River (Dang et al., 2014), which acts as an oceanographic barrier to the dispersal of marine planktonic larvae, could be one explanation for the separation of reef fish communities between the southwestern group in the Gulf of Thailand and the central and southern groups in the South China Sea. The recent results from oceanographic modeling indicate that a weak current flowed from the Gulf of Thailand (at the Phu Quoc Islands) to the Con Dao Islands, compared to a strong current from the Java Sea through the Karimata Strait, in Malaysia, up to the mouth of the Gulf of Thailand and over to the Con Dao Islands during the southwest monsoon (July–September), and that a weak current flowed from the Con Dao Islands to the Phu Quoc Islands, compared to a strong current from the Luzon Strait, between Taiwan and the Philippines, east to Hainan Island, in China, and down along the coast of Vietnam through the Con Dao Islands, to Malaysia and the Karimata Strait during the northeast monsoon (January–March) (Li et al., 2019). These currents may limit the larval dispersal of goldlined spinefoot and other marine organisms. Our findings on the separation of the 3 genetic groups are similar to the findings of distinct populations of this species sampled in Japan off Okinawa Island, Miyako Island, and Ishigaki Island on a geographical scale of about 100–2000 km (Iwamoto et al., 2009).

The spatial genetic structure found in our study for this species in the coastal waters of Vietnam could be related to differences in biological characteristics (Froukh and Kochzius, 2007). Larvae of goldlined spinefoot are in the pelagic stage, which lasts for about 24 d (Juario et al., 1985; Sheaves, 1995; Nabhitabhata and Ikeda, 2014). This factor may be the one that limits the dispersal of this species because larval dispersal of goldlined spinefoot is mainly driven by currents or tides (Kanashiro et al., 1999) and by seawater temperature (Collins and Nelson, 1993). The numbers of alleles for groups of goldlined spinefoot were similar between sampling locations, with the exception that the numbers for groups based on analysis of samples taken from specimens collected at the Phu Quoc Islands are twice as high as those for groups in other locations. This result indicates that there is distinguishable genetic diversity in this species at the Phu Quoc Islands. Therefore, the Phu Quoc Islands may be considered another functional location because of the differentiation in population genetics of this species. The differences in characteristics mentioned for goldlined spinefoot at the Phu Quoc Islands may play important roles in the creation of the differentiation in population genetics among distinct groups.

Conclusions

The coastal lagoons and estuaries in Vietnam with seagrass beds (especially, Tam Giang–Cau Hai Lagoon, Nha Phu Lagoon, and Thu Bon estuary) supported high yield of juvenile goldlined spinefoot, and the nearby MPAs (the Cu Lao Cham and Nha Trang Bay MPAs) had higher densities of adults of this species. There were 3 distinct genetic groups, with the central group including specimens from Con Co Island to Quy Nhon Bay, the southern group including individuals collected from Nha Trang Bay to the Con Dao Islands, and the southwestern group including fish from the Phu Quoc Islands in the Gulf of Thailand. Establishment of MPA networks on the basis of both ecological and social interconnectivity among crucial marine habitats, such as coral reefs, seagrass beds, and mangroves, is important because such efforts could help ensure that as many genetic units as possible are maintained for the overall resilience of fisheries. Creating networks of MPAs can further enhance the effectiveness of MPAs in protecting spawners in coral reefs and in increasing the survivorship of recruits in seagrass beds and mangroves in coastal lagoons and estuaries.

Resumen

Las evaluaciones del estado de las especies objetivo de la pesca y sus vínculos ecológicos con los hábitats marinos

están desempeñando un papel importante en mejorar la efectividad de las áreas marinas protegidas (AMP) y el manejo de otras zonas costeras. En este estudio, evaluamos el rendimiento de juveniles y la abundancia del sigano rayas doradas (*Siganus guttatus*) utilizando el conocimiento local y censos visuales en aguas costeras de Vietnam. La estructura genética se examinó mediante análisis de ADN de juveniles, colectados en pastos marinos y manglares en las principales lagunas y estuarios, y de adultos colectados en arrecifes de coral. Se colectados más de 38.6 millones de juveniles en 8 lagunas costeras y estuarios. Las lagunas costeras y los estuarios con pastos marinos albergaban un alto volumen de juveniles, y las AMP cercanas presentaban mayores densidades de adultos. Se identificaron tres grupos genéticos distintos: un grupo en la parte central de la costa oriental, desde la isla de Con Co hasta la bahía de Quy Nhon; un segundo grupo en la costa sudoriental, desde la bahía de Nha Trang hasta las islas Con Dao, situadas en el extremo sur de Vietnam; y un tercer grupo en la costa sudoccidental, en las islas Phu Quoc, en el golfo de Tailandia.

Acknowledgments

This study was developed within the framework of a national project (code: KC.09.41/16-20). In this study, unpublished data from current projects funded by the VAST (code: VAST06.02/17-18) and the U.S. Agency for International Development (code: AID-OAA-A-11-0012) were used for analysis. This publication is a contribution to celebrate the 100th anniversary of the Institute of Oceanography, VAST. We thank R. Winterbottom, A. Chung, and the anonymous reviewers who provided comments that helped improve the manuscript.

Literature cited

Ablan, M. C. A., J. W. McManus, C. A. Chen, K. T. Shao, J. Bell, A. S. Cabanban, V. S. Tuan, and I. W. Arthana.
2002. Meso-scale transboundary units for the management of coral reefs in the South China Sea area. Naga. Worldfish Cent. Q. 25(3–4):4–9.

Adamkewicz, S. L., and M. G. Harasewych.
1996. Systematics and biogeography of the genus *Donax* (Bivalvia: Donacidae) in eastern North America. Am. Malacol. Bull. 13:97–103.

Almany, G. R., M. L. Berumen, S. R. Thorrold, S. Planes, and P. G. Jones.
2007. Local replenishment of coral reef fish populations in a marine reserve. Science 316:742–744.

Begossi, A.
2015. Local ecological knowledge (LEK): understanding and managing fisheries. *In* Fishers' knowledge and the ecosystem approach to fisheries: applications, experiences and lessons in Latin America (J. Fischer, J. Jorgensen, H. Josupeit, D. Kalikoski, and C. M. Lucas, eds.), p. 7–18. FAO Fish. Aquac. Tech. Pap. 591. FAO, Rome. [Available from website.]

Berkström, C., M. Papadopoulos, N. S. Jiddawi, and L. M. Nordlund.
2019. Fishers' local ecological knowledge (LEK) on connectivity and seascape management. Front. Mar. Sci. 6:130.

Chen, C. A., M. C. A. Ablan, J. W. McManus, J. D. Bell, V. S. Tuan, A. S. Cabanban, and K.-T. Shao.
2004. Population structure and genetic variability of six bar wrasse (*Thallasoma hardwicki*) in northern South China Sea revealed by mitochondrial control region sequences. Mar. Biotechnol. 6:312–326.

Collins, L. A., and S. G. Nelson.
1993. Effects of temperature on oxygen consumption, growth, and development of embryos and yolk-sac larvae of *Siganus randalli* (Pisces: Siganidae). Mar. Biol. 117:195–204.

Conover, D. O., L. M. Clarke, S. B. Munch, and N. G. Wagner.
2006. Spatial and temporal scales of adaptive divergence in marine fishes and the implications for conservation. J. Fish Biol. 69:21–47.

Cowen, R. K., and S. Sponaugle
2009. Larval dispersal and marine population connectivity. Annu. Rev. Mar. Sci. 1:443–466.

Dang, B. T., D. H. Q. Vu, and T. O. Truong.
2014. Population genetics for marine resource conservation in Vietnam. *In* Proceedings of the 2nd National Scientific Conference on Marine Biology and Sustainable Development; Hai Phong, 13–14 November 2014, p. 33–40. Publ. House Nat. Sci. Technol., Ha Noi, Vietnam.

Dao, H. T., C. Smith-Keune, E. Wolanski, C. M. Jones, and D. R. Jerry.
2015. Oceanographic currents and local ecological knowledge indicate, and genetics does not refute, a contemporary pattern of larval dispersal for the ornate spiny lobster, *Panulirus ornatus* in the South-East Asian Archipelago. PLoS ONE 10(5):e0124568.

Do, D. S., N. B. Nguyen, D. Q. Ngo, and P. T. Vu.
2005. Review on mangroves in Vietnam, 136 p. Publ. House Argric., Ha Noi, Vietnam.

Duray, M. N.
1998. Biology and culture of siganids, rev. ed., 53 p. Aquac. Dep., Southeast Asian Fish. Dev. Cent., Tigbauan, Philippines.

Earl, D. A., and B. M. vonHoldt.
2012. STRUCTURE HARVESTER: a website and program for visualizing STRUCTURE output and implementing the Evanno method. Conserv. Genet. Resour. 4:359–361.

English, S., C. Wilkinson, and V. Baker (eds.).
1997. Survey manual for tropical marine resources, 2nd ed., 390 p. Aust. Inst. Mar. Sci., Townsville, Australia.

Evanno, G., S. Regnaut, and J. Goudet.
2005. Detecting the number of clusters of individuals using the software STRUCTURE: a simulation study. Mol. Ecol. 14:2611–2620.

Excoffier, L., G. Laval, and S. Schneider.
2005. Arlequin (version 3.0): an integrated software package for population genetics data analysis. Evol. Bioinform. Online. 1:47–50.

Fischer, J., J. Jorgensen, H. Josupeit, D. Kalikoski, and C. M. Lucas (eds.).
2015. Fishers' knowledge and the ecosystem approach to fisheries: applications, experiences and lessons in Latin America. FAO Fish. Aquac. Tech. Pap. 591, 278 p. FAO, Rome. [Available from website.]

Froese, R., and D. Pauly (eds.).
2021. FishBase, vers. 8/2021. [World Wide Web electronic publication.] [Available from website, accessed in August 2021.]

Froukh, T., and M. Kochzius.
2007. Genetic population structure of the endemic four-line wrasse (*Larabicus quadrilineatus*) suggests limited larval dispersal distances in the Red Sea. Mol. Ecol. 16:1359–1367.

Green, A. L., A. P. Maypa, G. R. Almany, K. L. Rhodes, R. Weeks, R. A. Abesamis, M. G. Gleason, P. J. Mumby, and A. T. White.
2015. Larval dispersal and movement patterns of coral reef fishes, and implications for marine reserve network design. Biol. Rev. 90:1215–1247.

Hellberg, M. E., R. S. Burton, J. E. Neigel, and R. S. Palumbi.
2002. Genetic assessment of connectivity among marine populations. Bull. Mar. Sci. 70(Suppl. 1):273–290.

Hodgson, G., J. Hill, W. Kiene, L. Maun, J. Mihaly, J. Liebeler, C. Shuman, and R. Torres.
2006. Reef check instruction manual: a guide to reef check coral reef monitoring, 86 p. Reef Check Found., Pacific Palisades, CA.

Honda, K., Y. Nakamura, M. Nakaoka, W. H. Uy, and D. M. Fortes.
2013. Habitat use by fishes in coral reefs, seagrass beds and mangrove habitats in the Philippines. PLoS ONE 8(8):e65735.

Iwamoto, K., A. Takemura, T. Yoshino, and H. Imai.
2009. Molecular ecological study of *Siganus spinus* and *S. guttatus* from Okinawan waters based on mitochondrial DNA control region sequences. J. Oceanogr. 65:103–112.

Jones, G. P., S. Planes, and R. S. Thorrold.
2005. Coral reef fish larvae settle close to home. Current Biol. 15:1314–1318.

Juario, J. V., M. N. Duray, V. M. Dwray, J. F. Nacario, and J. M. E. Almendras.
1985. Breeding and larval rearing of the rabbitfish, *Siganus guttatus* (Bloch). Aquaculture 44:91–101.

Kami, H. T., and I. I. Ikehara.
1976. Notes on the annual juvenile siganid harvest in Guam. Micronesica 12:323–325.

Kanashiro, K., F. Motonaga, and M. Kimura.
1999. Settlement of white-spotted spinefoot, *Siganus canaliculatus* (Pisces: Siganidae), in the coastal waters off Okinawa Island, Japan. Nippon Suisan Gakkaishi 65:19–25. [In Japanese.]

Kinlan, B. P., and S. D. Gaines.
2003. Propagule dispersal in marine and terrestrial environments: a community perspective. Ecology 84:2007–2020.

Knudsen, R., A. Klemetsen, P.-A. Amundsen, and B. Hermansen.
2006. Incipient speciation through niche expansion: an example from the Arctic charr in a subarctic lake. Proc. R. Soc. B 273:2291–2298.

Laikre, L., S. Palm, and N. Ryman.
2005. Genetic population structure of fishes: implications for coastal zone management. Ambio 34(2):111–119.

Lam, T. J.
1974. Siganids: their biology and mariculture potential. Aquaculture 3:325–354.

Le, D. Q., S. Y. Fui, R. M. Piah, T. Ishimura, Y. Sano, K. Tanaka, and K. Shirai.
2019. Isotopic evidence of connectivity between an inshore vegetated lagoon (nursery habitat) and coastal artificial reefs (adult habitats) for the reef fish *Lethrinus lentjan* on the Terengganu coast, Malaysia. Mar. Freshw. Res. 70:1675–1688.

Le, V. D., and D. N. Le.
2006. Preliminary data on development of gonad of *Siganus guttatus* in Thua Thien Hue lagoon. J. Agric. Rural Dev. 2:61–64. [In Vietnamese.]

Li, M., J. Wei, D. Wang, A. L. Gordon, S. Yang, P. Malanotte-Rizzoli, and G. Jiang.
2019. Exploring the importance of the Mindoro-Sibutu pathway to the upper-layer circulation of the South China Sea and the Indonesian throughflow. J. Geophys. Res. 124:5054–5066.

Luo, J., J. E. Serafy, S. Sponaugle, P. B. Teare, and D. Kieckbusch.
2009. Movement of gray snapper *Lutjanus griseus* among subtropical seagrass, mangrove, and coral reef habitats. Mar. Ecol. Prog. Ser. 380:255–269.

Luong, C. V., N. V. Thao, T. Komatsu, N. D. Ve, and D. D. Tien.
2012. Status and threats on seagrass beds using GIS in Vietnam. Proc. SPIE 8525, Remote Sens. Mar. Environ. II, 852512.

Magsino, R. M., and M. A. Juinio-Meñez.
2008. The influence of contrasting life history traits and oceanic processes on genetic structuring of rabbitfish populations *Siganus argenteus* and *Siganus fuscescens* along the eastern Philippine coasts. Mar. Biol. 154:519–532.

Maliao, R. J., A. T. White, A. P. Maypa, and R. G. Turingan.
2009. Trajectories and magnitude of change in coral reef fish populations in Philippine marine reserves: a meta-analysis. Coral Reefs 28:809.

Mao, X. Q., Z. B. Li, Y. F. Ning, J. B. Shangguan, Y. Yuan, Y. S. Huang, and B. B. Li.
2016. Development of novel polymorphic microsatellite markers in *Siganus fuscescens*. Genet. Mol. Res. 15(3):gmr.15037515.

McMillan, W. O., and S. R. Palumbi.
1995. Concordant evolutionary patterns among Indo-West Pacific Butterflyfishes. Proc. R. Soc. B. 260:229–236.

Nabhitabhata, J., and Y. Ikeda.
2014. *Sepioteuthis lessonana*. *In* Cephalopod culture (J. Iglesias, L. Fuentes, and R. Villanueva, eds.), p. 315–347. Springer, Dordrecht, Netherlands.

Nagelkerken, I.
2009. Evaluation of nursery function of mangroves and seagrass beds for tropical decapods and reef fishes: patterns and underlying mechanisms. *In* Ecological connectivity among tropical coastal ecosystems (I. Nagelkerken, ed.), p. 357–399. Springer, Dordrecht, Netherlands.

Nguyen, V. L., and T. S. Vo.
2014. Status of coral reefs in the coastal waters of Viet Nam. *In* Status of coral reefs of East Asian Seas Region: 2014 (Kimura T., Tune K. and L. M. Chou, eds.), p. 187–216. Minist. Environ. Jpn., Tokyo, Japan.

Nguyen, V. L., and D. X. Mai.
2018. Status of exploitation of marine resources in the World Biosphere Reserve of Cu Lao Cham–Hoi An. Vietnam J. Mar. Sci. Technol. 18(4A):115–128. [In Vietnamese.]
2020. Reef fish fauna in the coastal waters of Vietnam. Mar. Biodivers. 50:100.

Nguyen, A. K., S. T. Vo, T. T. T. Nguyen, V. L. Nguyen, T. T. Hua, X. D. Truong, X. H. Nguyen, K. H. Phan, X. V. Nguyen, T. T. T. Le, et al.
2010. The status of fishery resources and juveniles of Thi Nai Lagoon by using the participatory coastal resource assessment method. Collect. Mar. Res. Works 17:118–131. [In Vietnamese.]

Nguyen, V. Q., T. T. Nguyen, T. C. Chu, D. T. Nguyen, D. T. Dam, D. T. Tran, D. V. Vu, H. N. Dang, D. V. Nguyen, and N. V. Dinh.
2015. Degradation and solutions for restoration of lagoons in the central coast of Vietnam, 385 p. Publ. House Nat. Sci. Technol., Ha Noi, Vietnam.

Nguyen, V. H., K. B. Nguyen, V. N. Nguyen, and K. V. Do.
2019. Coral reef distribution and hard coral cover in the coastal area in Vietnam. Vietnam J. Agric. Rural Dev., special issue on marine fisheries 2019: 214–220. [In Vietnamese.]

Peakall, R., and P. E. Smouse.
2006. GENALEX 6: genetic analysis in Excel. Population genetic software for teaching and research. Mol. Ecol. Notes 6:288–295.

Planes, S., G. P. Jones, and R. S. Thorrold.
2009. Larval dispersal connects fish populations in a network of marine protected areas. Proc. Natl. Acad. Sci. U.S.A. 106:5693–5697.

Pritchard, J. K., M. Stephens, and P. Donnelly.
2000. Inference of population structure using multilocus genotype data. Genetics 155:945–959.

Randall, J. E., G. R. Allen, and R. C. Steene.
1990. Fishes of the Great Barrier Reef and Coral Sea, 507 p. Univ. Hawaii Press, Honolulu, HI.

Rice, W. R.
1989. Analyzing tables of statistics test. Evolution 43:223–225.

Rocha, L. A., A. L. Bass, D. R. Robertson, and B. W. Bowen.
2002. Adult habitat preferences, larval dispersal, and the comparative phylogeography of three Atlantic surgeonfishes (Teleostei: Acanthuridae). Mol. Ecol. 11:243–252.

Rosenberg, N. A., T. Burke, K. Elo, M. W. Feldman, P. J. Freidlin, M. A. Groenen, J. Hillel, A. Mäki-Tanila, M. Tixier-Boichard, A. Vignal, et al.
2001. Empirical evaluation of genetic clustering methods using multilocus genotypes from 20 chicken breeds. Genetics 159:699–713.

Russ, G. R.
2002. Yet another review of marine reserves as reef fishery management tools. *In* Coral reef fishes: dynamics and diversity in a complex ecosystem, p. 421–443. Acad. Press, San Diego, CA.

Russ, G. R., and A. C. Alcala.
2003. Marine reserves: rates and patterns of recovery and decline of predatory fish, 1983–2000. Ecol. Appl. 13:1553–1565.

Selkoe, K. A., S. D. Gaines, J. E. Caselle, and R. R. Warner.
2006. Current shifts and kin aggregation explain genetic patchiness in fish recruits. Ecology 87:3082–3094.

Sheaves, M.
1995. Large lutjanid and serranid fishes in tropical estuaries: are they adults or juveniles? Mar. Ecol. Prog. Ser. 129:31–40.

Tran, T. T. V., L. K. Phan, and J.-D. Durand.
2017. Diversity and distribution of cryptic species within the *Mugil cephalus* species complex in Vietnam. Mitochondrial DNA, A 28:493–501.

Van Oosterhout, C., W. F. Hutchinson, D. P. M. Wills, and P. Shipley.
2004. MICRO-CHECKER: software for identifying and correcting genotyping errors in microsatellite data. Mol. Ecol. Notes 4:535–538.

Verweij, M. C., I. Nagelkerken, I. Hans, S. M. Ruseler, and P. R. D. Mason.
2008. Seagrass nurseries contribute to coral reef fish populations. Limnol. Oceanogr. 53:1540–1547.

Vo, S. T.
2014. Fauna of reef corals in the Vietnam marine areas. *In* Proceedings of the 2nd National Scientific Conference on Marine Biology and Sustainable Development; Hai Phong, 13–14 November 2014, p. 315–322. Publ. House Nat. Sci. Technol., Ha Noi, Vietnam. [In Vietnamese.]

Vo, S. T., and L. V. Nguyen.
2022. Ecology and resources of coral reefs in Vietnam, 223 p. Publ. House Nat. Sci. Technol., Ha Noi, Vietnam. [In Vietnamese.]

Vrdoljak, D., S. Matić-Skoko, M. Peharda, H. Uvanović, K. Markulin, R. Mertz-Kraus, and P. Grønkjær.
2021. Otolith fingerprints and tissue stable isotope information enable allocation of juvenile fishes to different nursery areas. Water. 13(9):1293.

White, C., K. A. Selkoe, J. Watson, D. A. Siegel, D. C. Zacherl, and R. J. Toonen.
2010. Ocean currents help explain population genetic structure. Proc. R. Soc. B. 277:1685–1694.

Woodland, D. J.
1990. Revision of the fish family Siganidae with descriptions of two new species and comments on distribution and biology. Volume 19: Indo-Pacific fishes, 136 p. Bernice Pauahi Bishop Mus., Honolulu, HI.

National Marine Fisheries Service
NOAA

Fishery Bulletin
established in 1881

Spencer F. Baird
First U.S. Commissioner of Fisheries and founder of *Fishery Bulletin*

Exploring the biotic resistance of the invasive green crab (*Carcinus maenas*) by examining the diet of North American river otters (*Lontra canadensis*)

Bobbie M. Buzzell (contact author)[1]
Adrianne M. Akmajian[2]
Alejandro Acevedo-Gutiérrez[1]

Email address for contact author: bobbieb@lummi-nsn.gov

[1] Biology Department
Western Washington University
516 High Street
Bellingham, Washington 98225

[2] Marine Ecology Program
Makah Fisheries Management, Makah Tribe
150 Resort Drive
Neah Bay, Washington 98357

Abstract—We examined the potential of North American river otters (*Lontra canadensis*) to buffer the expansion of the invasion by green crab (*Carcinus maenas*) on the West Coast of the United States, documenting the diet of otters from scat remains on the Wa'atch and Tsoo-Yess Rivers, in Washington State, in 2018 and 2019. We tallied hard remains of prey and calculated frequency of occurrence, and we compared predation of the green crab to monthly values of catch per unit of effort for this crab species. North American river otters did not consume green crab in the Tsoo-Yess River and infrequently consumed green crab in the Wa'atch River (1.66% frequency of occurrence), likely because of the lower abundance of the green crab compared to the abundance of other prey in these rivers. Although our results indicate that North American river otters were not a biotic control of green crab, future studies on the population status of the green crab and North American river otter in both rivers and the long-term predator–prey dynamics could help to better gauge the potential for biotic resistance in populations of the green crab.

Manuscript submitted: 22 September 2022
Manuscript accepted: 25 January 2023
Fish. Bull. 121:30–35 (2023).
Online publication date: 15 February 2023.
doi: 10.7755/FB.121.1-2.3

The views and opinions expressed or implied in this article are those of the author (or authors) and do not necessarily reflect the position of the National Marine Fisheries Service, NOAA.

The green crab (*Carcinus maenas*) is an invasive species known for its effects on eelgrass beds and juvenile bivalves (Cohen et al., 1995; Curtis et al., 2012; Howard et al., 2019). Green crab have been documented in the waters of Makah Bay on the Makah Indian Reservation in northwest Washington through removal trapping efforts, specifically efforts in the estuaries of the Wa'atch and Tsoo-Yess Rivers (Yamada[1]) (Fig. 1). The absence of green crab in nearby Neah Bay might be a result of competition and predation by larger cancrid crab species, such as the red rock crab (*Cancer productus*) and adult Dungeness crab (*Metacarcinus magister*), both of which are more prevalent in Neah Bay than in the channels of the 2 coastal rivers that enter Makah Bay (Jensen et al., 2007). On the western coast of Vancouver Island, in Canada, increasing abundances of Dungeness crab, red rock crab, or graceful crab (*Metacarcinus gracilis*) have resulted in reduced densities of green crab (Howard, 2019). Hence, biological resistance might be a principal factor in mitigating the expansion of the invasion by green crab on the West Coast of the United States.

The North American river otter (*Lontra Canadensis*) often forages in coastal environments in Washington State and is known to predate several marine crab species (Guertin et al., 2010; Buzzell et al., 2014; Russell, 2015). Little attention has been given to North American river otters and their potential to act as a biotic control for invasive species (Feltrop et al., 2016). Latrines (sites of marking

[1] Yamada, S. B., C. Royer, S. Schooler, J. Fisher, A. Randall, C. Buffington, A. Stote, and A. Akmajian. 2022. Status of the European green crab, *Carcinus maenas*, in Oregon and Washington coastal estuaries: report for 2020 and 2021, 18 p. Report prepared for Aquatic Nuissance Species Project, Pacific State Marine Fisheries Commission. [Available from Aquat. Nuissance Species Proj., Pac. State Mar. Fish. Comm., 205 SE Spokane St., Ste. 100, Portland, OR 97202.]

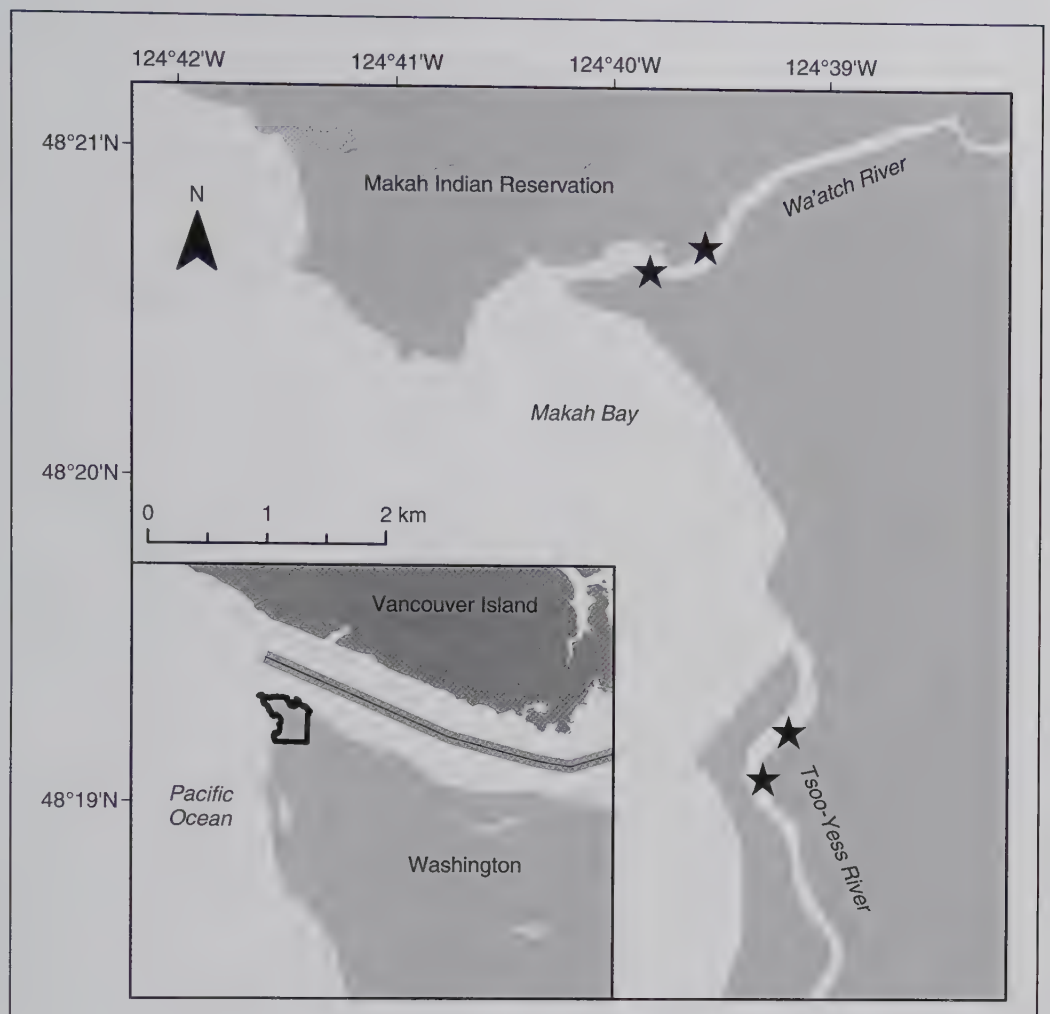

Figure 1

Map of the sites (stars) where samples of scat from North American river otters (*Lontra canadensis*) were collected during the summer of 2018 in the Wa'atch River and during the spring and summer of 2019 in the Wa'atch and Tsoo-Yess Rivers. Collection sites were latrines, areas of marking and defecation by otters, located within the boundaries of the Makah Indian Reservation in Washington State. Scat samples were used to examine the diet of North American river otters and the potential for predation by otters to control populations of the invasive green crab (*Carcinus maenas*). Map layer sources: WA State Parks GIS, ESRI, HERE, Garmin, SafeGraph, METI/NASA, USGS, EPA, USDA, NRCan, Parks Canada, GeoEye, Maxar, FAO, NOAA, Bureau of Land Management, NP.

and defecation) of North American river otters have been observed along the lower Wa'atch and Tsoo-Yess Rivers during removal efforts targeting green crab (A. Akmajian, personal observ.). Because of this apparent overlap of habitats of North American river otters and green crab and the known predation of North American river otters on green crab in other regions (Mason and Macdonald, 1980), we hypothesized that North American river otters are consuming green crab in both rivers and may act as a natural control for green crab in these estuaries.

The first step in assessing the potential of North American river otters to serve as a biotic control of green crab was to determine 1) if North American river otters consume green crab and 2) if such consumption varies relative to time or abundance of green crab. We analyzed the hard remains found in scat from North American river otters to describe their diet and the relative importance of prey items, focusing on consumption of green crab. We investigated differences in consumption of green crab between rivers, seasons (spring and summer of 2019), and years (summers of 2018 and 2019). Finally, to explore possible mitigation of the invasive green crab through their consumption by otters, we examined the consumption of green crabs by North American river otters in relation to the availability of green crab

based on average catch rates during removal trapping efforts in 2019.

Materials and methods

The estuaries of the Wa'atch River and Tsoo-Yess River of the Makah Indian Reservation are located on the northwest coast of the Olympic Peninsula in Washington State (Fig. 1). The 2 rivers extend inland more than 16 km and up to 600 m in elevation, with the 4 river kilometers at the lowest elevations classified as brackish emergent tidal marsh (Heady et al., 2014). Active latrine sites used by North American river otters were identified along both the Wa'atch and Tsoo-Yess Rivers (Fig. 1). On the Wa'atch River, 1 latrine site was located on each of the north and south banks less than 1.5 km upstream from the river mouth. On the lower Tsoo-Yess River, 2 latrine sites were found on the east bank, approximately 0.8 and 1.2 km upstream from the river mouth. The locations of the latrines in relation to the coast, bays, and one another are depicted in Figure 1.

Prey identification was conducted by using analysis of undigested remains (bones and shells) found in scat samples, a widely used method for documenting diet (Stenson et al., 1984; Day et al., 2015). Scat collection was completed every other week alongside green crab trapping efforts on the Wa'atch River in August and September 2018 and for a longer period in 2019 from April through September, but scat samples were collected on the Tsoo-Yess River only during May–September 2019. Samples of scat collected in the summer (July–September) from the latrines along the Wa'atch River were used to compare diet between years, but only samples collected in 2019 were used to compare diet between rivers and seasons (between spring, April–June, and summer). If latrines contained fewer than 15 scat samples, collections were made on additional days in the following week. Protocols for the collection and cleaning of scat were based on methods described for pinnipeds in Lance et al.[2]

Prey items were identified to the lowest possible taxon but for brevity are reported herein only to the family level, apart from green crab and Dungeness crab. Color, claw, texture, and carapace morphology were all factors used to identify remains of crab. Fish remains were identified by using reference bones and otoliths housed at the NOAA Marine Mammal Laboratory in Seattle, Washington. We used frequency of occurrence (Trites and Joy, 2005) to examine and describe spatial and temporal variations in the diet of North American river otters, meaning differences between the Tsoo-Yess and Wa'atch Rivers, between seasons (spring and summer), and between years. Minimum number of individuals was determined for crustaceans by using protocols adapted from Lance et al.[2] With the exception of green crab, frequency of occurrence (FO) is reported for all prey groups with FO of at least 2% and was calculated as follows:

$$FO_i = \frac{\sum_{k=1}^{s} O_{ik}}{s} \times 100,$$

where O_i = 0 if taxon i is absent in fecal sample k and 1 if taxon i is present in fecal sample k; and
s = total number of scat samples.

We used catch per unit of effort (CPUE), defined as the number of green crab caught per trap set per day, as a proxy for abundance because no other information was available on populations of green crab in the study area. Trapping catch data from Makah Fisheries Management, Makah Tribe, were used in calculations of CPUE. Trap descriptions and protocols can be found in the summary report on trapping efforts in 2019 (Akmajian[3]). Average monthly values for CPUE of green crab and Dungeness crab were generated for each river to explore relative densities of prey. Although fish were also caught in traps, CPUE for other species in bycatch were not included in this study.

Results and discussion

In this study, 722 scat samples were collected in both rivers combined (Table 1). Green crab were present in samples from the Wa'atch River (with FO of 1.66%) but absent in samples from the Tsoo-Yess River. Although green crab were scarce in the diet of North American river otters, green crab were observed in scat samples collected from both latrine sites along the Wa'atch River and on 7 separate dates, indicating that otters recognized green crab as prey (Suppl. Figure) (online only). Even so, green crab are elusive and aggressive, possibly making them more difficult to capture and a less-favored prey type overall (Cohen et al., 1995).

Fish composed the most frequently found and numerous group consumed by North American river otters in both rivers, a result that is consistent with those from other otter diet studies in coastal areas (Table 1) (Buzzell et al., 2014; Russell, 2015). Among fish taxa, sculpins (Cottidae) made up the most frequently consumed prey group overall (65.37% FO), followed by gunnels (Pholidae) (57.20% FO) and righteye flounders (Pleuronectidae) (49.45% FO). Cancrid crabs (mostly Dungeness crab) composed the most consumed crustacean prey group (28.54% FO), but FO of cancrid crabs has varied in other studies (Table 1) (Guertin et al., 2010; Russell, 2015).

The relative importance of prey groups in the diet of North American river otters was similar between 2018 and 2019; however, most prey taxa and groups, including the green crab, had increased occurrence in scat samples

[2] Lance, M. M., A. J. Orr, S. D. Riemer, M. J. Weise, and J. L. Laake. 2001. Pinniped food habits and prey identification techniques protocol. Alsk. Fish. Sci. Cent. Proc. Rep. 2001-04, 29 p. [Available from website, accessed November 2022.]

[3] Akmajian, A. 2020. European green crab trapping summary for the 2019 season, 30 p. [Available from Makah Fish. Manag., Makah Tribe, P.O. Box 115, Neah Bay, WA 98357.]

Table 1

Frequency of occurrence (FO) for prey items found in samples of scat from North American river otters (*Lontra canadensis*) collected during the summer of 2018 in the Wa'atch River and during the spring and summer of 2019 in the Wa'atch and Tsoo-Yess Rivers. Frequency of occurrence is reported for all prey groups that had FO >2%. The number of scat samples (*n*) is given for each collection period.

		Wa'atch River			Tsoo-Yess River	
		2018	2019		2019	
Prey	Overall FO (%) *n*=722	Summer FO (%) *n*=139	Spring FO (%) *n*=135	Summer FO (%) *n*=179	Spring FO (%) *n*=125	Summer FO (%) *n*=144
Teleostei						
Cottidae (sculpins)	65.37	66.91	73.33	79.89	44.00	56.94
Pholidae (gunnels)	57.20	48.20	62.96	65.92	44.00	61.11
Pleuronectidae (Righteye flounders)	49.45	42.45	45.93	66.48	31.20	54.17
Embiotocidae (surfperches)	24.79	21.58	25.19	44.13	8.80	17.36
Gasterosteidae (sticklebacks)	22.02	23.74	27.41	31.84	13.60	10.42
Syngnathidae (pipefishes and seahorses)	17.04	3.60	45.93	10.61	16.00	11.81
Salmonidae (salmons and trouts)	12.05	0.72	20.00	6.15	25.60	11.11
Stichaeidae (pricklebacks)	5.96	14.39	2.96	7.26	0.80	3.47
Teleostei (unidentified fish)	4.29	7.19	0.74	7.82	3.20	1.39
Liparidae (snailfishes)	3.46	4.32	–	8.94	2.40	–
Scorpaenidae (rockfishes)	2.91	0.72	13.33	1.12	–	–
Decapoda						
Cancridae (rock crabs)	28.53	36.69	37.78	40.78	7.20	15.28
Astacidae (crayfishes)	11.50	2.16	5.19	5.03	24.00	23.61
Varunidae (shore crabs)	3.05	1.44	1.48	8.94	1.60	–
Carcinus maenas (Portunidae)	1.66	0.72	5.19	2.23	–	–
Miscellaneous						
Ranidae (true frogs)	2.91	1.44	2.96	2.79	3.20	4.17

collected in 2019 (Table 1). With the exception of sticklebacks (Gasterosteidae) consumed by otters on the Tsoo-Yess River, the other 5 most frequently occurring prey groups increased in FO to some degree from spring to summer on both rivers. Seasonal change in the FO of green crab in the scat samples collected on the Wa'atch River was not apparent because of low consumption, where only 7 and 4 individuals occurred in scat samples collected in spring and summer, respectively (Suppl. Figure) (online only).

Dungeness crab had greater CPUE overall in trapping efforts in both rivers (1.40 individuals·set^{-1}·d^{-1}) than green crab (0.63 individuals·set^{-1}·d^{-1}). Such a difference coincides with the consumption of crabs by North American river otters, where both overall FO and the FO of Dungeness crab were higher than the FO of green crab (Table 1, Suppl. Figure) (online only). The CPUE of green crab was higher on the Tsoo-Yess River (0.84 individuals·set^{-1}·d^{-1}) than on the Wa'atch River (0.39 individuals·set^{-1}·d^{-1}), but this difference was marginal compared to the greater overall CPUE of Dungeness crab on both rivers during most of the trapping season. Although we used CPUE only as a proxy of prey abundance and availability, the difference between crab species in both CPUE and FO in the diet of North American river otters supports the hypothesis posited by others that this otter species consumes prey species in proportion to their relative abundance and availability (Ryder, 1955; Day et al., 2015). Therefore, low consumption of green crab was likely a result of the overall lower abundance of green crab in both rivers compared with the abundance of other prey items.

Several studies have documented the limitations of diet studies that use FO and minimum number of individuals (Crimmins et al., 2009; Tsukada et al., 2020). Scat collection is subjective and can lead to pseudoreplication, where there is a strong likelihood that multiple scat samples from a single collection are from the same individual, leading to an overestimate of frequently consumed species and an underestimate of infrequently consumed species (Tsukada et al., 2020). Estimating species abundance by using CPUE has limitations because of the high variability in trapping efficacy; in future studies, an aim should be to use methods, such as mark-recapture techniques, that are more accurate (Munch-Petersen et al., 1982, Bergshoeff et al., 2018; Bernier et al., 2020). Although it is important to consider these biases, the objective of this study was to detect green crab in the diet of North American river otters and to describe important prey types, which was possible because of the timeframe of our study.

On the basis of our results, it is unlikely that North American river otters currently serve as a natural control of green crab populations that are at low densities. However, in recent years, population densities of green crab have continued to increase in Makah Bay and elsewhere along the coastline of Washington. Predation of green crab by North American river otters will likely increase as green crab become more abundant and available, but gauging potential effects will require estimating population densities for both North American river otters and green crab. As such, future studies should focus on understanding predator–prey interactions involving green crab and other likely predators, such as adult Dungeness crab, that might cumulatively buffer a higher density of green crab and further mitigate effects of green crab invasions on sensitive coastal habitats along the West Coast.

Resumen

Examinamos el potencial de las nutrias de río norteamericanas (*Lontra canadensis*) para amortiguar la expansión de la invasión del cangrejo verde (*Carcinus maenas*) en la costa oeste de Estados Unidos, documentando la dieta de las nutrias a partir de restos de excrementos en los ríos Wa'atch y Tsoo-Yess, en el estado de Washington, en 2018 y 2019. Contamos los restos duros de presas, calculamos la frecuencia porcentual de ocurrencia, y comparamos la depredación del cangrejo verde con los valores mensuales de captura por unidad de esfuerzo para esta especie de cangrejo. Las nutrias de río norteamericanas no consumieron cangrejos verdes en el río Tsoo-Yess y consumieron con poca frecuencia cangrejos verdes en el río Wa'atch (1.66% de frecuencia de ocurrencia), probablemente debido a la menor abundancia del cangrejo verde en comparación con la abundancia de otras presas en dichos ríos. No obstante que nuestros resultados indican que las nutrias de río norteamericanas no constituyen un control biologico del cangrejo verde, futuros estudios sobre el estado de las poblaciones del cangrejo verde y nutria de río norteamericana en ambos ríos y la dinámica depredador-presa a largo plazo podrían ayudar a calibrar mejor el potencial de resistencia biótica de las poblaciones del cangrejo verde.

Acknowledgments

We would like to thank the Makah Tribe for allowing us to conduct this study on their land. W. Walker conducted all identifications, otolith counts, and measurements of fish prey. Makah Tribe technicians and several undergraduates at the Western Washington University (WWU) helped collect scat samples and sort hard remains. B. Miner provided writing and project adivce. Funding was provided by the North Pacific Coast Marine Resource Committee of Jefferson County, Conservation Research and Education Opportunities International, and the WWU Office of Research and Sponsored Programs.

Literature cited

Bergshoeff, J. A., C. H. McKenzie, K. Best, N. Zargarpour, and B. Favaro.
2018. Using underwater video to evaluate the performance of the Fukui trap as a mitigation tool for the invasive European green crab (*Carcinus maenas*) in Newfoundland, Canada. PeerJ 6:e4223.

Bernier, R. Y., L. A. Poirier, A. Ramsay, and A. LeBlanc.
2020. European green crab (*Carcinus maenas*) population monitoring surveys (2000–2016) and efficacy of traps used for their capture in the southern Gulf of St. Lawrence. Can. Tech. Rep. Fish. Aquat. Sci. 3388, 33 p.

Buzzell, B., M. M. Lance, and A. Acevedo-Gutiérrez.
2014. Spatial and temporal variation in river otter (*Lontra canadensis*) diet and predation on rockfish (Genus *Sebastes*) in the San Juan Islands, Washington. Aquat. Mamm. 40:150–161.

Cohen, A. N., J. T. Carlton, and M. C. Fountain.
1995. Introduction, dispersal and potential impacts of the green crab *Carcinus maeanas* in San Francisco Bay, California. Mar. Biol. 122:225–237.

Crimmins, S. M., N. M. Roberts, and D. A. Hamilton.
2009. Effects of prey size on scat analysis to determine river otter *Lontra canadensis* diet. Wildl. Biol. 15:449–453.

Curtis, D. L., L. Sauchyn, L. Keddy, T. W. Therriault, and C. M. Pearce.
2012. Prey preferences and relative predation rates of adult European green crabs (*Carcinus maenas*) feeding on various bivalve species in British Columbia, Canada. Can. Tech. Rep. Fish. Aquat. Sci. 3014, 14 p.

Day, C. C., M. D. Westover, and B. R. McMillan.
2015. Seasonal diet of the northern river otter (*Lontra canadensis*): what drives prey selection? Can. J. Zool. 93:197–205.

Feltrop, P. D., C. K. Nielsen, and E. M. Schauber.
2016. Asian carp in the diet of river otters in Illinois. Am. Midl. Nat. 176:298–305.

Guertin, D. A., A. S. Harestad, and J. E. Elliott.
2010. Summer feeding habits of river otters inhabiting a contaminated coastal marine environment. Northwest Sci. 84:1–8.

Heady, W. N., K. O'Connor, J, Kassakian, K. Doiron, C. Endris, D. Hudgens, R. P. Clark, J. Carter, and M. G. Gleason.
2014. An inventory and classification of U.S. West Coast estuaries, 81 p. Nat. Conserv., Arlington, VA. [Available from website.]

Howard, B. R.
2019. The context-dependent spread and impacts of invasive marine crabs. Ph.D. thesis, 109 p. Simon Fraser Univ., Burnaby, British Columbia, Canada. [Available from website.]

Howard, B. R., F. T. Francis, I. M. Côté, and T. W. Therriault.
2019. Habitat alteration by invasive European green crab (*Carcinus maenas*) causes eelgrass loss in British Columbia, Canada. Biol. Invasions 21:3607–3618.

Jensen, G. C., P. S. McDonald, and D. A. Armstrong.
2007. Biotic resistance to green crab, *Carcinus maenas*, in California bays. Mar. Biol. 151:2231–2243.

Mason, C. F., and S. M. Macdonald.
1980. The winter diet of otters (*Lutra lutra*) on a Scottish sea loch. J. Zool. 192:558–561.

Munch-Petersen, S., P. Sparre, and E. Hoffmann.
1982. Abundance of the shore crab, *Carcinus maenas* (L.), estimated from mark-recapture experiments. Dana 2:97–121.

Russell, A.
2015. Dietary patterns of *Lontra canadensis* in the Lower Snohomish River Estuary, Washington. Northwest Sci. 89:182–187.
Ryder, R. A.
1955. Fish predation by the otter in Michigan. J. Wildl. Manag. 19:497–498.
Stenson, G. B., G. A. Badgero, and H. D. Fisher.
1984. Food habits of the river otter *Lutra canadensis* in the marine environment of British Columbia. Can. J. Zool. 62:88–91.
Trites, A. W., and R. Joy.
2005. Dietary analysis from fecal samples: how many scats are enough? J. Mammal. 86:704–712.
Tsukada, H., K. Abe, S. Takatsuki, and M. Minami.
2020. How many feces should be sampled from latrines? Spatial sampling biases affecting the dietary analysis of island raccoon dogs. Wildl. Biol. 2020(2):wlb.00656.

National Marine
Fisheries Service
NOAA

Fishery Bulletin
established in 1881

Spencer F. Baird
First U.S. Commissioner
of Fisheries and founder
of *Fishery Bulletin*

Ovarian masculinization and reproductive impairment in 3 species of groundfish in and around the hypoxic zone in the Gulf of Mexico

Michael V. Cyrana (contact author)[1,2]
Alexander J. Ledet[2,3]
Henry L. Bart Jr.[2]

Email address for contact author: michael.cyrana@jhuapl.edu

[1] Applied Physics Laboratory
Johns Hopkins University
11100 Johns Hopkins Road
Laurel, Maryland 20723-6099

[2] Ecology and Evolutionary Biology Department
Tulane University
201 Lindy Claiborne Boggs Center
6823 St. Charles Avenue
New Orleans, Louisiana 70118-5698

[3] Albert Einstein College of Medicine
1300 Morris Park Avenue
Bronx, New York 10461

Abstract—The results of this study provide additional evidence of ovarian masculinization in the Atlantic croaker (*Micropogonias undulatus*) in and around the hypoxic zone in the Gulf of Mexico and the first evidence of ovarian masculinization in the spot (*Leiostomus xanthurus*) and bigeye searobin (*Prionotus longispinosus*). In some specimens of Atlantic croaker and spot, we observed this phenomenon to a degree that has not been reported in either species. We also found evidence of smaller gonads in spot from hypoxic sites compared with the gonads in spot from sites with normal oxygen concentrations. These findings indicate that ovarian masculinization and reproductive impairment associated with hypoxia exposure affect a wider range of species than was previously known, and they highlight the importance of continued research on this topic.

Manuscript submitted 20 May 2022.
Manuscript accepted 25 January 2023.
Fish. Bull. 121:36–49 (2023).
Online publication date: 16 February 2023.
doi: 10.7755/FB.121.1-2.4

The views and opinions expressed or implied in this article are those of the author (or authors) and do not necessarily reflect the position of the National Marine Fisheries Service, NOAA.

In the last century, hypoxia has emerged as a significant threat to coastal ecosystems. *Hypoxia*, or hypoxic conditions, refers to low levels of dissolved oxygen in bodies of water. Coastal hypoxia, which was first observed in the 1930s (Diaz and Rosenberg, 2008), has increased 3-fold during the last 30 years (Diaz and Rosenberg, 2008; Vaquer-Sunyer and Duarte, 2008). The range of dissolved oxygen values used to define an area as hypoxic is variable, and the term *hypoxia* conventionally indicates dissolved oxygen values below 2.0 mg/L (Rabalais et al., 2002; Vaquer-Sunyer and Duarte, 2008). Although hypoxic events are known to occur naturally throughout the world (Helly and Levin, 2004), the global increase in coastal hypoxia can mostly be attributed to the increased use of synthetic nitrogen fertilizers since their creation in the 1940s (Diaz and Rosenberg, 2008; Galloway et al., 2008). Increased nitrogen runoff from fertilizers can result in large algal blooms in coastal waters. When algal cells die, their decomposition consumes dissolved oxygen in the water column. This process can result in hypoxia if the water column is stratified, given that subsurface waters are unable to mix with oxygen-rich surface waters because of differences in water density.

Hypoxia has wide-ranging ecological and physiological effects on marine life. Exposure to hypoxic conditions alters the behavior (Eriksson and Baden, 1997) and interspecific interactions of marine organisms (Sandberg, 1997). Hypoxic conditions have also been associated with changes in community composition (Dauer, 1993; Pihl, 1994) and biomass (Rosenberg and Loo, 1988). Community recovery following episodes of hypoxia is highly variable and dependent upon a variety of environmental and biotic factors (Wu, 2002), including community complexity and the severity and duration of hypoxic conditions (Boesch and Rosenberg, 1981). At the organismal level, endocrine disruption (Wu et al., 2003) and reproductive impairment (Zhou, 2001) are 2 of the most well-documented physiological effects of hypoxia exposure in fish.

Fish exposed to hypoxic conditions tend to have lower values for the gonadosomatic index (GSI), an indicator of reproductive condition, than fish exposed to normal oxygen concentrations, as has been observed in the Gulf killifish (*Fundulus grandis*) (Cheek et al., 2009), common carp (*Cyprinus carpio*) (Zhou, 2001), and Atlantic croaker (*Micropogonias undulatus*) (Wu et al., 2003; Thomas et al., 2007; Thomas and Rahman, 2012). Both episodic (diel) and chronic hypoxia have been shown to reduce the reproductive capacity of estuarine fish species (Landry et al., 2007; Cheek et al., 2009). Chronic exposure to hypoxic conditions has been further linked to masculinization in female fish (Landry et al., 2007; Cheek et al., 2009; Thomas and Rahman, 2012) and to reduced sperm production and viability in male Atlantic croaker (Thomas et al., 2015). Masculinization of female Atlantic croaker resulting from chronic exposure to hypoxia has been documented in both field and laboratory studies (Thomas et al., 2007; Thomas and Rahman, 2012).

In this study, we assessed whether the well-established reproductive effects of seasonal hypoxia on Atlantic croaker in the Gulf of Mexico (GOM) (Thomas and Rahman, 2012) extend to other cohabiting species of fish, specifically the spot (*Leiostomus xanthurus*) and bigeye searobin (*Prionotus longispinosus*). Both the Atlantic croaker and spot are members of the family Sciaenidae (order Perciformes). The bigeye searobin belongs to the family Triglidae (order Scorpaeniformes). Finding evidence of reproductive abnormalities at the family and order levels would demonstrate that the effects of seasonal hypoxia in the GOM are more widespread taxonomically, with broader implications for fisheries management, than previously thought.

Materials and methods

Sample collection and study area

Fish were collected aboard the NOAA Ship *Oregon II* during legs I and II (June–August) of the Southeast Area Monitoring and Assessment Program (SEAMAP) summer groundfish surveys in 2016, 2017, and 2019 (Fig. 1). Sampling sites were scattered throughout the area in which hypoxia seasonally develops in the GOM, ranging from the coast of Texas to waters off Louisiana. Samples were collected as described in the SEAMAP sampling protocol (GSMFC[1]) at survey sites with depths ≤30 m because hypoxia in the GOM occurs less frequently at depths below 30 m. Whole specimens caught during trawl surveys were fixed in a 10% formalin solution and transferred to ethanol for storage. Dissolved oxygen values were recorded immediately prior to trawling, according to SEAMAP protocol for collecting data on water conditions, by using a shipboard array equipped with dissolved oxygen, conductivity, temperature, and depth sensors and water bottles for measuring other water properties (Table 1). A site was defined as hypoxic if dissolved oxygen was 2.0 mg/L or lower, a level that is consistent with the recent literature on hypoxia (Vaquer-Sunyer and Duarte, 2008).

Female specimens of Atlantic croaker, spot, and bigeye searobin were reproductively immature at the time of sampling, as they did not contain any oocytes past the previtellogenic stage (Anderson et al., 2018). Male specimens of Atlantic croaker and spot were also reproductively immature, as no spermatids or spermatozoa were present. Some male bigeye searobin were reproductively mature. The natural history of Atlantic croaker and spot and histological examination of gonads of bigeye searobin strongly indicate that specimens would have reproductively matured within the year, making any evidence of reproductive abnormalities indicative of reproductive impairment. It is important to note that, although the majority of specimens were reproductively immature, the sampled fish were not juveniles and the term *immature* is meant to describe the state of the gametes within the gonads.

We obtained reference samples of Atlantic croaker and spot from the Royal D. Suttkus Fish Collection at the Tulane University Biodiversity Research Institute (TUBRI). Reference samples consisted of whole, formalin-fixed specimens from which gonads were dissected. We selected reference samples collected during the summer (June–September) at either the Chandeleur Islands or the Rigolets, both located in Louisiana. We selected samples collected between 1955 and 1969 because we wanted specimens from a time before the 1980s, when eutrophication dramatically increased in the western GOM, as evidenced by increased carbon deposition (Rabalais et al., 2007). The Chandeleur Islands and the Rigolets are not known to be hypoxic during the summer; therefore, both the location and time of the collection of our references samples makes it unlikely that reference fish were exposed to hypoxic conditions prior to sampling.

Sample processing

Subsamples were selected from male and female Atlantic croaker, spot, and bigeye searobin collected from both hypoxic sites and sites with normal oxygen levels. These selected specimens were wet weighed (to the nearest 0.001 g) and measured for total length (to the nearest millimeter), and then they had their gonads removed and wet weighed. The gonads were mounted, sectioned, and stained with hematoxylin and eosin. Only a subsample of these gonads were histologically processed and examined.

Gonadosomatic index

The GSI was calculated by using this formula:

$$\frac{Weight_{\text{gonads}}}{\left(Weight_{\text{fish}} - Weight_{\text{gonads}}\right)} \times 100,$$

where $Weight_{\text{gonads}}$ = the wet weight of both gonads post fixation; and

$Weight_{\text{fish}}$ = the wet weight of the whole fish post fixation.

[1] GSMFC (Gulf States Marine Fisheries Commission). 2019. SEAMAP operations manual for trawl and plankton surveys, 63 p. Gulf States Mar. Fish. Comm., Ocean Springs, MS. [Available from website.]

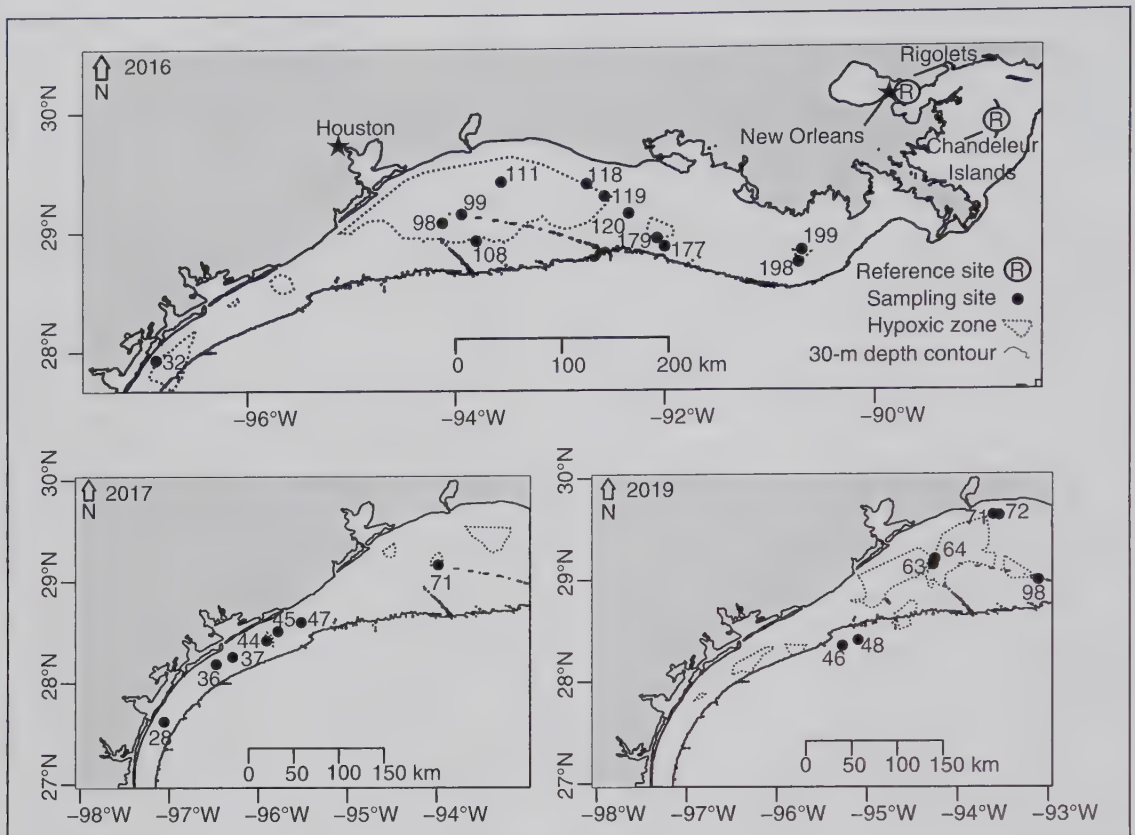

Figure 1

A map of the sites in the northern Gulf of Mexico where Atlantic croaker (*Micropogonias undulatus*), spot (*Leiostomus xanthurus*), and bigeye searobin (*Prionotus longispinosus*) were sampled in 2016, 2017, and 2019. All sampling for this study was conducted during Southeast Area Monitoring and Assessment Program (SEAMAP) summer groundfish surveys aboard the NOAA Ship *Oregon II* at sites with depths ≤30 m scattered throughout the hypoxic zone that develops seasonally in the Gulf of Mexico. Reference samples, collected during summer between 1955 and 1969 at sites known not to have hypoxic conditions, were obtained from the Royal D. Suttkus Fish Collection of the Tulane University Biodiversity Research Institute. Numerals next to the symbols for sites indicate the station numbers assigned by SEAMAP. Note that the shoreward boundaries of the polygons for hypoxic areas reflect the boundaries of the hydrographic survey used to generate the polygons and do not necessarily represent the extent of the hypoxic zone in a given year.

In order to compare the GSI of fish of varying sizes, a residual index of the GSI values was computed. The residual index has been shown to be an effective way to reduce the influence of body size in analyses of organismal condition (Jakob et al., 1996) and has been proven to be effective in the analysis of fish morphometric data (Reist, 1985; Jakob et al., 1996). The residual index is the difference between the observed GSI value and the predicted GSI value, which is determined by using a linear trendline generated with pooled data (for specimens from both hypoxic and normal oxygen concentrations). Positive values for the residual index indicate that the observed GSI is greater than the predicted GSI, whereas negative values indicate that the observed GSI is less than the predicted GSI.

Overall body condition

Overall body condition was calculated as wet weight divided by total length. These condition index values for specimens were compared between hypoxic and normal sites by using the residual index (polynomial trendline) of the length–weight relationship based on data pooled for males and females, under the assumption that there is no sexual dimorphism in any of the species included in this study. In order to compare both sexes simultaneously, the weight used for the overall condition analysis was the wet weight of each fish minus the weight of its gonads.

Statistical treatment

Mean residual GSI and condition index values were compared between fish from hypoxic sites and those from sites with normal oxygen levels by using sites as replicates. The residual indices of both overall body condition and GSI for both male (hypoxic: n=31; normal: n=28) and female (hypoxic: n=36; normal: n=31) spot and female Atlantic croaker (hypoxic: n=37; normal: n=44) were normally distributed (Shapiro–Wilk test: P>0.05) (Shapiro

Table 1

Recorded dissolved oxygen (DO) values and depths at the sites sampled for this study in the northern Gulf of Mexico during 2016, 2017, and 2019. The site numbers correspond to the numbers assigned to "Pascagoula" stations by the Southeast Area Monitoring and Assessment Program.

Site no.	Year	DO (mg/L)	Depth (m)
15	2016	5.7	22.4
32	2016	1.1	15.4
98	2016	1.4	19.6
99	2016	1.1	18.7
108	2016	2.3	22.8
111	2016	0.0	15.0
118	2016	0.9	14.4
119	2016	1.0	15.8
120	2016	5.1	13.9
177	2016	4.1	26.4
179	2016	2.2	23.8
198	2016	2.0	18.1
199	2016	1.8	18.8
28	2017	5.8	23.6
29	2017	6.3	19.4
36	2017	5.4	18.0
37	2017	2.5	21.6
44	2017	1.4	20.1
45	2017	3.4	18.8
47	2017	3.2	19.3
48	2017	5.9	15.6
71	2017	1.4	17.8
46	2019	3.0	33.0
63	2019	0.5	14.0
64	2019	0.5	13.0
72	2019	1.5	10.0
98	2019	1.5	26.0

and Wilk, 1965) and had statistically indistinguishable variances (Bartlett's test: $P>0.05$) (Bartlett, 1937). Therefore, we used a 2-way analysis of variance (ANOVA), and a significance level (α) of 0.05, to compare the residual indices of these samples. The residual GSI for male Atlantic croaker was not normally distributed (Shapiro–Wilk test: $P<0.05$); therefore, we used a Kruskal–Wallis test, with a α of 0.05, for these data (hypoxic: $n=48$; normal: $n=26$) (Kruskal and Wallis, 1952).

Results

Ovarian masculinization

Evidence of masculinization was found in 6 of the 17 ovaries from Atlantic croaker that were examined in this study, with masculinized ovaries observed only for specimens collected at hypoxic sites. In the masculinized ovaries from Atlantic croaker, testicular tissue was found primarily in connective tissue along the ovary periphery (Fig. 2). The testicular tissue consisted of clusters of spermatids within connective tissue, similar to the tissue conditions used in determinations of masculinization made in previous studies (Thomas and Rahman, 2012) (Fig. 2). The spermatogenic tissue observed within ovarian tissue resembled spermatogenic cysts of lobular type testes. One specimen, the gonads of which externally resembled testes, had gonadal tissue that is best described as transitional (i.e., an ovary that was transitioning to a testis). The gonads of this specimen organizationally resembled testes; however, degenerated oocytes were present and surrounded duct-like structures. Spermatogenic tissue was not present. The ovaries of reference specimens contained no evidence of spermatogenic tissue or ovarian anomalies.

The masculinized ovaries from spot (Fig. 3) had a masculinization profile similar to that of the masculinized ovaries from Atlantic croaker. Masculinization in peripheral connective tissue was found in 3 of the 7 ovaries from spot that were examined in this study, with one of the ovaries coming from a specimen collected at a site with normal oxygen concentrations.

Two of the spot we examined contained ovaries that are best described as in a transition from female to male tissue (Fig. 3). These transitional gonads had structures more like a typical testis, with ducts surrounded by connective tissue that was interspersed with spermatogenic tissue. One of these transitional gonads contained numerous atretic follicles and a large lumen filled with what looked like ovum remnants and large melano-macrophage centers (Agius and Roberts, 2003). The other transitional gonad contained atretic follicles and a testicular-like structure but lacked ovum remnants and melano-macrophage centers. The ovaries of the reference specimens used in this study appeared more organized compared with the gonads of specimens collected in 2016, and no evidence of spermatogenic tissue was found within them.

Masculinization in bigeye searobin manifested as spermatogenic cells in various stages of development interspersed among oocytes and peripheral tissue (Fig. 4). Evidence of this phenomenon was found in 1 of the 7 ovaries from bigeye searobin that were examined in this study.

Gonadosomatic index and body condition

The mean residual index of overall body condition based on pooled data for female and male Atlantic croaker was significantly higher for fish from hypoxic sites than for fish from sites with normal oxygen concentrations (Kruskal–Wallis test: $P<0.05$) (Figs. 5 and 6.). The residual GSI of both male and female Atlantic croaker from hypoxic sites did not significantly differ from that of males and females from sites with normal levels of oxygen (males: $P=0.65$, df=7, $f=0.21$; females: $P=0.77$, df=11, $f=0.08$) (Figs. 5 and 6).

The mean residual index of overall body condition for female and male spot combined did not significantly differ between specimens from hypoxic sites and specimens from normal sites ($P=0.12$, df=14, $f=0.60$) (Figs. 7 and 8). The mean residual GSI of female spot from hypoxic sites

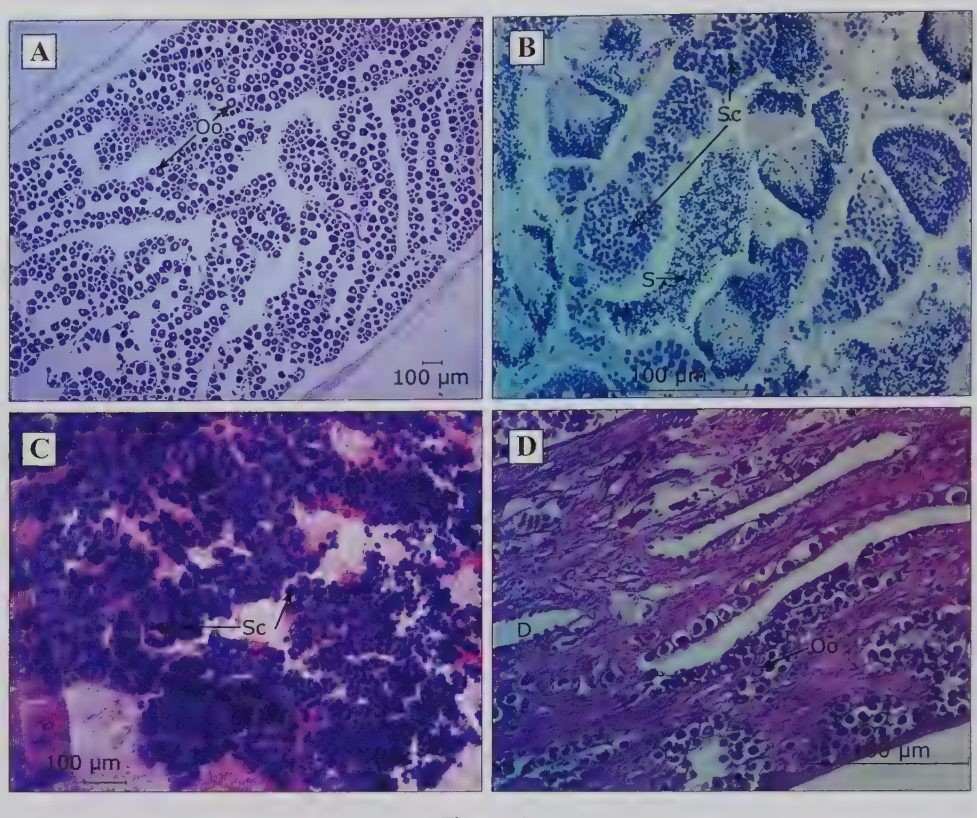

Figure 2

Microphotographs of the gonads of Atlantic croaker (*Micropogonias undulatus*) collected from the northern Gulf of Mexico, showing the effects of hypoxia on gonadal development. (**A**) This ovary of a reference specimen, acquired from the Tulane University Biodiversity Research Institute and sampled between 1955 and 1959, has previtellogenic oocytes (Oo) and no signs of spermatogenic tissue or oocyte degradation. (**B**) In this mature testis of a male, from a control treatment of a laboratory study conducted in 2020 (senior author, in prep.), spermatocytes (Sc) in various stages of development are visible, as are fully developed spermatids (S). No cells in this mature testis resemble oocytes. (**C**) In this section of an ovary, from a specimen collected in 2016 at a site in a hypoxic area (site 99, which had a dissolved oxygen [DO] level of 1.1 mg/L), both spermatocytes are in various stages of development. (**D**) This transitional gonad, from a specimen externally classified as male and sampled in a hypoxic zone (in an area with a DO level of 1.4 mg/L) in 2016, has clear ducts (D) surrounded by degrading or degenerating oocytes. The structure resembles a testis, with reproductive cells surrounding duct-like structures. Degenerating oocytes in this gonad are larger than and visually distinct from spermatocytes in the mature testes shown in panel C.

was significantly lower (ANOVA: $P<0.05$) than that of females from sites with normal oxygen concentrations (Figs. 7 and 8), and male spot from hypoxic sites also had significantly lower GSI values than males from normal sites (ANOVA: $P<0.05$).

Discussion

Scope and possible causes of ovarian masculinization

Prior to this study, the only species from the GOM for which evidence of ovarian masculinization had been reported was the Atlantic croaker (Thomas and Rahman, 2012). This study is the first to report this phenomenon in 2 additional GOM species, the spot and bigeye searobin, with 2 of 7 subsampled ovaries from spot (Fig. 3) and 1 of 7 subsampled ovaries from bigeye searobin (Fig. 4) containing male reproductive cells. Additionally, such evidence was found in 6 of 17 ovaries of Atlantic croaker examined in this study (Fig. 2).

The cause of the ovarian masculinization found in this study cannot be determined. However, hypoxia is a likely possibility. It is well known that estrogen, the synthesis of which is regulated by the enzyme aromatase, is a primary factor in the sex determination of fish. Guiguen et al. (2010) discussed results of a number of experiments that indicate that suppression of estrogen synthesis (aromatase inhibition) in fish can result in the formation of testicular tissue. Aromatase inhibitors have been shown to induce

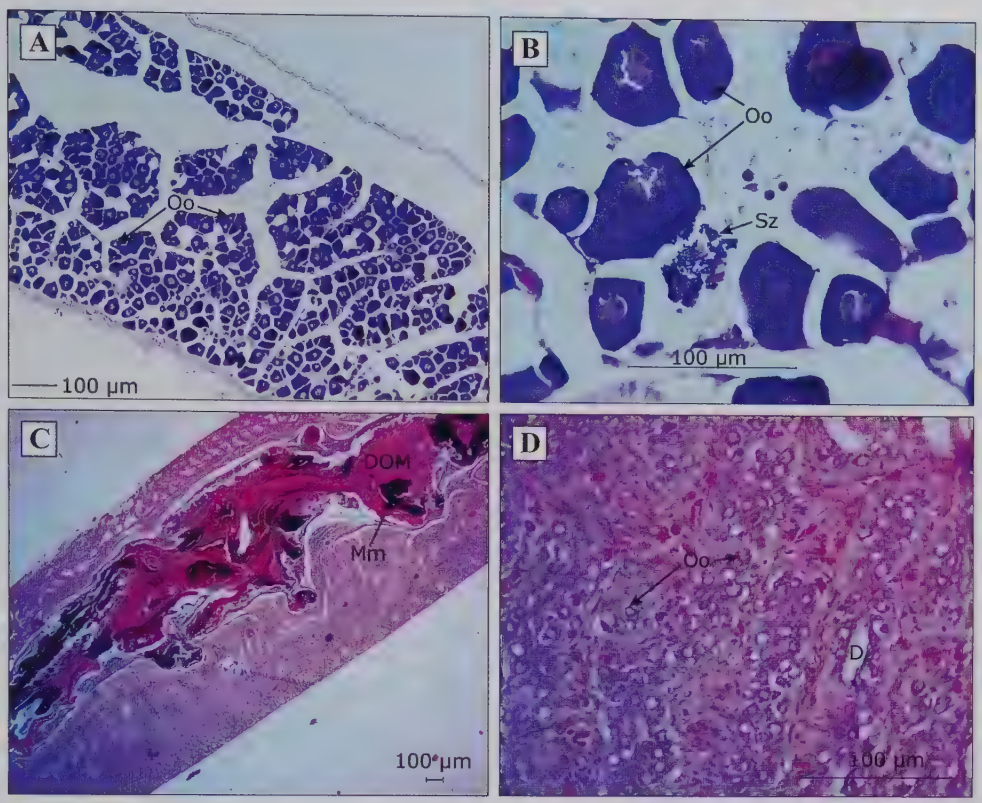

Figure 3

Microphotographs of the gonads of spot (*Leiostomus xanthurus*) collected from the northern Gulf of Mexico, showing the effects of hypoxia on gonadal development. (**A**) This ovary of a reference specimen, acquired from the Tulane University Biodiversity Research Institute and sampled in 1969, has previtellogenic oocytes (Oo) and no evidence of spermatogenic tissue or oocyte degradation. (**B**) In this ovary of a specimen collected in 2016, at a site adjacent to an area of hypoxia (site 177, which had a level of dissolved oxygen [DO] of 4.1 mg/L), oocytes are visible, as are clustered spermatozoa (Sz). (**C**) This transitional gonad, from a specimen sampled in 2016 at a site in a hypoxic zone (site 198, which had a DO level of 2.0 mg/L), has testicular features, like ducts (D) and a preponderance of connective tissue, and evidence of previous oocyte degradation, such as degraded oocyte material (DOM) and melano-macrophage aggregations (Mm). (**D**) In the same specimen featured in panel C, shown here at a higher magnification, degraded or degenerating oocytes are embedded in the connective tissue. Testicular-like ducts are also visible.

masculinization in several species of fish, including the naturally hermaphroditic honeycomb grouper (*Epinephelus merra*) (Bhandari et al., 2004), red grouper (*E. morio*) (Guiguen et al., 2010), and European seabass (*Dicentrarchus labrax*) (Navarro-Martín et al., 2009) and in the naturally gonochoristic common carp (Ogawa et al., 2008). Long-term aromatase suppression has even been reported to convert functional ovaries into functional testes in tilapia (Sun et al., 2014). Hypoxic conditions have been shown to function as an aromatase inhibitor in Atlantic croaker, decreasing mRNA expression and aromatase activity in fish exposed to hypoxia both in the wild and in the lab (Thomas and Rahman, 2012).

It is likely that the ovarian masculinization observed in fish from hypoxic sites in our study could be a consequence of hypoxia-induced inhibition of aromatase and the concomitant suppression of estrogen synthesis. The well-documented connection between aromatase suppression and the development of intersex gonads in fish, coupled with the broad geographic extent of hypoxia encountered during the sampling for this study, strongly indicates that the ovarian masculinization observed in this study was hypoxia related.

The presence of intersex specimens from sites with normal oxygen levels is a novel discovery; however, the relatively low sample size prevents us from offering a definitive interpretation. Specifically, the normal sites that yielded intersex specimens were immediately adjacent to areas of hypoxia (Fig. 1) and differed by only 0.2 mg/L in the level of dissolved oxygen, with the concentration at these normal sites falling right on the line between our definition of hypoxic and normal conditions. Although this closeness in

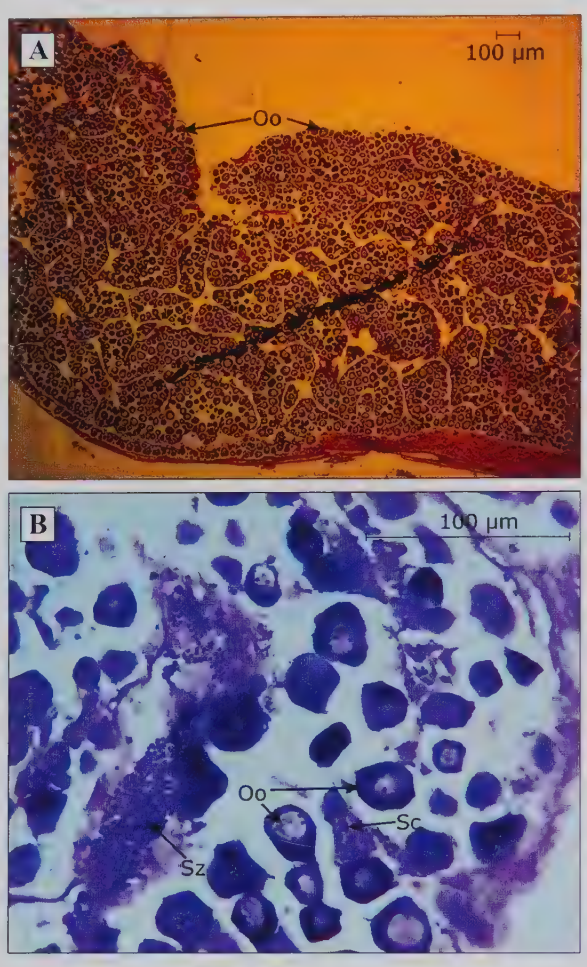

Figure 4

Microphotographs of ovaries of bigeye searobin (*Prionotus longispinosus*) collected in the northern Gulf of Mexico in 2016. (**A**) This ovary has no signs of masculinization or oocyte degradation: previtellogenic oocytes (Oo) are visible throughout the ovary. (**B**) In this ovary, there is evidence of masculinization: both oocytes and spermatocytes (Sc) are in various stages of development, and spermatozoa (Sz) are present.

location and dissolved oxygen could indicate either that the intersex specimens had passed through the hypoxic area and were subsequently masculinized or that the dissolved oxygen concentration at the normal site was low enough to induce the development of intersex gonads, there are not enough data to identify a causal relationship. Sampling numbers were not sufficient to explain the source of ovarian masculinization in fish from normal sites; therefore, further sampling efforts and laboratory exposure experiments are needed to fully explain this phenomenon. Similarly, it is unclear what effect the masculinization observed in this study would have had on fish if they had reached reproductive maturity. Although the molecular pathway involved in ovarian masculinization in fish is well understood, the parameters that trigger this pathway and how they affect fish at different stages of reproductive development is not well understood and should be further studied.

Our findings highlight the importance of continued work in this area, particularly in the development of intersex gonads in additional fish species and the exposure parameters (e.g., duration of exposure, dissolved oxygen level, and reproductive stage at time of exposure). A better understanding of the exposure parameters that trigger the development of intersexuality in fish would help not only elucidate the findings of this study but also better inform management decisions regarding resources in the GOM and in other areas affected by hypoxia.

Our observation of ovarian masculinization in Atlantic croaker and 2 other groundfish species in the GOM extends the taxonomic breadth of this phenomenon, which was first reported by Thomas and Rahman (Thomas et al., 2007). If our finding of testicular tissue in the ovaries of wild-caught specimens is not related to hypoxia, the phenomenon either is due to some other environmental factor or it represents naturally occurring background intersexuality. Bahamonde et al. (2013) reviewed this phenomenon in great detail, with his work including studies of gonochoristic species in which intersex individuals were found to occur naturally (Bahamonde et al., 2013). In one such study involving the freshwater species smallmouth bass (*Micropterus dolomieu*), significantly more occurrences of intersex fish during the prespawning period were observed than during the reproductive period (Blazer et al., 2007). The spawning period of Atlantic croaker in the GOM begins as early as October and ends as late as June (Parker, 1971), a protracted spawning period. Results from research on bigeye searobin in the GOM indicate that this species also has a protracted spawning period, from January through June (Hoff, 1992). The spot has been reported to be a winter spawner in the GOM, with the exact timing of spawning contingent on longitude (Parker, 1971). Even though our ovarian samples were taken from fish collected primarily in the prespawning period for their species, it is unlikely that the evidence of masculinization we observed was the result of the inherent intersex characteristics described by Bahamonde et al. (2013).

The vast majority of examples of naturally occurring intersex individuals in gonochoristic fishes outlined by Bahamonde et al. (2013) are male fish with testicular tissue that contained oocytes, given that the study was focused primarily on the process of male feminization. The feminization of testicular tissue indicates aromatization of androgens into estrogens—the opposite hormonal mechanism from that presumed to occur in ovarian masculinization, making it incompatible with our interpretation. Additionally, our observation of heavily masculinized specimens, including a specimen of spot best characterized as in the process of undergoing a sex change, with degenerating oocytes, indicates that specimens were transitioning from female to male, similar to the transition of ovaries to functional testes in tilapia as a result of aromatase suppression (Sun et al., 2014).

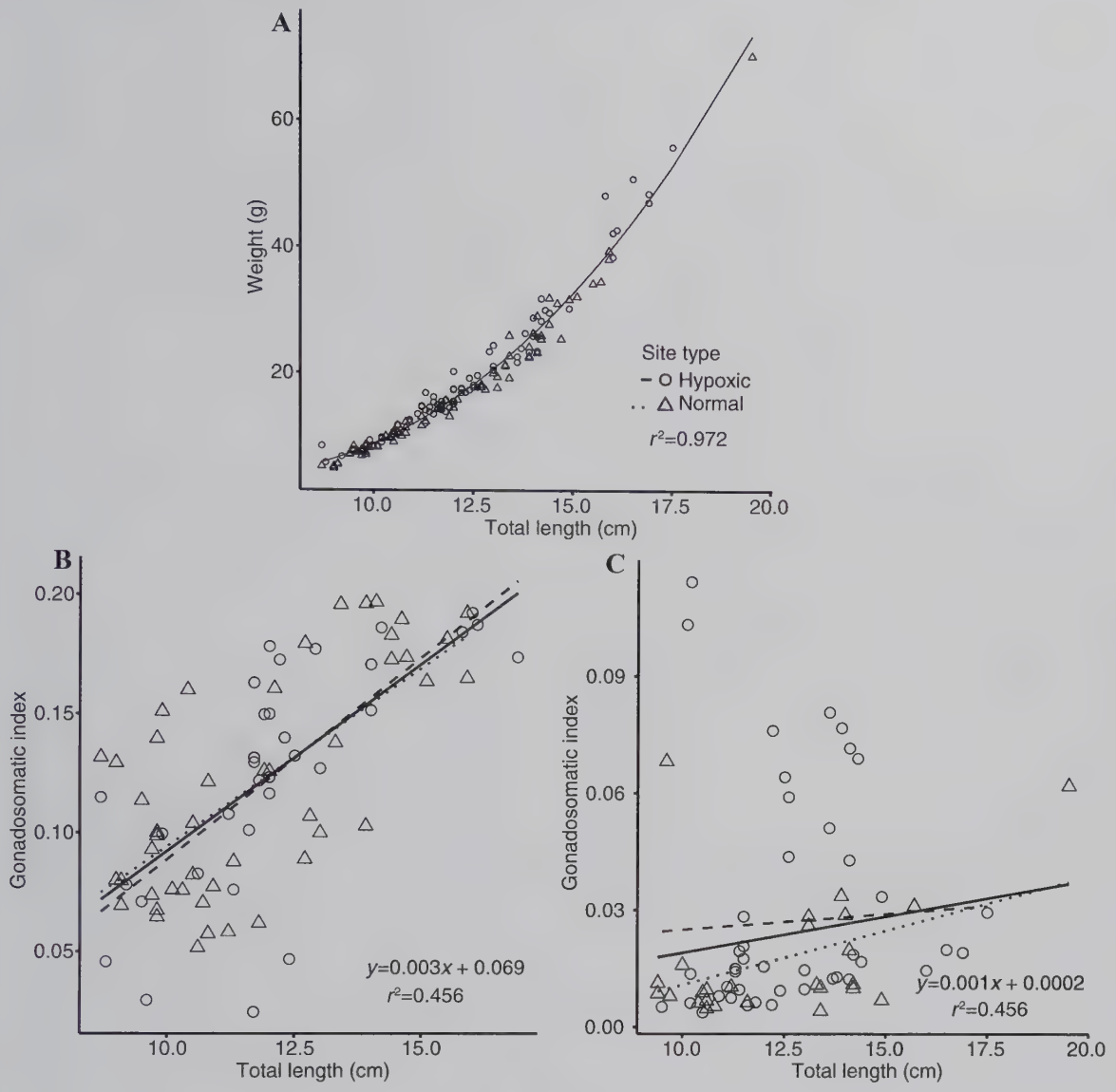

Figure 5

(**A**) Weight–length relationship for Atlantic croaker (*Micropogonias undulatus*), males and females combined, and the relationship between length and the gonadosomatic index for (**B**) female and (**C**) male Atlantic croaker collected in the northern Gulf of Mexico during 2016, 2017, and 2019. All specimens were caught off the coasts of Texas and Louisiana at sites in hypoxic areas and sites with normal levels of oxygen. The solid trend lines were calculated by using data pooled for fish from both hypoxic and normal sites, and the dashed and dotted trend lines represent data only for fish from hypoxic sites or only for fish from normal sites, respectively. Also provided are the coefficient of determination (r^2) in each graph and the equation for the solid trend line in each of the bottom graphs.

Therefore, although the occurrence of naturally intersex individuals in otherwise gonochoristic fishes should be seriously considered, the low number of examples of naturally masculinized individuals in the literature, compared to the high degree of masculinization in some of our specimens, as well as the lack of any observable intersexuality in our reference samples indicate that naturally occurring intersexuality is not a likely explanation for our observations.

Manifestation of masculinization

In previous reports of masculinization in Atlantic croaker, the process is described as "spermatogenic cyst-like structures" (Thomas and Rahman, 2012). This description fits the majority of masculinized ovaries from Atlantic croaker and the masculinized specimens of spot from a site in this study that had normal oxygen concentrations but was adjacent to the area with hypoxic conditions. In addition to

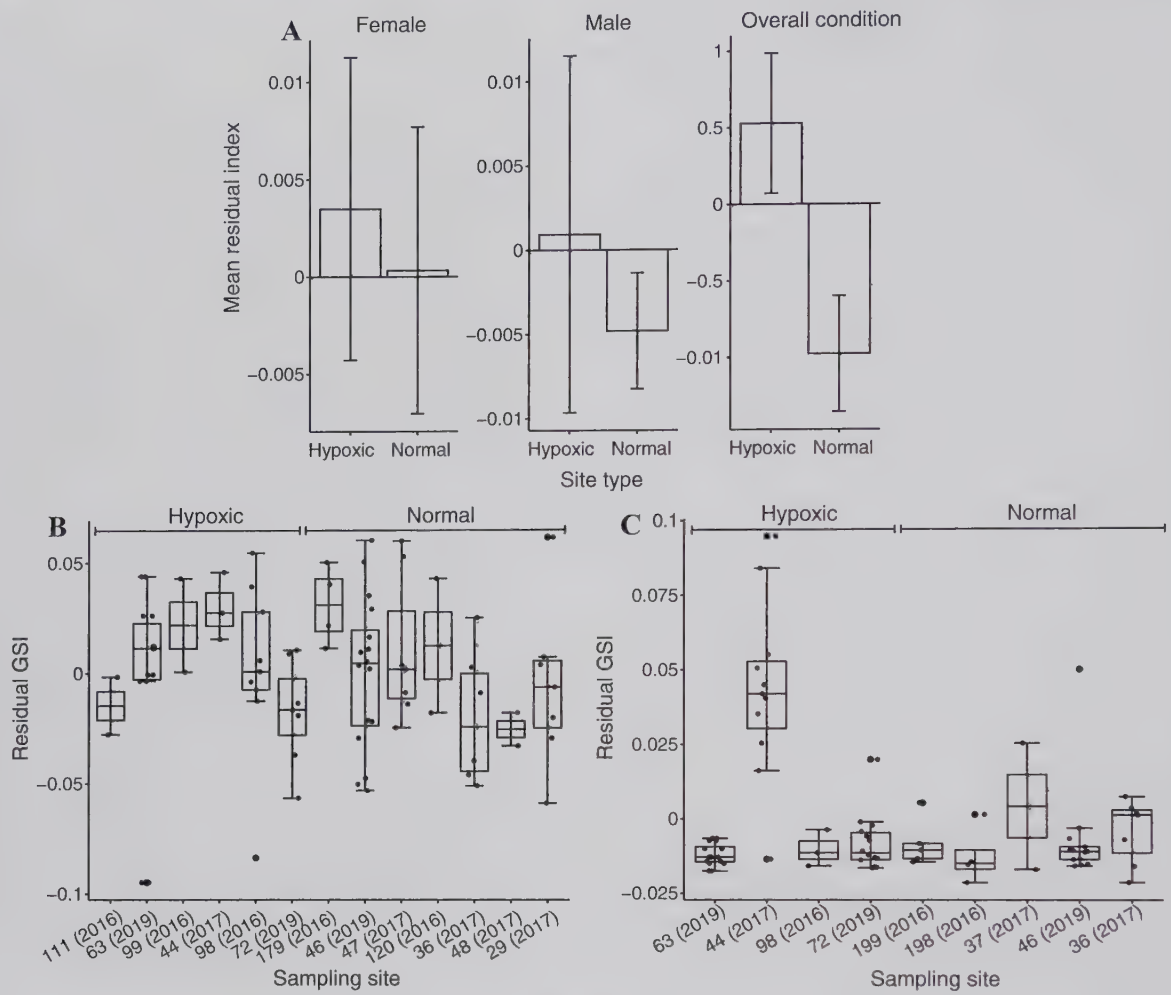

Figure 6

Mean residual gonadosomatic index (GSI), mean residual overall body condition index, and box plots of GSI values for Atlantic croaker (*Micropogonias undulatus*) caught at hypoxic sites and sites with normal oxygen concentrations in the northern Gulf of Mexico in 2016, 2017, and 2019. (**A**) Mean residual GSI and mean residual index of overall body condition, calculated as wet weight divided by total length, for females and males (analysis of variance: $P<0.05$; hypoxic sites: $n=9$; normal sites: $n=11$) are provided. Sampling sites served as replicates for all analyses. Error bars indicate standard errors of the means. For (**B**) female and (**C**) male Atlantic croaker, box plots present residual GSI values by site and site type. Numerals along the x-axis indicate the numbers assigned to sampling sites by the Southeast Area Monitoring and Assessment Program and the year during which specimens were collected. The upper and lower parts of each box represent the first and third quartiles (the 25th and 75th percentiles), and the horizontal line is the median. The whiskers extend above and below the box no more than 1.5 times the interquartile range. Data points inside and outside the boxes represent residual GSI values for individual fish.

observing this more typical manifestation of masculinization in sampled fish, we also examined 3 specimens that were undergoing this phenomenon to a degree that has yet to be described in wild specimens from the GOM.

In 2 specimens of spot and 1 specimen of Atlantic croaker, we observed masculinization to the extent that their gonads were in transition from female to male tissue, as these specimens had degenerating or regressing female reproductive cells and a testes-like overall structure. The gonads of these specimens contained well-defined ducts that were surrounded by highly degraded oocytes. The gonad of one of the spot specimens also contained a large duct or lumen space filled with material consistent with follicular atresia and melano-macrophages. The other specimen of spot had similarly degraded oocytes and well-defined male tissue; however, the gonad of this individual lacked a large lumen and melano-macrophage aggregations.

The evidence of oocyte degradation combined with the well-defined testicular structure and spermatogenic tissue in these specimens indicate masculinization beyond what has been observed previously in fish from the GOM.

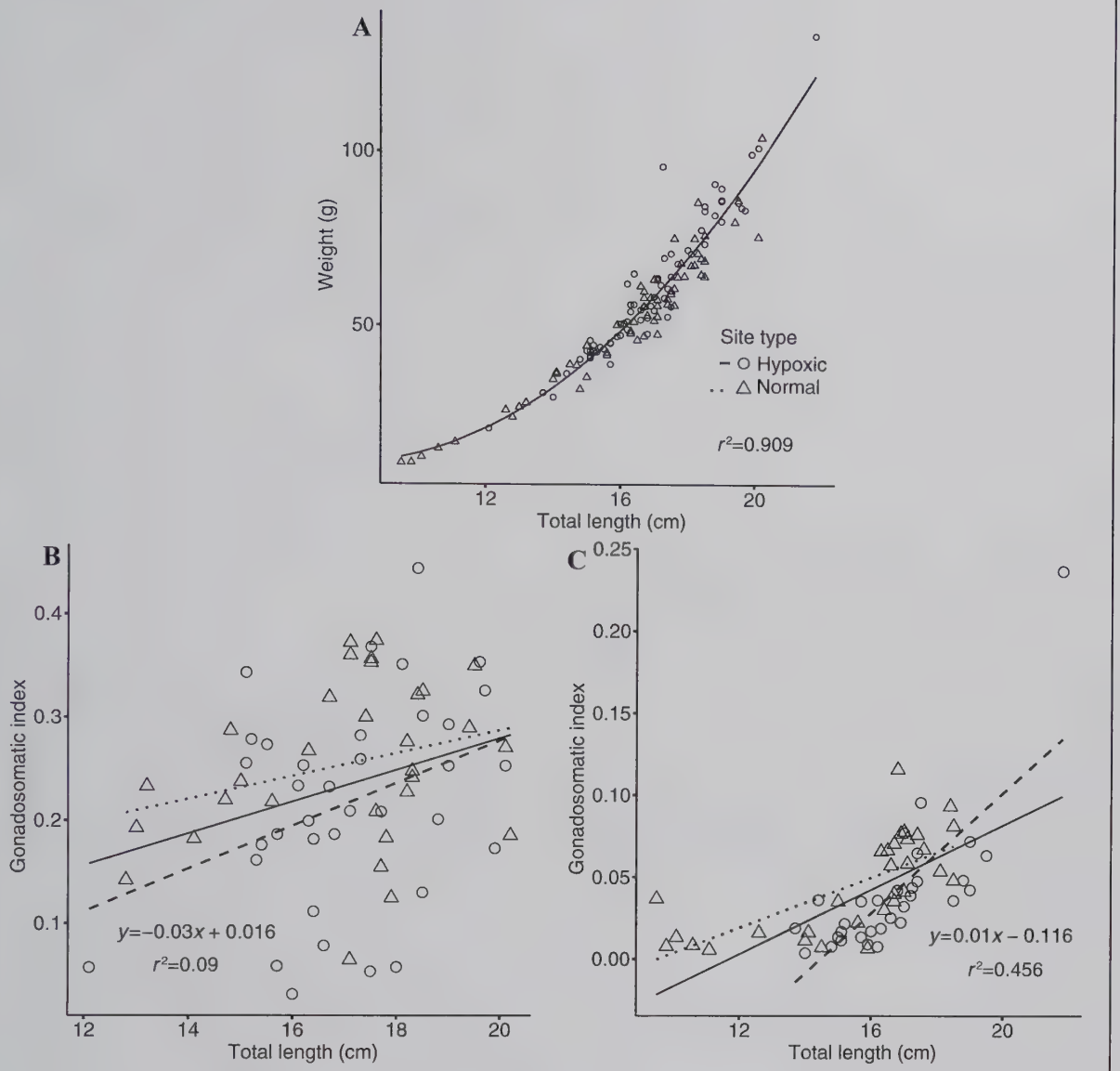

Figure 7

(**A**) Weight–length relationship for spot (*Leiostomus xanthurus*), males and females combined, and the relationship between length and the gonadosomatic index for (**B**) female and (**C**) male spot collected in the northern Gulf of Mexico during 2016, 2017, and 2019. All specimens were caught off the coasts of Texas and Louisiana at sites in hypoxic areas and sites with normal levels of oxygen. The solid trend lines were calculated by using data pooled for fish from both hypoxic and normal sites, and the dashed and dotted trend lines represent data only for fish from hypoxic sites or only for fish from normal sites, respectively. Also provided are the coefficient of determination (r^2) in each graph and the equation for the solid trend line in each of the bottom graphs.

The characterization of these individuals as females undergoing masculinization, as opposed to males undergoing feminization, is supported by work on tilapia by Sun et al. (2014) in which aromatase suppression led to a complete sex change in females, a change characterized by a degradation of oocytes and replacement of the oocytes by spermatogenic cells (Sun et al., 2014). Histological observations in naturally hermaphroditic fish transitioning from female to male provide similar evidence of oocyte breakdown prior to the transition from female to male (Wang et al., 2017; Maxfield and Cole, 2019). Centers of melano-macrophages have been considered pathological signs of environmental degradation and hypoxia in fish (Agius and Roberts, 2003), including individuals of species such as the Atlantic croaker in the GOM (Fournie et al., 2001), albeit the aggregations were found in the spleen.

The more structurally complex nature of the examples of masculinization we observed in this study, coupled with

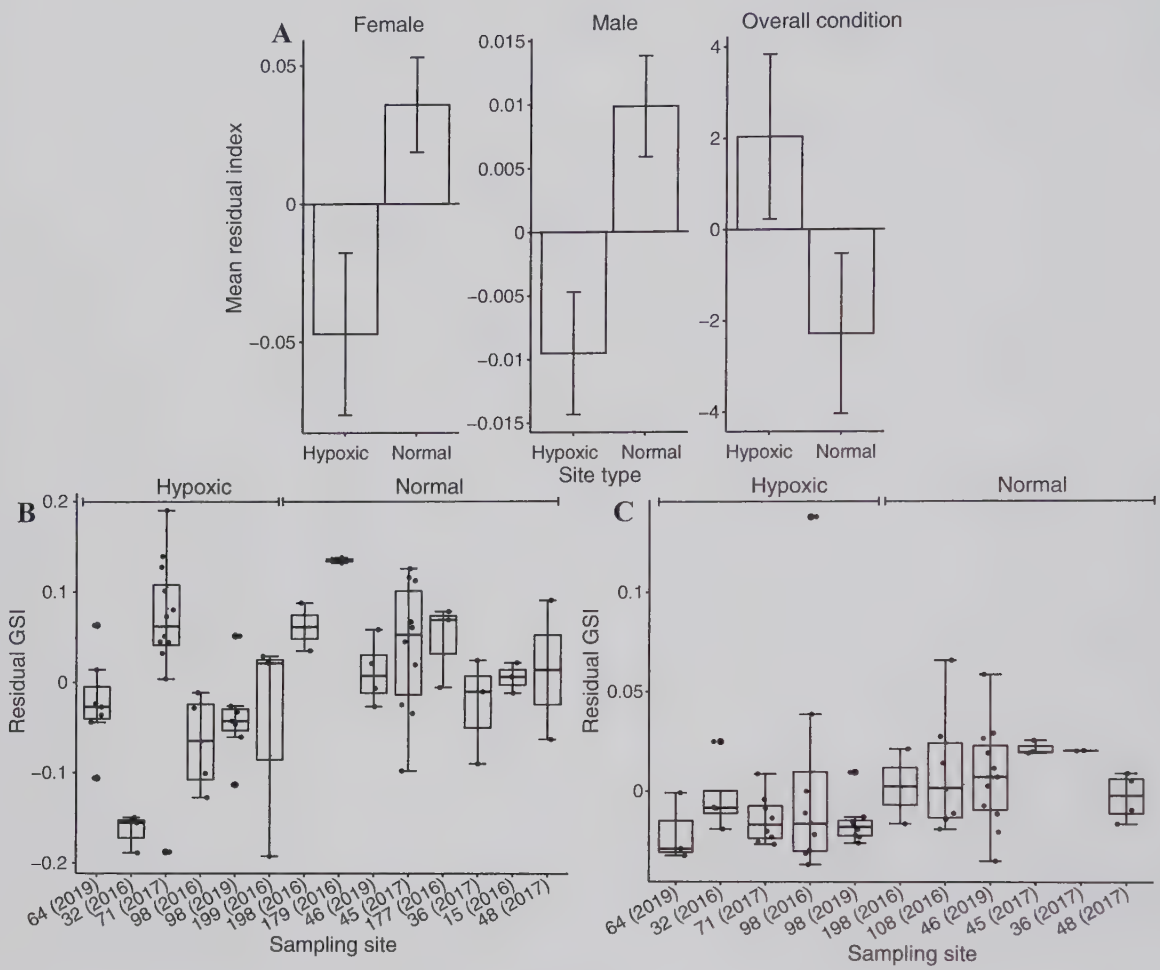

Figure 8

Mean residual gonadosomatic index (GSI), mean residual overall body condition index, and box plots for spot (*Leiostomus xanthurus*) caught at hypoxic sites and sites with normal oxygen concentrations in the northern Gulf of Mexico in 2016, 2017, and 2019. (**A**) Mean residual GSI for females (ANOVA: $P<0.05$; hypoxic sites: $n=6$; normal sites: $n=8$) and males (ANOVA: $P< 0.05$; hypoxic sites: $n=5$; normal sites: $n=6$) and mean residual index of overall body condition, calculated as wet weight divided by total length (analysis of variance (ANOVA): $P>0.05$; hypoxic sites: $n=6$; normal sites: $n=10$), are provided. Sampling sites served as replicates for all analyses. Error bars indicate the standard errors of the means. For (**B**) female and (**C**) male spot, box plots present residual GSI values by site and site type. Numerals along the x-axis indicate the numbers assigned to sampling sites by the Southeast Area Monitoring and Assessment Program and the year during which specimens were collected. The upper and lower parts of each box represent the first and third quartiles (the 25th and 75th percentiles), and the horizontal line is the median. The whiskers extend above and below the box no more than 1.5 times the interquartile range. Data points inside and outside the boxes represent residual GSI values for individual fish.

the discovery of transitional individuals, highlights the need for further research into this phenomenon. Fish specimens examined in previous work were sampled later in the season and were more reproductively developed than the fish examined in this study (Thomas and Rahman, 2012), indicating that hypoxia-induced reproductive impairment in fish in the GOM is more widespread and develops earlier than previously known. It is important to note that, although the results of this study indicate that ovarian masculinization in fish can occur earlier in gonadal development than previously thought, more research is needed to understand how this early impairment translates to reproductive success later in the season.

Ovarian masculinization and reproductive impairment

For both female and male Atlantic croaker, no statistically significant differences were found in the residual GSI between hypoxic sites and sites with normal oxygen concentrations, although a trend of increased GSI in specimens from normal sites was observed. This finding contradicts those of previous studies in which

statistically significant decreases in GSI values were found for Atlantic croaker from hypoxic sites (Thomas and Rahman, 2012). Although unexpected, the results of our study could be explained by the difference in the severities of hypoxic conditions between the investigations, given that hypoxia in 2016 was less patchy and more widespread compared to that in 2007 (the year of Thomas and Rahman's field collections), or by differences in the sexual maturity of sampled specimens due to differences in how far into the seasons fish were sampled. These discrepancies highlight the importance of continued research into hypoxia and its effects, especially those on fish at different levels of reproductive maturity.

Both female and male spot from hypoxic sites had significantly lower ($P<0.05$) residual GSI values than those for females and males from sites with normal oxygen levels. This finding supports observations from previous studies of Atlantic croaker and further highlights the potential effects of an environmental stressor, such as hypoxia, on fish reproduction at population and ecosystem levels.

Female and male Atlantic croaker and female spot sampled from hypoxic sites in 2017 had some of the highest GSI values observed for both species and both sexes (Figs. 6 and 8). The patchy areas of hypoxia from which these specimens were sampled in 2017 were a fraction of the size of the large, more continuous hypoxic zones sampled in 2016 and 2019 (the hypoxic zone was patchier in 2019 than in 2016, but the patches of hypoxia were much larger in 2019 than in 2017) (Fig. 1). The patchiness of hypoxia in 2017 could have led to hypoxia exposure that was less severe than that to which fish were exposed in 2016 and 2019. Although we have no diet data to support this interpretation, it is possible that the smaller areas of hypoxia in 2017 could have allowed benthic fish to feed on hypoxia-stressed infaunal invertebrates, similar to what has been observed in the more episodic zones of hypoxia that develop in Chesapeake Bay (Pihl et al., 1992). This interpretation could also explain why fish from hypoxic sites in 2017 had such high GSI values. Balancing the potential for increased foraging opportunities associated with hypoxic conditions with the physiological costs associated with hypoxia exposure is one explanation for the context-dependent nature of thresholds for hypoxia avoidance in groundfish in the GOM (Craig, 2012), highlighting the need for more research to place the reproductive costs of hypoxia in the broader ecological context of the GOM.

Conclusions

The results of our study indicate that reproductive impairment, specifically the presence of intersex individuals associated with hypoxic conditions, affects more species of fish than previously documented. We also found evidence of reproductive anomalies, such as the presence of ovum remnants in early stages of ovarian development, in fish in and around the hypoxic zone in the GOM in 2016. These findings, along with the lack of ovarian masculinization and reproductive anomalies in reference fish and the significantly lower GSI values for spot from hypoxic sites than from sites with normal oxygen concentrations, strongly support the idea that hypoxic conditions can alter the reproductive health of fish.

The findings of this study expand upon previous reports of ovarian masculinization and reproductive impairment in fish in the GOM. They increase the number of species affected and provide novel examples and pathologies of this phenomenon. This study also resulted in evidence of ovarian masculinization occurring in fish sampled at sites bordering hypoxic areas and in fish at earlier developmental stages than have been reported previously. However, these findings need to be further explored to fully understand how they fit within the broader context of hypoxia-induced ovarian masculinization in fish in the GOM.

Resumen

Los resultados de este estudio aportan evidencia adicional de masculinización ovárica en la corvina (*Micropogonias undulatus*) dentro de la zona hipóxica del Golfo de México y sus alrededores, así como las primeras pruebas de masculinización ovárica en la croca (*Leiostomus xanthurus*) y el rubio ojón (*Prionotus longispinosus*). En algunos ejemplares de corvina y croca observamos este fenómeno en un grado que no se había reportado antes en ninguna de las dos especies. También, encontramos evidencia de gónadas más pequeñas en crocas de sitios hipóxicos en comparación con las gónadas crocas de sitios con concentraciones normales de oxígeno. Estos hallazgos indican que la masculinización ovárica y la deficiencia reproductiva asociados con la exposición a la hipoxia, afectan a una gama de especies más amplia de lo que se conocía hasta ahora y destacan la importancia de seguir investigando sobre este tema.

Acknowledgments

We would like to thank the scientists and staff at the National Marine Fisheries Service lab in Pascagoula, Mississippi, and the crew of the NOAA Ship *Oregon II* for all their time, expertise, kindness, and guidance during the sample collection process. We would also like to recognize J. Mann, the collections manager of the Royal D. Suttkus Fish Collection at the TUBRI, for helping to process and integrate the sizeable number of specimens generated by this work into the collection at the TUBRI.

Literature cited

Agius, C., and R. J. Roberts.
2003. Melano–macrophage centres and their role in fish pathology. J. Fish Dis. 26:499–509.

Anderson, J., D. McDonald, B. Bumguardner, Z. Olsen, and J. W. Ferguson.
2018. Patterns of maturity, seasonal migration, and spawning of Atlantic croaker in the western Gulf of Mexico. Gulf Mex. Sci. 34(1):19–31.

Bahamonde, P. A., K. R. Munkittrick, and C. J. Martyniuk.
2013. Intersex in teleost fish: are we distinguishing endocrine disruption from natural phenomena? Gen. Comp. Endocrinol. 192:25–35.

Bartlett, M. S.
1937. Properties of sufficiency and statistical tests. Proc. R. Soc. Lond. A 160:268–282.

Bhandari, R. K., H. Komuro, M. Higa, and M. Nakamura.
2004. Sex inversion of sexually immature honeycomb grouper (*Epinephelus merra*) by aromatase inhibitor. Zool. Sci. 21:305–311.

Blazer, V. S., L. R. Iwanowicz, D. D. Iwanowicz, D. R. Smith, J. A. Young, J. D. Hedrick, S. W. Foster, and S. J. Reeser.
2007. Intersex (testicular oocytes) in smallmouth bass from the Potomac River and selected nearby drainages. J. Aquat. Anim. Health 19:242–253.

Boesch, D. F., and R. Rosenberg.
1981. Response to stress in marine benthic communities. *In* Stress effects on natural ecosystems (G. W. Barrett and R. Rosenberg, eds.), p. 179–200. John Wiley and Sons, New York.

Cheek, A. O., C. A. Landry, S. L. Steele, and S. Manning.
2009. Diel hypoxia in marsh creeks impairs the reproductive capacity of estuarine fish populations. Mar. Ecol. Prog. Ser. 392:211–221.

Craig, J. K.
2012. Aggregation on the edge: effects of hypoxia avoidance on the spatial distribution of brown shrimp and demersal fishes in the northern Gulf of Mexico. Mar. Ecol. Prog. Ser. 445:75–95.

Dauer, D. M.
1993. Biological criteria, environmental health and estuarine macrobenthic community structure. Mar. Pollut. Bull. 26:249–257.

Diaz, R. J., and R. Rosenberg.
2008. Spreading dead zones and consequences for marine ecosystems. Science 321:926–929.

Eriksson, S. P., and S. P. Baden.
1997. Behaviour and tolerance to hypoxia in juvenile Norway lobster (*Nephrops norvegicus*) of different ages. Mar. Biol. 128:49–54.

Fournie, J. W., J. K. Summers, L. A. Courtney, V. D. Engle, and V. S. Blazer.
2001. Utility of splenic macrophage aggregates as an indicator of fish exposure to degraded environments. J. Aquat. Anim. Health 13:105–116.

Galloway, J. N., A. R. Townsend, J. W. Erisman, M. Bekunda, Z. Cai, J. R. Freney, L. A. Martinelli, S. P. Seitzinger, and M. A. Sutton.
2008. Transformation of the nitrogen cycle: recent trends, questions, and potential solutions. Science 320:889–892.

Guiguen, Y., A. Fostier, F. Piferrer, and C.-F. Chang.
2010. Ovarian aromatase and estrogens: a pivotal role for gonadal sex differentiation and sex change in fish. Gen. Comp. Endocrinol. 165:352–366.

Helly, J. J., and L. A. Levin.
2004. Global distribution of naturally occurring marine hypoxia on continental margins. Deep Sea Res., I 51:1159–1168.

Hoff, J. G., Jr.
1992. Comparative biology and population dynamics of searobins (genus *Prionotus*) with emphasis on populations in the northwestern Gulf of Mexico. Ph.D. diss., 229 p. Va. Inst. Mar. Sci., Coll. William Mary, Gloucester Point, VA. [Available from website.]

Jakob, E. M., S. D. Marshall, and G. W. Uetz.
1996. Estimating fitness: a comparison of body condition indices. Oikos 77:61–67.

Kruskal, W. H., and W. A. Wallis.
1952. Use of ranks in one-criterion variance analysis. J. Am. Stat. Assoc. 47:583–621.

Landry, C. A., S. L. Steele, S. Manning, and A. O. Cheek.
2007. Long term hypoxia suppresses reproductive capacity in the estuarine fish, *Fundulus grandis*. Comp. Biochem. Physiol., A 148:317–323.

Maxfield, J. M., and K. S. Cole.
2019. Patterns of structural change in gonads of the divine dwarfgoby *Eviota epiphanes* as they sexually transition. J. Fish Biol. 94:142–153.

Navarro-Martín, L., M. Blázquez, and F. Piferrer.
2009. Masculinization of the European sea bass (*Dicentrarchus labrax*) by treatment with an androgen or aromatase inhibitor involves different gene expression and has distinct lasting effects on maturation. Gen. Comp. Endocrinol. 160:3–11.

Ogawa, S., M. Akiyoshi, M. Higuchi, M. Nakamura, and T. Hirai.
2008. 'Post-sex differentiational' sex reversal in the female common carp (*Cyprinus carpio*). Cybium 32(2 suppl.): 102–103.

Parker, J. C.
1971. The biology of the spot, *Leiostomus xanthurus* Lacepede, and Atlantic croaker, *Micropogon undulatus* Linnaeus, in two Gulf of Mexico nursery areas. Sea Grant Publ. TAMU-SG-71-210, 194 p. Tex. A&M Univ., College Station, TX. [Available from website.]

Pihl, L.
1994. Changes in the diet of demersal fish due to eutrophication-induced hypoxia in the Kattegat, Sweden. Can. J. Fish. Aquat. Sci. 51:321–336.

Pihl, L., S. P. Baden, R. J. Diaz, and L. C. Schaffner.
1992. Hypoxia-induced structural changes in the diet of bottom-feeding fish and Crustacea. Mar. Biol. 112:349–361.

Rabalais, N. N., R. E. Turner, and W. J. Wiseman Jr.
2002. Gulf of Mexico hypoxia, A.K.A. "the Dead Zone." Annu. Rev. Ecol. Syst. 33:235–263.

Rabalais, N. N., R. E. Turner, B. K. S. Gupta, D. F. Boesch, P. Chapman, and M. C. Murrell.
2007. Hypoxia in the northern Gulf of Mexico: does the science support the plan to reduce, mitigate, and control hypoxia? Estuar. Coasts 30:753–772.

Reist, J. D.
1985. An empirical evaluation of several univariate methods that adjust for size variation in morphometric data. Can. J. Zool. 63:1429–1439.

Rosenberg, R., and L.-O. Loo.
1988. Marine eutrophication induced oxygen deficiency: effects on soft bottom fauna, western Sweden. Ophelia 29:213–225.

Sandberg, E.
1997. Does oxygen deficiency modify the functional response of *Saduria entomon* (Isopoda) to *Bathyporeia pilosa* (Amphipoda)? Mar. Biol. 129:499–504.

Shapiro, S. S., and M. B. Wilk.
1965. An analysis of variance test for normality (complete samples). Biometrika 52:591–611.

Sun, L.-N., X.-L. Jiang, Q.-P. Xie, J. Yuan, B.-F. Huang, W.-J. Tao, L.-Y. Zhou, Y. Nagahama, and D.-S. Wang.
2014. Transdifferentiation of differentiated ovary into functional testis by long-term treatment of aromatase inhibitor in Nile tilapia. Endocrinology 155:1476–1488.

Thomas, P., and M. S. Rahman.
2009. Biomarkers of hypoxia exposure and reproductive function in Atlantic croaker: a review with some preliminary findings from the northern Gulf of Mexico hypoxic zone. J. Exp. Mar. Biol. Ecol. 381(Suppl.):S38–S50.
2012. Extensive reproductive disruption, ovarian masculinization and aromatase suppression in Atlantic croaker in the northern Gulf of Mexico hypoxic zone. Proc. R. Soc. B 279:28–38.

Thomas, P., M. S. Rahman, I. A. Khan, and J. A. Kummer.
2007. Widespread endocrine disruption and reproductive impairment in an estuarine fish population exposed to seasonal hypoxia. Proc. R. Soc. B 274:2693–2702.

Thomas, P., M. S. Rahman, M. E. Picha, and W. Tan.
2015. Impaired gamete production and viability in Atlantic croaker collected throughout the 20,000 km^2 hypoxic region in the northern Gulf of Mexico. Mar. Pollut. Bull. 101:182–192.

Vaquer-Sunyer, R., and C. M. Duarte.
2008. Thresholds of hypoxia for marine biodiversity. Proc. Natl. Acad. Sci. U.S.A. 105:15452–15457.

Wang, Q., Y. Liu, C. Peng, X. Wang, L. Xiao, D. Wang, J. Chen, H. Zhang, H. Zhao, S. Li, and H. Lin.
2017. Molecular regulation of sex change induced by methyltestosterone-feeding and methyltestosterone-feeding withdrawal in the protogynous orange-spotted grouper. Biol. Reprod. 97:324–333.

Wu, R. S. S.
2002. Hypoxia: from molecular responses to ecosystem responses. Mar. Pollut. Bull. 45:35–45.

Wu, R. S. S., B. S. Zhou, D. J. Randall, N. Y. S. Woo, and P. K. S. Lam.
2003. Aquatic hypoxia is an endocrine disruptor and impairs fish reproduction. Environ. Sci. Technol. 37:1137–1141.

Zhou, B. S.
2001. Effects of hypoxia on metabolism, bioenergetics, growth, and reproduction of the common carp (*Cyprinus carpio* L.). Ph.D. thesis. City Univ. Hong Kong, Hong Kong, China.

National Marine
Fisheries Service
NOAA

Fishery Bulletin
established in 1881

Spencer F. Baird
First U.S. Commissioner
of Fisheries and founder
of *Fishery Bulletin*

Reducing uncertainty in survey abundance estimates by considering alternative designs and estimators: a case study with 3 species in the Gulf of Alaska

Paul G. von Szalay (contact author)
Stan Kotwicki
Lewis A. K. Barnett
Lou J. Rugolo
Kotaro Ono

Email address for contact author: paul.von.szalay@noaa.gov

Alaska Fisheries Science Center
National Marine Fisheries Service, NOAA
7600 Sand Point Way NE
Seattle, Washington 98115

Abstract—A bottom-trawl survey with a stratified-random sampling design has been used to inform stock assessments for commercially important species in the Gulf of Alaska since 1984. A new stratified sampling design was evaluated to determine whether its use could improve the precision and accuracy of abundance estimates. In this proposed approach to defining strata, historical survey data are used to generate what we refer to as *information scores* (ISes). We compared the traditional stratification scheme with the new method and 2 other sampling designs, using both a design-based estimator and a model-based estimator with each design, to determine if the existing approach is optimal. Statistical robustness, measured in terms of coefficient of variation, bias, and root mean square error, was compared among 7 scenarios with different combinations of estimators and sampling designs by using simulation with a spatiotemporal generalized linear mixed model conditioned on historical observations of catch per unit of effort of 3 species. The combination of the design-based estimator with the IS-based stratification scheme was the best scenario across all performance metrics for all species. This scenario consistently had the lowest variance and smallest total error, and it was generally unbiased. In contrast, the pairing of the model-based estimator with this sampling design was by far the worst-performing scenario. The performance of the existing approach was average.

Manuscript submitted 29 September 2022.
Manuscript accepted 17 April 2023.
Fish. Bull. 121:50–66 (2023).
Online publication date: 2 May 2023.
doi: 10.7755/FB.121.1-2.5

The views and opinions expressed or implied in this article are those of the author (or authors) and do not necessarily reflect the position of the National Marine Fisheries Service, NOAA.

Surveys for estimating abundance of natural resources, and the precision of abundance estimates based on survey data, are limited in scope by a number of logistical constraints, including but not limited to funding, staffing, time, and access to appropriate and sufficient sampling tools and platforms. The precision of abundance estimates, including those of biomass, generally increases with sample size, which is limited by available resources, assuming the availability of a species to sampling remains constant. In practice, the scope of a survey effort, as indicated by the number of stations where sampling occurs, is typically known before the sampling design is generated and is dictated by logistical constraints. The goal of a sampling design, therefore, is to optimize the geographical distribution of the predetermined number of survey stations to achieve the highest possible precision for survey data products. A potential problem for survey continuity arises when circumstances compel a reduction or increase in sampling effort, especially after a survey time series is well established. In such an event, it may be appropriate to review the existing sampling design of the survey for optimality and to consider changes to the design while assuring continuity of the time series. The long-established and relatively large-scale multispecies bottom-trawl survey that has been conducted in the Gulf of Alaska (GOA) since 1984 can serve as an illustrative example of how these issues can be addressed.

The NOAA Alaska Fisheries Science Center has conducted a bottom-trawl survey in summer in the GOA biennially since 1999 (and triennially between 1984 and 1999), using a stratified-random sampling design to assess the distribution and abundance of groundfish for the purposes of fisheries management (von Szalay and Raring, 2018). Traditionally, the survey effort consisted of 3 vessels sampling approximately 820 stations in 59 different strata. Prior to 1990, the focal survey areas in a given year were adapted to meet specific scientific or management needs, and as a result the effort levels in the different strata could be highly variable from one survey year

to another. This practice was discontinued in 1990, when the sampling design of the survey was standardized to adhere to a modified Neyman allocation scheme. A variety of factors in recent years, such as funding limitations and inability to acquire a sufficient number of suitable charter vessels, have resulted in the need to reduce the survey effort in some years (von Szalay, 2015). Other fisheries resource management agencies, both domestic and international, similarly have had to or are preparing to contend with potential unavoidable reductions in survey effort for a variety of reasons, including vessel breakdowns, lack of enough survey vessels or staff due to the COVID-19 pandemic, bad weather, and failure to obtain sampling permits for all parts of the survey area (Peel et al., 2013; ICES, 2020).

The reduction of survey effort has amplified the need not only to ensure the use of the optimal sampling design but also to seek the most robust and precise abundance estimator possible that would perform well in years with fewer data. This issue can be addressed by comparing the statistical robustness of the existing approach with that of alternative scenarios based on different combinations of estimators and sampling designs, a valuable exercise even if survey effort has not been reduced. Until recently, it has been difficult to make direct comparisons between different estimators and sampling designs because of a lack of an appropriate simulation framework. However, Kotwicki and Ono (2019) developed a framework for simulating distributions of fish population density with a spatiotemporal model conditioned on historical catch and environmental survey data for a number of commercially important species in the GOA. We used this operating model to simulate the "true" distribution of abundance and the results of simulated sampling with different designs.

When the existing stratified-random sampling design was first devised in the early 1980s, no historical catch or environmental data were available to refine the stratification scheme. Now that a long-running time series is well established, it is possible to use these data to explore alternative stratification schemes and sampling designs, which may potentially reduce the uncertainty in abundance estimates by yielding more accurate and precise estimates of biomass and its associated variance. In recent studies, optimization-based methods of stratifying finite populations (Hidiroglou and Kozak, 2018; Oyafuso et al., 2021, 2022) have been proven to be superior to the traditional stratification scheme used for the bottom-trawl survey in the GOA. In our study, we evaluated the performance of 3 different traditional sampling designs, which are among the most commonly used in the world and have already been implemented by the Alaska Fisheries Science Center: simple random, stratified random, and systematic.

For these evaluations, we used a proposed new technique for determining stratum boundaries in the GOA, one in which estimates of abundance and its variability from historical survey data are used to derive an empirical metric referred to herein as an *information score* (IS). This technique, which ensures that more stations are allocated to strata with higher abundance and variance in abundance based on historical survey data, fine-tunes the stratification process by decreasing the variance within strata while increasing the variance among strata. This approach contrasts with the traditional stratification scheme whose performance may be compromised by including an ad hoc management area and depth bounds to define strata. Management area boundaries are unlikely to have any bearing on fish density, and arbitrary depth boundaries in regular 100-m intervals are unlikely to coincide with breaks in fish density distributions.

There has recently been a rapid development of methods for estimating population density by using spatial model-based estimators to calculate biomass or abundance (e.g., Thorson and Barnett, 2017; Anderson et al.[1]). Design-based estimators, such as the one developed by Wakabayashi et al. (1985), are simpler and faster, but spatial model-based estimators, such as vector autoregressive spatiotemporal (VAST) models (Thorson, 2019), may be more accurate or precise under some scenarios because they allow for spatial and temporal correlation and covariate effects. In addition, model-based designs can be both efficient and flexible in allowing uneven sampling due to survey logistics and in providing a general framework to answer specific design questions (Peel et al., 2013).

The objective of this study was to compare the statistical robustness of 7 scenarios with different combinations of sampling designs and estimators in order to identify whether an approach improves the accuracy and precision of estimates of biomass, which we used as a measure of abundance. As a case study, we evaluated the statistical robustness of 7 scenarios by simulating the distribution and abundance of 3 species in the GOA: Pacific cod (*Gadus macrocephalus*), Pacific ocean perch (*Sebastes alutus*), and arrowtooth flounder (*Atheresthes stomias*). These species were chosen on the basis of their ecological or commercial importance as well as the diversity of their spatial distribution patterns. In 6 scenarios, a random sampling design was paired with a design-based or model-based estimator, and in 1 scenario a systematic sampling design was paired with a model-based estimator.

Materials and methods

Survey characteristics

The GOA forms the northeastern border of the Pacific Ocean and has complex bathymetric features ranging from jagged, mountainous pinnacles to flat, muddy areas (von Szalay and Raring, 2018). These features provide a variety of habitats, creating a complex ecosystem. The standard survey area of the biennial bottom-trawl survey in the GOA is approximately 320,000 km^2 and includes

[1] Anderson, S. C., E. J. Ward, P. A. English, and L. A. K. Barnett. Unpubl. manuscript. sdmTMB: an R package for fast, flexible, and user-friendly generalized linear mixed effects models with spatial and spatiotemporal random fields. bioRxiv 2022.03.24.485545. [Available from website.]

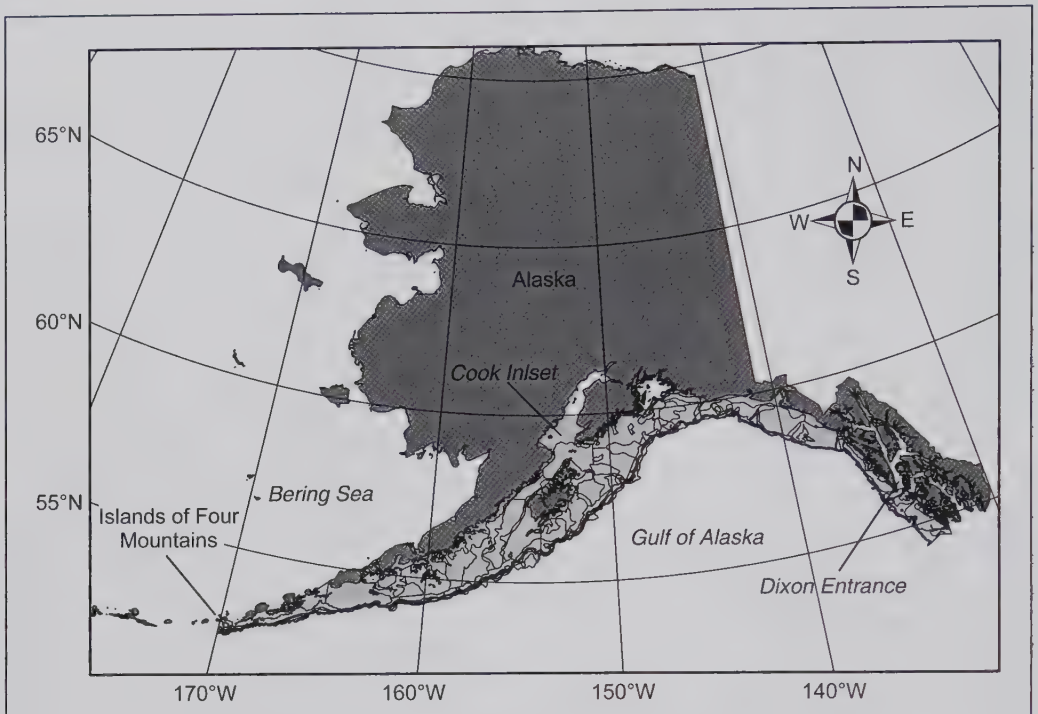

Figure 1

Map showing the 59 strata of the bottom-trawl survey conducted biennially in the Gulf of Alaska by the NOAA Alaska Fisheries Science Center. The survey area includes the portion of the continental shelf from the Islands of Four Mountains eastward approximately 2800 km to Dixon Entrance and from nearshore waters to a depth of 1000 m. The stratum boundaries have been fixed since the inception of the survey in 1984.

the portion of the continental shelf from the Islands of Four Mountains, in the Aleutian Islands, eastward to Dixon Entrance, near the border of Canada and the United States, and from nearshore waters to a depth of 1000 m (Fig. 1). The continental shelf, which makes up 82% of the survey area, is bordered by the continental slope, a region that is approximately 20 km in width, but only the portion of the slope at depths between 200 and 1000 m, is sampled in the standard surveys. The total survey area has been effectively decreased to 308,415 km^2 in recent surveys as reductions in survey effort have resulted in the deepest strata (700–1000 m) not being sampled.

In the bottom-trawl surveys conducted in the GOA by the Resource Assessment and Conservation Engineering Division of the Alaska Fisheries Science Center, approximately 820 locations within 59 strata traditionally have been sampled with a stratified-random sampling design. Abundance estimates are generated by using the estimator developed by Wakabayashi et al. (1985). Henceforth, this combination of sampling design and estimator will be referred to as the *TRS*.

The same standard trawl gear has been used since the beginning of the survey, a Poly Nor'Eastern 4-seam bottom trawl with 24.2-m roller gear constructed with 36-cm rubber bobbins separated by 10-cm rubber disks (Stauffer, 2004). Surveys start in the western end of the survey area and proceed eastward. Tow duration is approximately 15 min at 1.54 m/s (3 kt). The catch per unit of effort (CPUE) is estimated by using the area-swept method (e.g., Alverson and Pereyra, 1969), which defines the effort as the product of the distance fished and the average distance between wing tips (for details, see von Szalay and Raring, 2018).

A grid with a resolution of 5 km superimposed on the survey area is used for sampling design. Each 5-by-5-km cell in the grid is a potential survey station, but some potential stations are excluded from the pool of stations eligible for survey selection because they are untrawlable as a result of rough bottom or other factors. Furthermore, because they are truncated by the coastline and the deepest edge of the sampling domain, grid cells along the boundaries of the survey area have an area smaller than a standard 25-km^2 grid cell. Only grid cells large enough to accommodate a complete tow path (those with an area >5 km^2) are eligible for sampling.

Simulated distributions of catch per unit of effort

Simulated CPUE distributions of Pacific cod, Pacific ocean perch, and arrowtooth flounder were created by fitting a spatiotemporal delta model to historical GOA survey data from 1996 through 2015, with the package

R-INLA (vers. 18.07.12; available from website, accessed October 2018; Rue et al., 2009) in R (vers. 3.6.1; R Core Team, 2019); this package accounts for both environmental covariates and spatiotemporal dependency in catches (Kotwicki and Ono, 2019) (Fig. 2). The delta model has 2 components: one that models the species occurrence and another that models positive CPUE.

Species occurrence at locations s during year t, $\pi_t(s)$, was modeled by using a binomial generalized linear mixed model with the logit link function (see Lindgren et al., 2011):

$$\text{logit}\left(\pi_t\left(s\right)\right) = X_t\left(s\right)b + \omega_t\left(s\right), \text{where} \quad (1)$$

$$\omega_t\left(s\right) \sim N\left(\rho_1\omega_{t-1}\left(s\right), \Sigma_1\right)$$

and $X_t(s)$ = the matrix of covariates at locations s during year t;
b = the vector of regression coefficients;
ω = the spatiotemporal variation that follows a first-order autoregressive process;
N = normal distribution;
ρ_1 = the degree of autoregression in encounter probability between successive years; and
Σ_1 = the spatial covariance modeled as a Mátern function with smoothness of 1.

The covariates used in this study were log(*depth*), $(\log(depth))^2$, *bottom temperature*, *bottom temperature* squared, *surface temperature*, *surface temperature* squared, and a fixed year effect (Kotwicki et al., 2005, 2015).

The non-zero species density at a set of locations s during year t, $\mu_t(s)$, was modeled by using a lognormal distribution:

$$\log\left(\mu_t\left(s\right)\right) = Z_t\left(s\right)a + \delta_t(s), \text{where} \quad (2)$$

$$\delta_t\left(s\right) \sim N\left(\rho_2\delta_{t-1}\left(s\right), \Sigma_2\right)$$

and $Z_t(s)$ = a matrix of covariates at locations s during year t;
a = the vector of regression coefficients;
δ_t = the spatial field for year t assumed to follow an autoregressive 1 process;
ρ_2 = autocorrelation of the autoregressive 1 process in which the current value is based on the immediately preceding value; and
Σ_2 = the spatial covariance modeled as a Mátern function with smoothness of 2.

Annual distributions of simulated CPUE within the survey area were predicted over a nominal grid with a

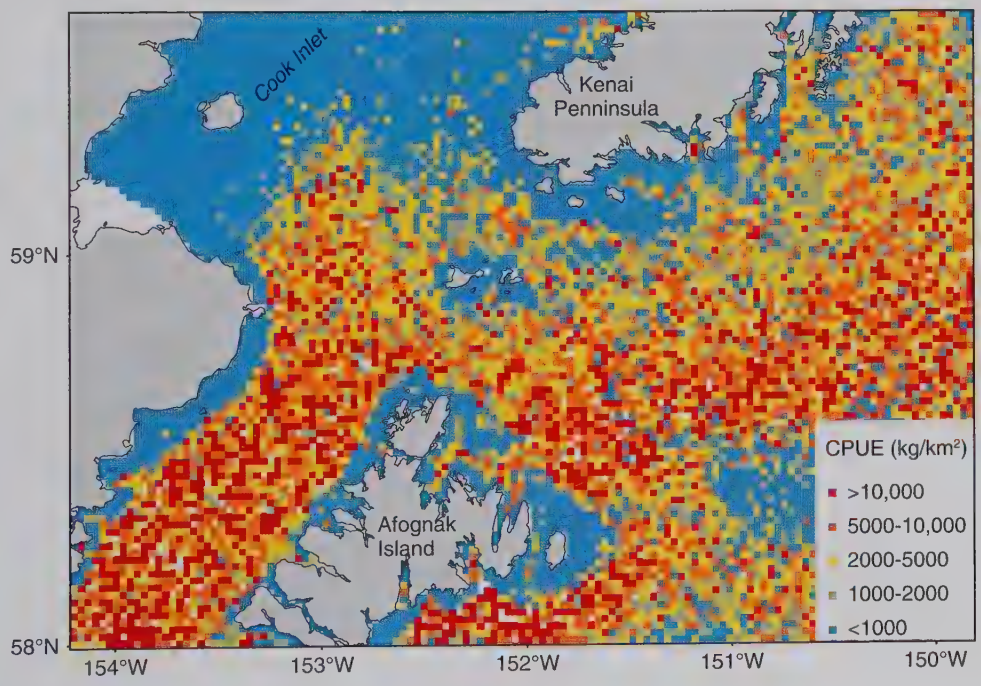

Figure 2

Simulated distribution of catch per unit of effort (CPUE) of arrowtooth flounder (*Atheresthes stomias*) in 2015 at the entrance to Cook Inlet in southcentral Alaska. The simulations were created by fitting a spatiotemporal delta model that accounts for both environmental covariates and spatiotemporal dependency in catches to historical data from the bottom-trawl survey in the Gulf of Alaska. Each pixel on the map is 2 km^2 and represents the CPUE realized when a station is sampled at that location in the simulated surveys conducted in this study.

2-km resolution on the basis of a single but random sample from the posterior predictive distribution of the models while accounting for the sampling process. In other words, simulated CPUE was calculated as the product of sampled fish occurrence and sampled density. Sampled fish occurrence was estimated by using a Bernoulli trial with the probability determined by the parameter samples taken from the posterior predictive distribution (in practice, a random Markov chain Monte Carlo [MCMC] run was chosen and parameter values were taken from it). Sampled density was estimated by using a sample from a Gaussian distribution on the link scale with the mean and variance derived from parameter values taken from a randomly chosen MCMC run (the sample value was exponentiated by using the natural exponential function to convert it to real space).

With this approach, predictions accounted for all sources of uncertainty included in the model and created a noisier CPUE distribution that was more reflective of "true" patterns than the mean MCMC prediction. Environmental covariate values were determined by kriging with the semivariogram model that best fit the historical survey data (Kotwicki and Ono, 2019), as implemented by the function autofitVariogram in the R package automap (vers. 1.0-16; Hiemstra et al., 2009). All geographic coordinates were converted into an Albers projection in order to preserve distances prior to analysis.

Simulation of surveys

The CPUE distributions defined over the grid with the finer resolution of 2 km were superimposed on the grid with a 5-km resolution for the surveys in the GOA before the simulated surveys were generated. Each station sampled during surveys in the GOA (i.e., each 25-km^2 grid cell), therefore, contained an average of approximately 4–7 of the 2-km^2 grid cells with density data. A variety of scenarios with different combinations of estimators and sampling designs were then implemented to generate simulated surveys over the modeled CPUE distributions for each of the 10 survey years between 1996 and 2015 and for each of 3 commercially important species: Pacific cod, Pacific ocean perch, and arrowtooth flounder.

In addition to the traditional stratified-random sampling design and the proposed stratification sampling design based on an IS, we considered 2 additional sampling designs, simple random sampling and systematic sampling, in conjunction with both the model-based estimator and the design-based estimator, for a total of 8 potential scenarios. The scenario in which the design-based estimator is paired with the systematic sampling design was excluded from this analysis because of its unsuitability for the survey area in the GOA. Because the survey area is characterized by relatively wide strata on the continental shelf but extremely narrow strata along the continental slope, stations are too far apart to adequately cover the slope area. The remaining 7 scenarios consisted of the use of the design-based estimator with 3 different sampling designs—simple random sampling (SRS), stratified-random sampling based on ISes (WIS) (described later in the "Stratified-random sampling based on information scores" section), and TRS—and the use of the model-based estimator in the R package VAST (vers. 3.3.0; Thorson, 2019) with 4 different sampling designs—systematic sampling (VSY), simple random sampling (VRS), stratified-random sampling based on ISes (VIS), and traditional stratified-random sampling (VTRS).

We simulated 100 replicate surveys, each consisting of 820 stations, for each of the 10 years in which surveys had been conducted, resulting in 82,000 simulated stations per survey year for each scenario. All analyses were conducted in R, vers. 3.6.1 (R Core Team, 2019).

Design-based approaches

Traditional stratified-random sampling In the stratified-random sampling design used since the inception of the bottom-trawl survey of the GOA in 1984, the survey area is divided into 59 strata defined by water depth, bottom terrain (e.g., shelf, gully, and slope), and statistical management areas (von Szalay and Raring, 2018). Following this traditional design, we allocated stations among the strata for species k by using a modified Neyman strategy for optimal allocation (Cochran, 1977):

$$n_{hk} = \frac{\frac{nN_h s_{hk} a_h}{\sqrt{c_h}}}{\sum_h \frac{N_h s_{hk} a_h}{\sqrt{c_h}}}, \quad (3)$$

where n_{hk} = the sample size for species k in stratum h;
n = the total sample size;
N_h = the population size for stratum h;
s_{hk} = the standard deviation of species k in stratum h;
a_h = the area of stratum h; and
c_h = the cost to conduct a trawl tow in stratum h.

Catch rates, stratum variances, and stratum areas from the surveys conducted in 1990–2015 were used to allocate sampling effort among strata for each previous survey year and for each of the 50 principal GOA groundfish species that the historical survey was designed to sample. The estimated time to perform a trawl tow in a given stratum was used as a cost variable because tows in deeper strata have a greater probability of unacceptable gear performance and take longer to complete. A mean sample size was calculated across years for each principal species, and the sample size for each species was then weighted by each species' commercial value, which was defined as the product of the mean biomass and its ex-vessel value in 2015. The calculated sample sizes, representing the numbers of trawl tows allocated to the various strata, were rounded to whole numbers while ensuring that each stratum was allocated at least 2 samples.

The allocated stations within each stratum were randomly selected without replacement from the 2-km-resolution grid described earlier. Sample mean ($\bar{x}_{hk}$)

and standard deviation (S_{hk}) for species k were calculated by stratum and were used to generate the survey mean ($\overline{X}_k$) and variance ($S^2_{\overline{x}k}$) for a stratified-random sampling design according to the following equations:

$$\overline{X}_k = \frac{1}{N}\sum_{h=1}^{20} N_h \overline{x}_{hk}, \text{ and} \quad (4)$$

$$S^2_{\overline{x}k} = \sum_{h=1}^{20}\left(\frac{N_h}{N}\right)^2 \left(\frac{N_h - n_{hk}}{N_h}\right)\left(\frac{s^2_{hk}}{n_{hk}}\right). \quad (5)$$

Stratified-random sampling based on information scores As an alternative method of stratification to the traditional scheme, we propose the IS approach to stratified-random sampling. This novel approach uses spatial and temporal information of abundance and temporal information of variation in abundance to derive an IS for each sampling unit. A high IS should identify areas where abundance tends to be high, areas where the abundance is highly variable over time, or a combination of these characteristics. Sampling in such areas is likely to provide most information about population abundance, composition, and trends in abundance, all of which are critical for use in stock assessment models and for acquisition of other types of information about sampled populations and temporal trends in population parameters. Information scores could be used to stratify the survey area and provide a basis for prioritizing areas with high fish density and high variance in fish density to ensure that more stations are allocated to strata with higher expected abundance and variability in abundance. Given this logic, we propose an IS that is calculated for each of the 15,718 eligible 5-by-5-km grid cells in the survey area as follows:

$$IS_{ik} = \overline{\widehat{CPUE}}_{ik}^2 + \frac{\mathrm{Var}(\widehat{CPUE}_{ik})}{n}, \quad (6)$$

where $\overline{\widehat{CPUE}}_{ik}$ = the mean predicted CPUE of species k in grid cell i over the 10 survey years between 1996 and 2015.

The $\widehat{CPUE}_{ik}$ of grid cell i (5-by-5 km) for a given year was calculated as the mean prediction of the simulated densities of all 2-by-2-km grid cells within it. By squaring the mean predicted CPUE, we ensure that the 2 terms have the same units and equal weight.

To determine how to stratify on the basis of discretizing the ISes into bins of similar values, we first examined how the scores were distributed. We found the distribution of the 15,718 ISes to be highly positively skewed for all species (Pearson's coefficient of skewness ranged between 8.7 for arrowtooth flounder and 43.5 for Pacific ocean perch; Suppl. Fig. 1 [online only]).

These values were sorted from low to high, and evenly spaced breakpoints were inserted to generate 20 strata, each with 786 stations. The choice to use 20 strata resulted from observations about the scores. These observations were that approximately 5% of the ISes were equal to zero, and a similar proportion of the scores on the opposite end of the distribution were of the same order of magnitude, resulting in 2 strata that contained the extreme values on both ends of the distribution with other strata having intermediate values. In a sensitivity analysis, we found no indication of substantial differences in results when either 19 or 21 strata were used. Furthermore, 20 strata is a reasonable number for the survey in the GOA and is also the number of strata being considered for a revised sampling design for this survey.

The number of survey stations allocated to the different strata was weighted by the mean IS of each stratum. First, we used the Neyman algorithm to determine the sample allocation (Lavrakas, 2008):

$$n_h = \frac{n(N_h s_h)}{\sum_{h=1}^{20} N_h s_h}. \quad (7)$$

Then, to weight the allocation among strata by using the mean IS of each stratum, the weights were calculated as follows:

$$w_h = \frac{\sqrt{\overline{IS}_h}}{\sum_{h=1}^{20}\sqrt{\overline{IS}_h}}, \quad (8)$$

where w_h = the weight of stratum h, and

$\overline{IS}_h$ = the mean information score for stratum h.

In this equation, substituting $\sqrt{\overline{IS}_h}$ for s_h in Equation 7 and algebraically simplifying the new equation (N_h is a constant and cancels out) results in n_h being equal to nw_h, which is the sample size of stratum h weighted by its information score.

Some stations originally assigned to the strata with the highest ISes were reallocated to strata receiving fewer than 2 stations to make variance calculations possible for all strata. This procedure for station allocation among strata was repeated for each species.

The allocated stations within each stratum were randomly selected without replacement from the grid with a 5-km resolution for the survey in the GOA. A random grid cell from the 2-km-resolution grid was then sampled to represent the CPUE of the entire station. Sample mean and standard deviation were calculated by stratum and were used to generate the survey mean and variance for a stratified-random sampling design similar to the procedure used for the traditional stratified-random approach described in the previous section.

Model-based approaches

The model-based estimator was a spatiotemporal delta model consisting of a binomial model for the probability of encounter and a user-selected model for positive catch rates, as implemented in the VAST package (Thorson, 2019). In a report of their recent work, Thorson et al. (2021) noted that the choice of distributional assumptions can

have a substantial effect on the scale of the biomass index estimated from such spatiotemporal models; therefore, we tested a range of assumptions to determine which provided the best fit and accuracy. We considered 2 different observation error distributions for positive catch rates, lognormal and gamma, and whether or not to correct values for retransformation bias (Thorson and Kristensen, 2016).

The hurdle models included *year* as a fixed effect, a spatial random field for each model component (encounter and positive catch rate), and independent spatiotemporal random fields for the positive catch rate component (Suppl. Table) (online only). The spatiotemporal term for encounter probability was not estimated because of the lack of consistent convergence among replicate simulated surveys. A model resolution of 500 knots was used, and bilinear interpolation was implemented to extrapolate from knot locations in order to generate predictions at each location in the same 2-km-resolution grid used in the operating model. Anisotropy was estimated. The models for each scenario differed only in terms of the observation error model used for positive catch rates (gamma versus lognormal distribution) and by whether retransformation bias was addressed (i.e., with or without epsilon bias correction) (Thorson and Kristensen, 2016). All models were run with the VAST package (Thorson et al., 2015) and the tools available in FishStatsUtils (vers. 2.6.0; available from website, accessed October 2019).

A customized 2-km-resolution extrapolation grid was created as a subset of the standard GOA survey grid (depths <1000 m), which excluded all grid cells known to be untrawlable. This custom grid was used to ensure that the VAST estimation model only integrated densities from trawlable areas or areas with an unknown trawlability status in order to make the estimates of biomass and its variance from the model-based approaches comparable to those from the design-based approaches. The results of the 4 different combinations of settings, between the 2 observation models for positive catch rates and whether or not the retransformation bias was addressed, for each scenario and species were compared with respect to the performance metrics described later in the "Performance metrics" section. The combination of settings that resulted in the lowest relative root-mean-square error (rRMSE) for a given scenario and species was selected for final comparison with the other scenarios (Table 1).

Simple random sampling Simulated CPUE values from the operating model were sampled by using simple random sampling. These values were then used as input to the VAST estimation model, along with the associated data on location and year for CPUE observations.

Systematic sampling A rectangular grid encompassing the entire survey area in the GOA was created by identifying the extreme latitudes and longitudes spanning the survey area. An iterative procedure was used to determine that the length of the square grid cells that would result in approximately 820 uniformly spaced stations falling within the survey area was approximately 20 km. To generate multiple iterations of systematic surveys, the origin of the survey grid was altered between iterations by randomly sampling a set of coordinates from within the grid cell in the extreme southeast corner of the survey grid. This 20-km^2 survey grid was, in turn, superimposed on the nominal 2-km-resolution grid of simulated fish densities. The 2-km^2 density grid cells within each of the 820 uniformly spaced grid cells were identified, and the density associated with the 2-km^2 grid cell closest to the center of the survey grid cell was used to represent the density of the entire survey grid cell.

Stratified-random sampling based on information scores Simulated CPUE estimates from the operating model were sampled by using an IS-based stratified-random sampling design. These values were then used as input to the VAST estimation model, along with the associated data on location and year for CPUE observations.

Traditional stratified-random sampling Based on the same principles described for the traditional stratified-random sampling in the "Design-based approaches" section, the station allocation by stratum scheme replicated the sampling design used for the bottom-trawl survey in the GOA in 2007 that consisted of 825 stations allocated to the 59 survey strata. However, rather than sampling directly from the 2-km-resolution CPUE grid, the stations were sampled from the grid with a 5-km resolution used for the survey in the GOA, and the CPUE associated with each station was based on the mean of the 2-km^2 CPUE grid cells within it.

Performance metrics

Three performance metrics were used to evaluate the relative performance of the 7 scenarios that were used to simulate abundance: coefficient of variation (CV), relative bias, and rRMSE. Each metric was applied to estimates of biomass and its associated variance and was calculated separately for each year and species. The true biomass was calculated as the product of the trawlable area of the survey area in the GOA and the arithmetic mean of simulated CPUE (with observation error) from all 65,863 trawlable grid cells. The true variance was calculated for each year as the variance of the replicate simulated biomass estimates:

$$\sigma_T^2 = \frac{\sum_S (B_S - B_T)^2}{N}, \quad (9)$$

where σ_T^2 = a "true" variance of the abundance index based on 100 simulated surveys;
N = the total number of simulated surveys (i.e., 100);
B_S = the estimated biomass realized in simulation survey s; and
B_T = the "true" biomass estimated from simulated density grids.

Bias of both biomass and its variance was defined as the mean of the deviations between the respective value of each simulation and the true value. The relative bias (RB)

Table 1

Relative root-mean-square errors (rRMSEs) for 7 scenarios with different combinations of estimators and sampling designs used to estimate biomass and its variance for arrowtooth flounder (*Atheresthes stomias*) (ATF), Pacific cod (*Gadus macrocephalus*) (COD), and Pacific ocean perch (*Sebastes alutus*) (POP) in the Gulf of Alaska. The observation error model for positive catch rates and the approach to bias correction are indicated for the scenarios in which the model-based estimator was used. The model-based estimator was the vector autoregressive spatiotemporal (VAST) model in the R package VAST. The design-based estimator was developed by Wakabayashi et al. (1985). One of the sampling designs was a stratified-random design based on information scores. The scenarios with the best overall performance for each species have the lowest values for biomass and its variance, which are indicated with asterisks. Analysis of scenarios was based on data from the bottom-trawl surveys conducted in the Gulf of Alaska during 1996–2015 by the NOAA Alaska Fisheries Science Center. The abbreviations in parentheses represent the 7 scenarios.

Species	Estimator and sampling design (scenario)	Observation error model	Bias correction	rRMSE	
				Biomass	Variance
Model-based approaches					
ATF	VAST systematic (VSY)	delta-gamma	Off	0.16	>1.00
	VAST simple random (VRS)	delta-lognormal	Off	0.05	0.30
	VAST information score (VIS)	delta-gamma	On	0.24	0.25
	VAST stratified random (VTRS)	delta-gamma	On	0.04*	0.18*
COD	VAST systematic (VSY)	delta-lognormal	On	0.07	0.69
	VAST simple random (VRS)	delta-lognormal	On	0.10	0.18
	VAST information score (VIS)	delta-gamma	On	0.13	0.15*
	VAST stratified random (VTRS)	delta-gamma	On	0.05*	0.15*
POP	VAST systematic (VSY)	delta-gamma	On	0.17	0.98
	VAST simple random (VRS)	delta-lognormal	On	0.14	0.31
	VAST information score (VIS)	delta-gamma	Off	0.40	0.18*
	VAST stratified random (VTRS)	delta-gamma	On	0.12*	0.28
Design-based approaches					
ATF	Simple random (SRS)	–	–	0.07	0.19
	Information score (WIS)	–	–	0.02*	0.05*
	Stratified random (TRS)	–	–	0.08	0.28
COD	Simple random (SRS)	–	–	0.06	0.15
	Information score (WIS)	–	–	0.03*	0.09*
	Stratified random (TRS)	–	–	0.06	0.19
POP	Simple random (SRS)	–	–	0.17	0.39
	Information score (WIS)	–	–	0.03*	0.10*
	Stratified random (TRS)	–	–	0.16	0.40

of these estimates was calculated within each year and species as follows:

$$RB = \frac{\frac{1}{n}\sum_{i=1}^{n}\left(\theta_i - \theta_{True}\right)}{\theta_{True}}, \quad (10)$$

where θ_i = the value (biomass or variance) of the ith simulation replicate, and

θ_{True} = the true value (biomass or variance), over 100 simulation replicates.

The CV was defined as follows:

$$CV = \frac{\sqrt{Var(\theta)}}{\theta_{True}}, \text{ where} \quad (11)$$

$$Var(\theta) = \frac{1}{n}\sum_{i=1}^{n}\left(\theta_i - \theta_{mean}\right)^2,$$

and $Var(\theta)$ = the mean of the square deviations between the value (biomass or variance) of each simulation and the mean biomass or variance.

The mean square error was defined as the sum of the bias squared and variance, and the rRMSE was calculated as follows:

$$rRMSE = \frac{\sqrt{Bias^2 + Var}}{\theta_{True}}, \quad (12)$$

where $Bias$ = the absolute bias as defined by the numerator in Equation 10.

Results

Of the 7 scenarios with different combinations of estimators and sampling designs that were considered in this

study, the best scenario for estimating biomass and its variance across all performance metrics and all species was the design-based estimator coupled with the stratified-random sampling design in which strata were defined by ISes. This IS scenario consistently had the lowest CV and rRMSE and was generally unbiased (Table 1, Figs. 3–8). In contrast, the scenario that paired the model-based estimator of biomass with this sampling design (VIS scenario) was by far the worst-performing scenario by all 3 performance metrics for all species. It had the highest CV and rRMSE and was the most biased for all species. However, for variance, the VIS scenario performed considerably better, with no bias for 2 of the species and with an rRMSE similar to or smaller than that of the other model-based variance scenarios.

The performance of the combination of the design-based estimator with the traditional stratified-random sampling design (TRS scenario) was generally average for estimates of biomass and its variance among the 7 scenarios. The performance of this scenario was most similar to that of the scenario that pairs the design-based estimator with a simple random sampling design (Figs. 3–8).

The performance of scenarios differed among species. Of the 7 scenarios for estimating biomass, 5 scenarios performed relatively well for arrowtooth flounder (VRS, VTRS, SRS, WIS, and TRS). A sixth scenario (VSY) performed well for Pacific cod in terms of rRMSE (rRMSE <0.10). However, only the WIS had an rRMSE below 0.10 for Pacific ocean perch (Table 1). All of the scenarios with the designed-based estimator of biomass were consistently unbiased (mean relative bias <0.005 for all species), whereas the scenarios with the model-based estimator were generally negatively biased, except the VRS for arrowtooth flounder and the VIS across all species (Figs. 3–5).

Of the 7 scenarios for estimating variance in biomass, only the WIS consistently performed well as measured by rRMSE (rRMSE: 0.06–0.10). Although most of the other scenarios were relatively unbiased for Pacific cod and

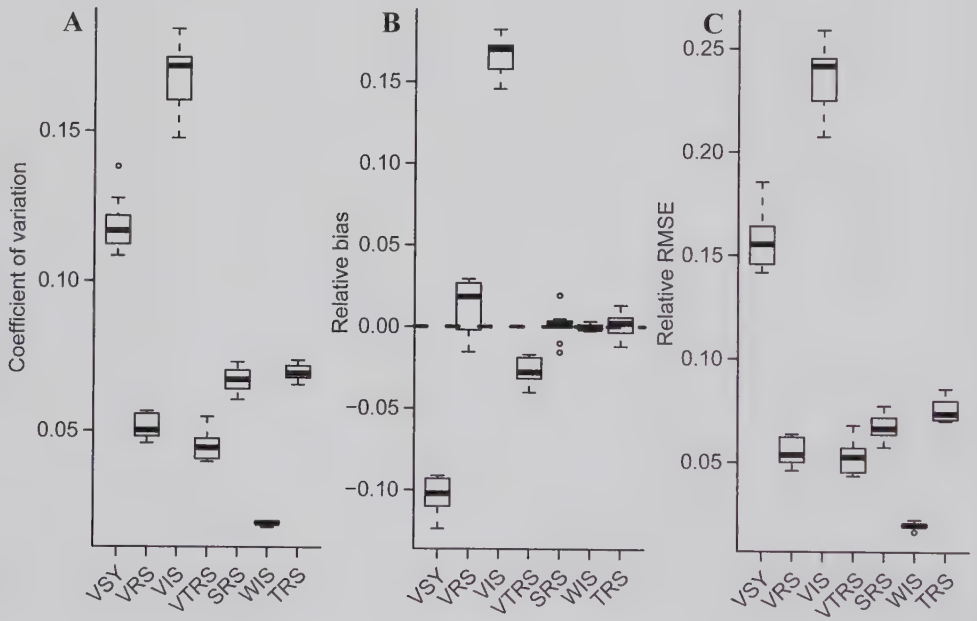

Figure 3

Relative performance of the 7 scenarios with different combinations of estimators and sampling designs in estimating biomass for arrowtooth flounder (*Atheresthes stomias*) based on 100 simulated bottom-trawl surveys in the Gulf of Alaska. Each box plot represents the distribution of a performance metric, (**A**) coefficient of variation, (**B**) relative bias, or (**C**) relative root-mean-square error (RMSE), for a scenario over the 10 survey years between 1996 and 2015. The model-based estimator, the vector autoregressive spatiotemporal (VAST) model in the R package VAST, was paired with 4 sampling designs: systematic (VSY scenario), simple random (VRS scenario), stratified random based on information scores (VIS scenario), and traditional stratified random (VTRS scenario). The designed-based estimator was paired with 3 sampling designs: simple random (SRS scenario), stratified random based on information scores (WIS scenario), and traditional stratified random based on Neyman allocation (TRS scenario). In each box plot, the thick black line is the median. The lower and upper hinges of the box plots correspond to the 25th and 75th percentiles. The whiskers extend from the hinge to the farthest value no more than 1.5 times the interquartile range (distance between the 25th and 75th percentiles). Data points beyond the end of the whiskers, outliers, are plotted individually.

Pacific ocean perch (with VSY being the only exception), they produced relatively large variances, which resulted in relatively large rRMSEs (Figs. 6–8).

The VTRS scenario performed better in estimating biomass than 2 of the design-based methods (TRS and SRS), as well as all of the other model-based scenarios in terms of CV and rRMSE, but this scenario was somewhat negatively biased (mean relative bias ranged between −0.02 and −0.05). The only scenario with the model-based estimator of biomass that had a comparable rRMSE was the one with the simple random sampling design (VRS scenario), but only for arrowtooth flounder and Pacific ocean perch (Figs. 3–5). The performance of the VTRS in estimating variance in biomass, on the other hand, was generally similar to that of the other methods (except for the poorly performing VSY and the best performing WIS) across all performance metrics (Figs. 6–8).

The VSY scenario for estimating the variance of biomass had extreme values of all performance metrics for Pacific cod and Pacific ocean perch (CV: 0.64–0.78; mean relative bias: from −0.28 to −0.60; rRMSE: 0.7–1.0; Figs. 7–8) but even more extreme values for arrowtooth flounder (CV and rRMSE >1.0). The VSY scenario for estimating biomass variance for arrowtooth flounder, therefore, was excluded from the boxplots in Figure 6 because it was an extreme outlier, which if included, would have made comparisons of the other scenarios difficult. The poor performance of the VSY scenario for estimating variance was due to the highly skewed variance distributions for all species, with ranges spanning as much as 5 orders of magnitude for arrowtooth flounder (Suppl. Fig. 2) (online only).

Apart from the differences in the relative performance of the various scenarios for estimating biomass and variance, differences in the performance of each scenario among species are notable. All of the scenarios performed considerably worse in estimating biomass for Pacific ocean perch than for the other 2 species in terms of rRMSE. The difference in performance across species was small for the

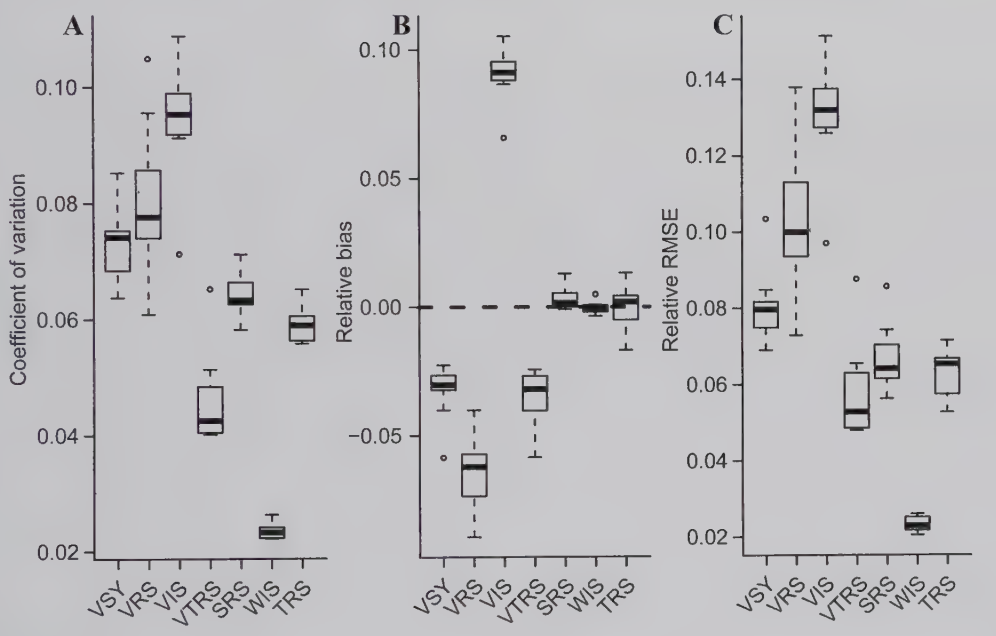

Figure 4

Relative performance of the 7 scenarios with different combinations of estimators and sampling designs in estimating biomass for Pacific cod (*Gadus macrocephalus*) based on 100 simulated bottom-trawl surveys in the Gulf of Alaska. Each box plot represents the distribution of a performance metric, (**A**) coefficient of variation, (**B**) relative bias, or (**C**) relative root-mean-square error (RMSE), for a scenario over the 10 survey years between 1996 and 2015. The model-based estimator, the vector autoregressive spatiotemporal (VAST) model in the R package VAST, was paired with 4 sampling designs: systematic (VSY scenario), simple random (VRS scenario), stratified random based on information scores (VIS scenario), and traditional stratified random (VTRS scenario). The designed-based estimator was paired with 3 sampling designs: simple random (SRS scenario), stratified random based on information scores (WIS scenario), and traditional stratified random based on Neyman allocation (TRS scenario). In each box plot, the thick black line is the median. The lower and upper hinges of the box plots correspond to the 25th and 75th percentiles. The whiskers extend from the hinge to the farthest value no more than 1.5 times the interquartile range (distance between the 25th and 75th percentiles). Data points beyond the end of the whiskers, outliers, are plotted individually.

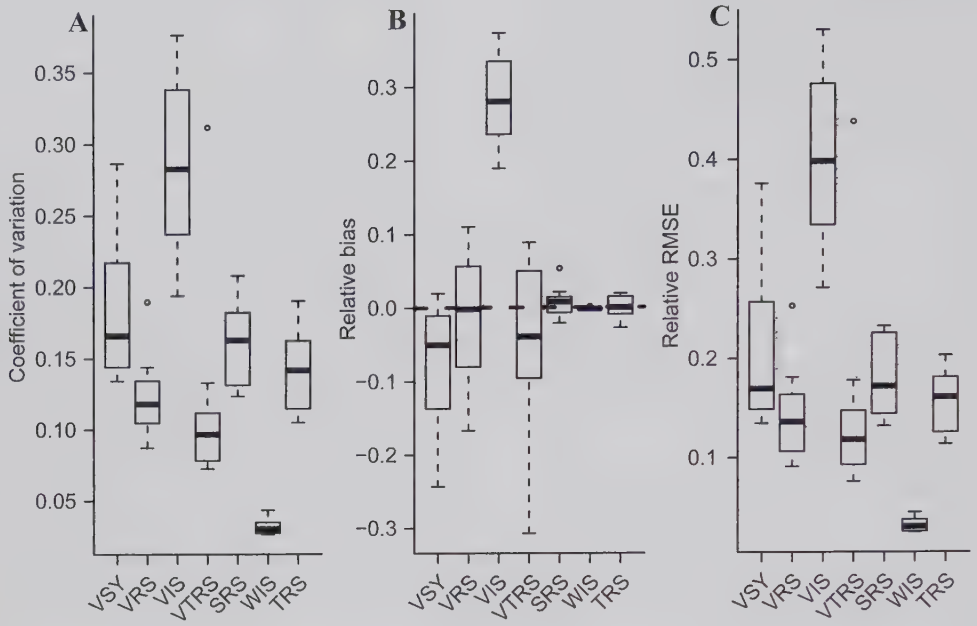

Figure 5

Relative performance of the 7 scenarios with different combinations of estimators and sampling designs in estimating biomass for Pacific ocean perch (*Sebastes alutus*) based on 100 simulated bottom-trawl surveys in the Gulf of Alaska. Each box plot represents the distribution of a performance metric, (**A**) coefficient of variation, (**B**) relative bias, or (**C**) relative root-mean-square error (RMSE), for a scenario over the 10 survey years between 1996 and 2015. The model-based estimator, the vector autoregressive spatiotemporal (VAST) model in the R package VAST, was paired with 4 sampling designs: systematic (VSY scenario), simple random (VRS scenario), stratified random based on information scores (VIS scenario), and traditional stratified random (VTRS scenario). The designed-based estimator was paired with 3 sampling designs: simple random (SRS scenario), stratified random based on information scores (WIS scenario), and traditional stratified random based on Neyman allocation (TRS scenario). In each box plot, the thick black line is the median. The lower and upper hinges of the box plots correspond to the 25th and 75th percentiles. The whiskers extend from the hinge to the farthest value no more than 1.5 times the interquartile range (distance between the 25th and 75th percentiles). Data points beyond the end of the whiskers, outliers, are plotted individually.

top-performing WIS scenario (an rRMSE of 0.03 for Pacific ocean perch versus values of 0.02 and 0.025 for arrowtooth flounder and Pacific cod, respectively). However, the difference was much higher for all of the other scenarios for estimating biomass, with absolute differences in rRMSE between Pacific ocean perch and the other 2 species ranging from 0.01 to 0.16 for arrowtooth flounder and from 0.04 to 0.27 for Pacific cod (Table1). In contrast, all but one of the scenarios for estimating variance of biomass performed best for Pacific cod, with absolute differences in the rRMSE between Pacific cod and the other 2 species ranging from 0.03 to >0.31 for arrowtooth flounder and from 0.01 to 0.29 for Pacific ocean perch. The single exception was the WIS scenario, which had a smaller rRMSE for arrowtooth flounder (0.05 for arrowtooth flounder versus a value of 0.09 for Pacific cod) but a larger rRMSE for Pacific ocean perch (0.10). The differences in relative performance of the scenarios between Pacific ocean perch and arrowtooth flounder were mixed.

Discussion

The objective of this study was to assess the performance of 7 scenarios with different combinations of sampling designs and estimators and to compare their statistical robustness. Although we used 3 different performance metrics to evaluate statistical robustness, for conciseness, we highlight herein the best-performing scenarios on the basis of only rRMSE (those with the lowest rRMSEs are considered the best performing), which includes both the bias and variance components teased apart by the other performance metrics.

The results of the simulation analyses indicate that, compared to the scenario that paired the design-based estimator with the existing sampling design (TRS), 4 scenarios performed better for arrowtooth flounder, 3 scenarios performed the same or better for Pacific cod, and 3 scenarios performed better for Pacific ocean perch. Of these scenarios, only the design-based WIS and the model-based VTRS scenarios performed better than the

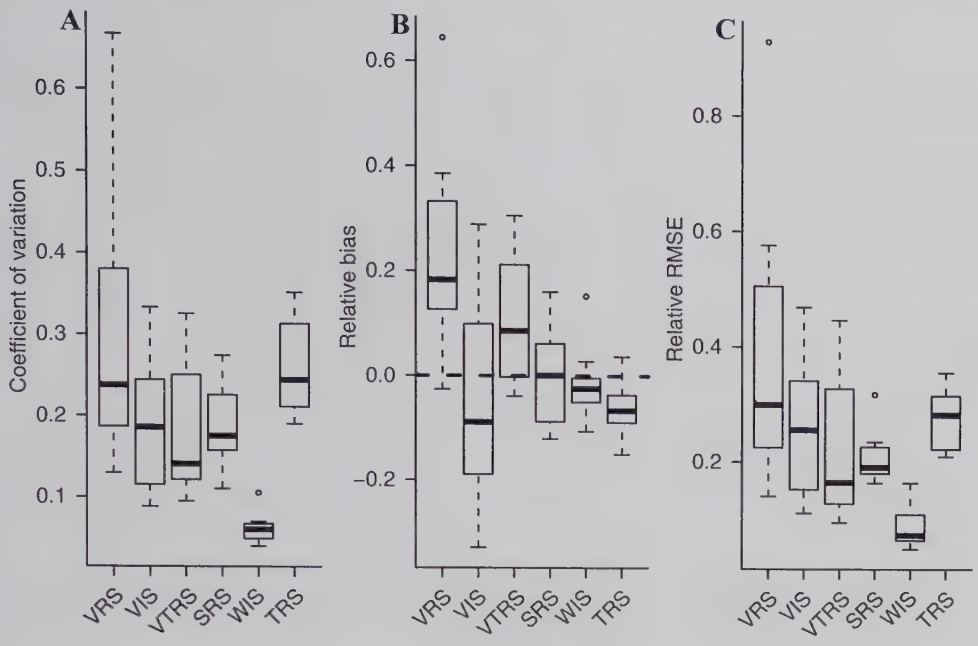

Figure 6

Relative performance of the 7 scenarios with different combinations of estimators and sampling designs in estimating the variance of biomass for arrowtooth flounder (*Atheresthes stomias*) based on 100 simulated bottom-trawl surveys in the Gulf of Alaska. Each box plot represents the distribution of a performance metric, (**A**) coefficient of variation, (**B**) relative bias, or (**C**) relative root-mean-square error (RMSE), for a scenario over the 10 survey years between 1996 and 2015. The box plots for the VSY scenario for this species have been omitted for readability of the vertical axis values of the other methods. The model-based estimator, the vector autoregressive spatiotemporal (VAST) model in the R package VAST, was paired with 4 sampling designs: systematic (VSY scenario), simple random (VRS scenario), stratified random based on information scores (VIS scenario), and traditional stratified random (VTRS scenario). The designed-based estimator was paired with 3 sampling designs: simple random (SRS scenario), stratified random based on information scores (WIS scenario), and traditional stratified random based on Neyman allocation (TRS scenario). In each box plot, the thick black line is the median. The lower and upper hinges of the box plots correspond to the 25th and 75th percentiles. The whiskers extend from the hinge to the farthest value no more than 1.5 times the interquartile range (distance between the 25th and 75th percentiles). Data points beyond the end of the whiskers, outliers, are plotted individually.

TRS scenario for all 3 species, with only the WIS scenario consistently performing substantially better than the TRS scenario for estimates of both biomass and its variance for all species (with rRMSEs >50% lower than those for the TRS). The reduction in rRMSE from the WIS scenario to the TRS scenario ranged among species between 58% and 81% for biomass and between 53% and 82% for variance in biomass, with the greatest reduction observed for Pacific ocean perch. It is likely that the traditional sampling design is not as suitable for assessing abundance of Pacific ocean perch because of the patchy distribution of this species in the GOA (Lunsford et al., 2001; Clausen and Fujioka, 2007), a pattern that requires larger sample sizes in areas of high density than in other areas. In summary, our results indicate that the combination of stratified-random sampling with model-based estimation methods is likely to produce the best results.

These results have at least 2 important implications for the redesign of and improvements to the method of abundance estimation for the bottom-trawl survey conducted in the GOA. First, in the short term, estimates of abundance can be improved immediately by using model-based estimators in combination with traditional stratified-random sampling. Second, in the long term, basing stratification on ISes could be an additional change that can improve estimates for species with spatially restricted or patchy distributions, when used in combination with design-based estimators.

Recommendation to develop model-based estimators

Our results indicate clear improvements in estimation for all species when the model-based estimator was used with a stratified-random sampling design. This finding is important because it indicates that some of the losses in

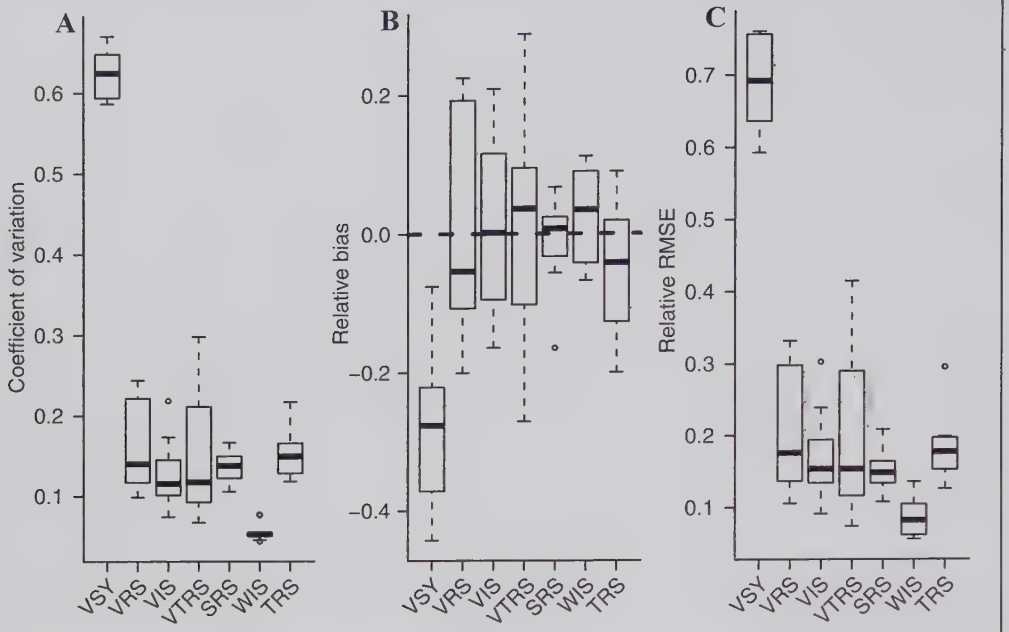

Figure 7

Relative performance of the 7 scenarios with different combinations of estimators and sampling designs in estimating the variance of biomass for Pacific cod (*Gadus macrocephaluls*) based on 100 simulated bottom-trawl surveys in the Gulf of Alaska. Each box plot represents the distribution of a performance metric, (**A**) coefficient of variation, (**B**) relative bias, or (**C**) relative root-mean-square error (RMSE), for a scenario over the 10 survey years between 1996 and 2015. The model-based estimator, the vector autoregressive spatiotemporal (VAST) model in the R package VAST, was paired with 4 sampling designs: systematic (VSY scenario), simple random (VRS scenario), stratified random based on information scores (VIS scenario), and traditional stratified random (VTRS scenario). The designed-based estimator was paired with 3 sampling designs: simple random (SRS scenario), stratified random based on information scores (WIS scenario), and traditional stratified random based on Neyman allocation (TRS scenario). In each box plot, the thick black line is the median. The lower and upper hinges of the box plots correspond to the 25th and 75th percentiles. The whiskers extend from the hinge to the farthest value no more than 1.5 times the interquartile range (distance between the 25th and 75th percentiles). Data points beyond the end of the whiskers, outliers, are plotted individually.

precision expected from design-based estimators in cases with reduced survey effort (Oyafuso et al., 2021) can perhaps be mitigated by the use of spatiotemporal model-based methods, such as those in the VAST package. Similar improvements were also observed when simple random sampling was used with the model-based estimator.

In a related study, in which the effect of sampling density changes on biomass estimates was examined for the same 3 species analyzed here, the model-based estimator when used with the stratified-random sampling design performed better than the design-based estimator for all 3 species at 4 different levels of survey effort (von Szalay et al.[2]). In other studies, the advantages of a spatiotemporal model-based estimator have been demonstrated more broadly. O'Leary et al. (2020) found that the spatial and temporal scope of total biomass for walleye pollock (*G. chalcogrammus*) in the northern Bering Sea was improved in a stock assessment model when a model-based biomass index from multiple surveys was used as model input in combination with the standard design-based estimates. In addition, stock assessment models for dusky rockfish (*S. ciliatus*) and northern rockfish (*S. polyspinis*) in the GOA have incorporated such model-based estimates because they are less noisy than the sampling-design-based CVs (Lunsford et al., 2015; Cunningham et al., 2018).

The improvements we observed with the model-based estimator are likely due to an increase in the effective sample size when data from multiple surveys are used to derive biomass estimates. Thorson and Haltuch (2019) showed that the effective sample size increased by 17% and that the model fit was better, resulting in smaller standard errors of estimated spawning biomass, when a spatiotemporal model-based estimator was used in a stock synthesis assessment

[2] von Szalay, P. G., E. A. Laman, S. Kotwicki, L. A. K. Barnett, and K. Ono. In preparation. Quantifying the effects of sample size and species distribution on the precision and accuracy of abundance estimates from bottom trawl surveys in the Gulf of Alaska.

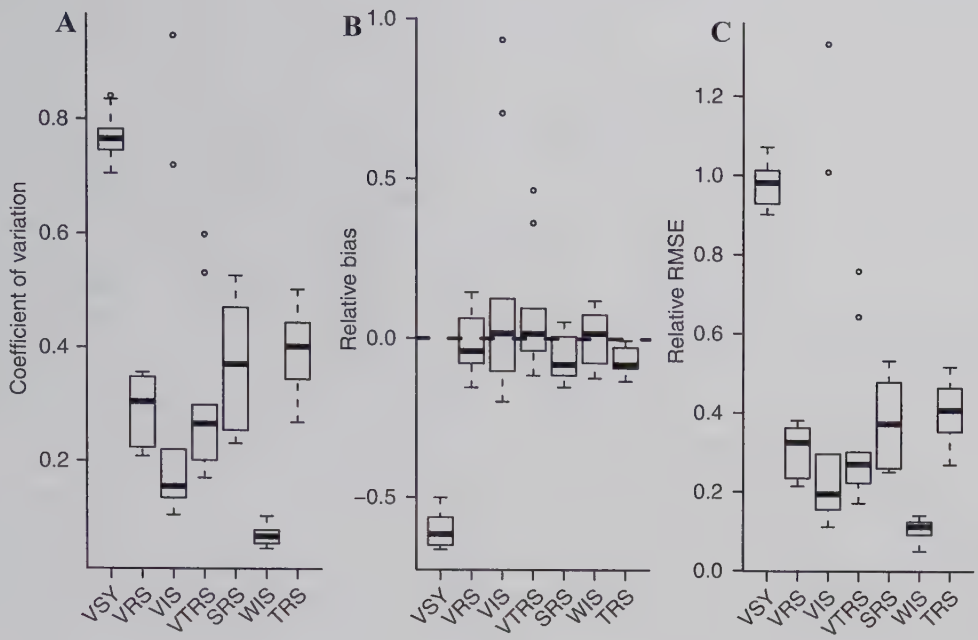

Figure 8

Relative performance of 7 scenarios with different combinations of estimators and sampling designs in estimating the variance of biomass for Pacific ocean perch (*Sebastes alutus*) based on 100 simulated bottom-trawl surveys in the Gulf of Alaska. Each box plot represents the distribution of a performance metric, (**A**) coefficient of variation, (**B**) relative bias, or (**C**) relative root-mean-square error (RMSE), for a scenario over the 10 survey years between 1996 and 2015. The model-based estimator, the vector autoregressive spatiotemporal (VAST) model in the R package VAST, was paired with 4 sampling designs: systematic (VSY scenario), simple random (VRS scenario), stratified random based on information scores (VIS scenario), and traditional stratified random (VTRS scenario). The designed-based estimator was paired with 3 sampling designs: simple random (SRS scenario), stratified random based on information scores (WIS scenario), and traditional stratified random based on Neyman allocation (TRS scenario). In each box plot, the thick black line is the median. The lower and upper hinges of the box plots correspond to the 25th and 75th percentiles. The whiskers extend from the hinge to the farthest value no more than 1.5 times the interquartile range (distance between the 25th and 75th percentiles). Data points beyond the end of the whiskers, outliers, are plotted individually.

model for lingcod (*Ophiodon elongatus*) in the California Current. However, we acknowledge that additional work with more than the 3 species examined in our study is needed before our results can be generalized. It is possible that the VAST estimator does not perform as well for species with a more limited spatial distribution.

Furthermore, both bias and variance tended to be high for the model-based estimator when the sampling design is highly unbalanced. This was the case for all 3 species when the VAST estimation model was paired with the IS-based sampling design (VIS scenario), which concentrated sampling density in areas of high biomass.

Recommendation to develop stratification methods based on information scores

For all 3 species, IS-based stratification in combination with design-based estimation yielded results that were by far better than any other method. The main reason this method outperformed the traditional design schemes (random and systematic) was that stratification was informed by historical data in the form of ISes, which can be described as estimated expectation of population abundance and its temporal variability. Of course, for this approach to be valid, one must be confident in the predictions of density based on historical data to adequately represent current and perhaps future species distributions. In contrast, the stratum boundaries in traditional random sampling are defined by depth and management area. Using ISes to stratify the survey area resulted in strata with more homogenous variances than the strata in the traditional Neyman allocation. This difference is due to the variance component of the IS, which increases the efficiency of IS-based stratification compared to that of the traditional stratification scheme. Furthermore, in contrast to using Neyman allocation, the use of ISes ensures that samples are representative in areas where density is persistently high and temporal variance is low. In Neyman allocation, strata with high density

but low variance are apportioned a relatively small number of stations. Such allocation is undesirable for fisheries surveys because, in addition to precise estimates of abundance, representative samples for other population measures, such as age and size compositions, are also needed. In the extreme case of the abundance of a stratum being very high but uniform, the Neyman strategy would allocate no samples to that stratum.

In the future, it may be problematic to use historical data to define stratum boundaries under the IS approach if fish distributions change in response to climate change as they are in many regions (Hobday and Evans, 2013; Maureaud et al., 2021; Hollowed et al., 2022). If the shift in distributions is relatively gradual over time, it may still be appropriate to use relatively recent data while excluding older data to define stratum boundaries on the basis of ISes. However, if the shift in distribution patterns is more abrupt, it may not be appropriate to use any sampling design that defines strata on the basis of historical data, as is the case for both the WIS and TRS approaches. In this situation, it may be necessary to conduct a pilot survey prior to the main survey to establish new stratum boundaries.

The finding that the design based on ISes outperformed the traditional sampling design is not surprising given that the stratification was performed individually for each species in the case of the WIS scenario. Therefore, this method would be applicable to only single-species surveys. In contrast, the stratification scheme used for the TRS scenario was first optimized for each species, but because the GOA survey is a multispecies survey, the realized station allocation to each stratum was based on a weighted average of several principal species. This weighting effectively resulted in less than optimal station allocation for each species. The comparison is nevertheless informative because it illustrates how much better the biomass and variance estimates are if we can focus on sampling individual species, given their importance to the fishery. Perhaps it has been a mistake to make so many compromises with the traditional weighting across too many species.

More research is needed to investigate how the relative performance of the WIS scenario compares with the TRS scenario in the context of a multispecies survey, in which the IS-based station allocation scheme would be subjected to the same compromises among several principal species as the traditional stratified-random sampling design. We envision generating multispecies ISes, which are linear combinations of the single-species scores associated with each of the principal species included in the TRS scenrio. Each component of these combinations could be weighted by a number of different factors important to management (e.g., the commercial value of each species, ecological importance of each species, or non-biological elements, such as cultural or political considerations).

Although both the absolute and relative performance of a multispecies version of the WIS would necessarily be lower than the performance of the single-species version, we expect it to perform better than the TRS scenario because the stratum boundaries and station allocation scheme are strictly driven by historical data and determined by the objective factors of fish density and its variance. Furthermore, it is likely that the IS approach can be improved by optimizing for both the relative weighting of the variance component and the number of strata used. In contrast, in the TRS scenario, strata are defined by ad hoc boundaries and depth of the management area, likely reducing the efficiency of the traditional sampling design. The allocation scheme of the TRS scenario also includes a penalty against strata that are relatively costly to sample in terms of time. This cost penalty may be problematic for estimating biomass and its variance for slope species, such as Pacific ocean perch and sablefish (*Anoplopoma fimbria*), which primarily inhabit these high-cost strata and are also more patchily distributed than species, such as Pacific cod and arrowtooth flounder, that inhabit the continental shelf. As a compromise with the objective to preserve the TRS approach, it may be feasible in the future to introduce a hybrid sampling design in which sampling for some species is done with the traditional design and sampling for other species, such as Pacific ocean perch, may be enhanced by sampling more in areas with high ISes.

The relatively poor performance of the model-based VIS scenario can likely be attributed to the unbalanced sampling design resulting from stratification based on ISes. Under this stratification scheme, in which the distributions of the ISes were highly skewed (Suppl. Fig. 1) (online only), the bulk of the stations were assigned to just a few strata while the minimum of 2 required stations were assigned to all of the remaining strata, concentrating the spatial distribution of samples used to extrapolate to the entire survey area. The performance of the VIS in estimating biomass was particularly poor for Pacific ocean perch because this species is primarily confined to a depth range of approximately 150–300 m, which exists only in a relatively narrow band on the upper continental slope of the survey area. Pacific cod and arrowtooth flounder, on the other hand, are more evenly distributed over a larger portion of the survey area (primarily over the relatively wide continental shelf); therefore, the effect of the unbalanced sampling design is less pronounced for them. The IS-based sampling design tailors the station allocation to individual strata, resulting in better performance than the traditional stratification scheme with designed-based estimators because stations are allocated to areas where fish are most likely to be, thereby reducing the variance in biomass estimates while having no effect on bias. However, it does not work well with the model-based estimator, which is sensitive to the highly unbalanced sampling dictated by the IS-based stratification.

Conclusions

The results of our analysis of 6 scenarios with different combinations of sampling designs and estimators, in comparison to the method used for the bottom-trawl survey conducted in the GOA since 1984, not only identify which scenario consistently outperformed the traditional approach but also indicate that the traditional approach of using a stratified-random sampling design with a design-based

estimator is not optimal for any of the 3 species considered in this study. Estimates of abundance can likely be improved immediately by using the model-based estimator in the VAST package in combination with the traditional stratified-random sampling design (VTRS scenario). In the long term, stratification based on the IS proposed in this study, when used with a design-based estimator, could be a useful alternative to the traditional approach in improving estimates of abundance for species, such as Pacific ocean perch, with spatially restrictive or patchy distributions. However, in subsequent work, interspecific tradeoffs in a multispecies context will be required to justify reconsidering the traditional sampling design. Nonetheless, this approach of combining an IS-based sampling design with a design-based Wakabayashi estimator is promising, particularly for single-species surveys or for multispecies surveys in areas with few interspecific differences in distribution.

Resumen

Desde 1984, se han utilizado prospecciones de arrastre de fondo con un diseño de muestreo aleatorio estratificado para la evaluación de poblaciones de especies de importancia comercial en el Golfo de Alaska. Se evaluó un nuevo diseño de muestreo estratificado para determinar si su uso podría mejorar la precisión y exactitud de las estimaciones de abundancia. En el enfoque propuesto para definir los estratos, se utilizaron datos de estudios históricos para generar lo que denominamos puntajes de información (ISes). Para determinar si el enfoque existente es óptimo, se comparó el esquema de estratificación tradicional con el nuevo método y otros 2 diseños de muestreo, utilizando tanto un estimador basado en el diseño como un estimador basado en el modelo con cada diseño. La robustez estadística, medida en términos del coeficiente de variación, sesgo y la raíz del error cuadrático medio, se comparó entre 7 escenarios con diferentes combinaciones de estimadores y diseños de muestreo mediante simulación con un modelo lineal generalizado mixto espaciotemporal condicionado a observaciones históricas de capturas por unidad de esfuerzo de 3 especies. La combinación del estimador basado en el diseño con el esquema de estratificación basado en los ISes fue el mejor escenario en todas las medidas de desempeño para todas las especies. Este escenario consistentemente presentó la varianza más baja y el menor error total, y en general, no estuvo sesgado. En contraste, la comparación del estimador basado en el modelo con este diseño de muestreo fue por mucho, el escenario con peor desempeño. El desempeño del enfoque existente fue promedio.

Acknowledgments

We thank J. Thorson for the development of the R package VAST and the working group formed during the International Council for the Exploration of the Sea Workshop on Unavoidable Survey Effort Reduction for providing valuable feedback and inspiration. We are grateful for N. Laman's development of a revised extrapolation grid used in the model-based methods, and we greatly appreciate the labor-intensive work of the many scientists and volunteers who have contributed to the bottom-trawl surveys conducted in the GOA over the years. Finally, we thank C. O'Leary, Z. Oyafuso, and 3 anonymous reviewers for their informative comments that helped to improve this manuscript.

Literature cited

Alverson, D. L., and W. T. Pereyra.
1969. Demersal fish explorations in the northeastern Pacific Ocean—an evaluation of exploratory fishing methods and analytical approaches to stock size and yield forecasts. J. Fish. Res. Board Can. 26:1985–2001.

Clausen, D. M., and J. T. Fujioka.
2007. Variability in trawl survey catches of Pacific ocean perch, shortraker rockfish, and rougheye rockfish in the Gulf of Alaska. *In* Biology, assessment, and management of North Pacific rockfishes. Univ. Alsk. Sea Grant Coll. Program Rep. AK-SG-07-01 (J. Heifetz, J. Dicosimo, A. J. Gharrett, M. S. Love, V. M. O'Connell, and R. D. Stanley, eds.), p. 411–428. Univ. Alsk. Sea Grant Coll. Program, Fairbanks, AK. [Available from website.]

Cochran, W. G.
1977. Sampling techniques, 3rd ed., 428 p. John Wiley and Sons, New York.

Cunningham, C. J., P.-J. F. Hulson, C. R. Lunsford, and D. H. Hanselman.
2018. Assessment of the northern rockfish stock in the Gulf of Alaska. *In* Stock assessment and fishery evaluation report for the groundfish resources of the Gulf of Alaska, 87 p. North Pac. Fish. Manag. Counc., Anchorage, AK. [Available from website.]

Hidiroglou, M. A., and M. Kozak.
2018. Stratification of skewed populations: a comparison of optimisation-based versus approximate methods. Int. Stat. Rev. 86:87–105.

Hiemstra, P. H., E. J. Pebesma, C. J.W. Twenhöfel, and G. B.M. Heuvelink.
2009. Real-time automatic interpolation of ambient gamma dose rates from the Dutch radioactivity monitoring network. Comp. Geosci. 35:1711–1721.

Hobday, A. J., and K. Evans.
2013. Detecting climate impacts with oceanic fish and fisheries data. Clim. Change 119:49–62.

Hollowed, A. B., A. C. Haynie, A. J. Hermann, K. K. Holsman, A. E. Punt, and C. S. Szuwalski.
2022. Implications of climate change on the Bering Sea and other cold water systems. Deep-Sea Res., II 201:105110.

ICES (International Council for the Exploration of the Sea).
2020. ICES workshop on unavoidable survey effort reduction (WKUSER). ICES Sci. Rep. vol. 2, issue 72, 92 p. [Available from website.]

Kotwicki, S., and K. Ono.
2019. The effect of random and density-dependent variation in sampling efficiency on variance of abundance estimates from fishery surveys. Fish Fish. 20:760–774.

Kotwicki, S., T. W. Buckley, T. Honkalehto, and G. Walters.
2005. Variation in the distribution of walleye pollock (*Theragra chalcogramma*) with temperature and implications for seasonal migration. Fish. Bull. 103:574–587.

Kotwicki, S., J. K. Horne, A. E. Punt, and J. N. Ianelli.
2015. Factors affecting the availability of walleye pollock to acoustic and bottom trawl survey gear. ICES J. Mar. Sci. 72:1425–1439.

Lavrakas, P. J. (ed.).
2008. Encyclopedia of survey research methods, 2 vols., 1072 p. SAGE Publ. Inc., Thousand Oaks, CA.

Lindgren, F., H. Rue, and J. Lindström.
2011. An explicit link between Gaussian fields and Gaussian Markov random fields: the stochastic partial differential equation approach. J. R. Stat. Soc., B 73:423–498.

Lunsford, C., L. Haldorson, J. T. Fujioka, and T. J. Quinn II.
2001. Distribution patterns and survey design considerations of Pacific ocean perch (*Sebastes alutus*) in the Gulf of Alaska. *In* Spatial processes and management of marine populations. Univ. Alsk. Sea Grant Coll. Program Rep. AK-SG-01-02 (G. H. Kruse, N. Bez, A. Booth, M. W. Dorn, S. Hills, R. N. Lipcius, D. Pelletier, C. Roy, S. J. Smith, and D. Witherell, eds.), p. 281–302. Univ. Alsk. Sea Grant Coll. Program, Fairbanks, AK. [Available from website.]

Lunsford, C. R., P.-J. F. Hulson, S. K. Shotwell, and D. H. Hanselman.
2015. Assessment of the dusky rockfish stock in the Gulf of Alaska. *In* Stock assessment and fishery evaluation report for the groundfish resources of the Gulf of Alaska, p. 1013–1102. North Pac. Fish. Manag. Counc., Anchorage, AK. [Available from website.]

Maureaud, A. A., R. Frelat, L. Pécuchet, N. Shackell, B. Mérigot, M. L. Pinsky, K. Amador, S. C. Anderson, A. Arkhipkin, A. Auber, et al.
2021. Are we ready to track climate-driven shifts in marine species across international boundaries? A global survey of scientific bottom trawl data. Glob. Change Biol. 27:220–236.

O'Leary, C. A., J. T. Thorson, J. N. Ianelli, and S. Kotwicki.
2020. Adapting to climate-driven distribution shifts using model-based indices and age composition from multiple surveys in the walleye pollock (*Gadus chalcogrammus*) stock assessment. Fish. Oceanogr. 29:541–557.

Oyafuso, Z. S., L. A. K. Barnett, and S. Kotwicki.
2021. Incorporating spatiotemporal variability in multispecies survey design optimization addresses trade-offs in uncertainty. ICES J. Mar. Sci. 78:1288–1300.

Oyafuso, Z. S., L. A. K. Barnett, M. C. Siple, and S. Kotwicki.
2022. A flexible approach to optimizing the Gulf of Alaska groundfish bottom trawl survey design for abundance estimation. NOAA Tech. Memo. NMFS-AFSC-434, 142 p.

Peel, D., M. V. Bravington, N. Kelly, S. N. Wood, and I. Knuckey.
2013. A model-based approach to designing a fishery-independent survey. J. Agric. Biol. Environ. Stat. 18:1–21.

R Core Team.
2019. R: a language and environment for statistical computing. R Foundation for Statistical Computing, Vienna, Austria. [Available from website, accessed August 2019.]

Rue, H., S. Martino, and N. Chopin.
2009. Approximate Bayesian inference for latent Gaussian models using integrated nested Laplace approximations (with discussion). J. R. Stat. Soc., B 71:319–392.

Stauffer, G.
2004. NOAA protocols for groundfish bottom trawl surveys of the nation's fishery resources. NOAA Tech. Memo. NMFS-F/SPO-65, 205 p.

Thorson, J. T.
2019. Guidance for decisions using the Vector Autoregressive Spatio-Temporal (VAST) package in stock, ecosystem, habitat and climate assessments. Fish. Res. 210:143–161.

Thorson, J. T., and K. Kristensen.
2016. Implementing a generic method for bias correction in statistical models using random effects, with spatial and population dynamics examples. Fish. Res. 175:66–74.

Thorson, J. T., and L. A. K Barnett.
2017. Comparing estimates of abundance trends and distribution shifts using single- and multispecies models of fishes and biogenic habitat. ICES J. Mar. Sci. 75:1311–1321.

Thorson, J. T., and M. A. Haltuch.
2019. Spatiotemporal analysis of compositional data: increased precision and improved workflow using model-based inputs to stock assessment. Can. J. Fish. Aquat. Sci. 76:401–414.

Thorson, J. T., A. O. Shelton, E. J. Ward, and H. J. Skaug.
2015. Geostatistical delta-generalized linear mixed models improve precision for estimated abundance indices for West Coast groundfishes. ICES J. Mar. Sci. 72:1297–1310.

Thorson, J. T., C. J. Cunningham, E. Jorgensen, A. Havron, P.-J. F. Hulson, C. C. Monnahan, and P. von Szalay.
2021. The surprising sensitivity of index scale to delta-model assumptions: recommendations for model-based index standardization. Fish. Res. 233:105745.

von Szalay, P. G.
2015. The impact of sample size reduction on the precision of biomass estimates in the Gulf of Alaska. NOAA Tech. Memo. NMFS-AFSC-297, 17 p.

von Szalay, P. G., and N. W. Raring.
2018. Data report: 2017 Gulf of Alaska bottom trawl survey. NOAA Tech. Memo. NMFS-AFSC-374, 260 p.

Wakabayashi, K., R. G. Bakkala, and M. S. Alton.
1985. Methods of the U.S.–Japan demersal trawl surveys. *In* Results of cooperative U.S.–Japan groundfish investigations in the Bering Sea during May–August 1979 (R. G. Bakkala and K. Wakabayashi, eds.), p. 7–29. Int. North Pac. Fish. Comm. Bull. 44. [Available from website.]

Errata

Fishery Bulletin 118:275–283 (2020).
Mercaldo-Allen, Renee, Paul Clark, Dylan Redman, Yuan Liu, Shannon Meseck, Lisa Milke, Julie M. Rose, and Ronald Goldberg
Temperature-related changes in species composition of juvenile finfish on a rock reef in Long Island Sound

Corrections

On Page 280, Figure 4 should read as follows, with corrected values on the *y*-axis of graphs in all panels except in the top 2 panels for black sea bass and cunner:

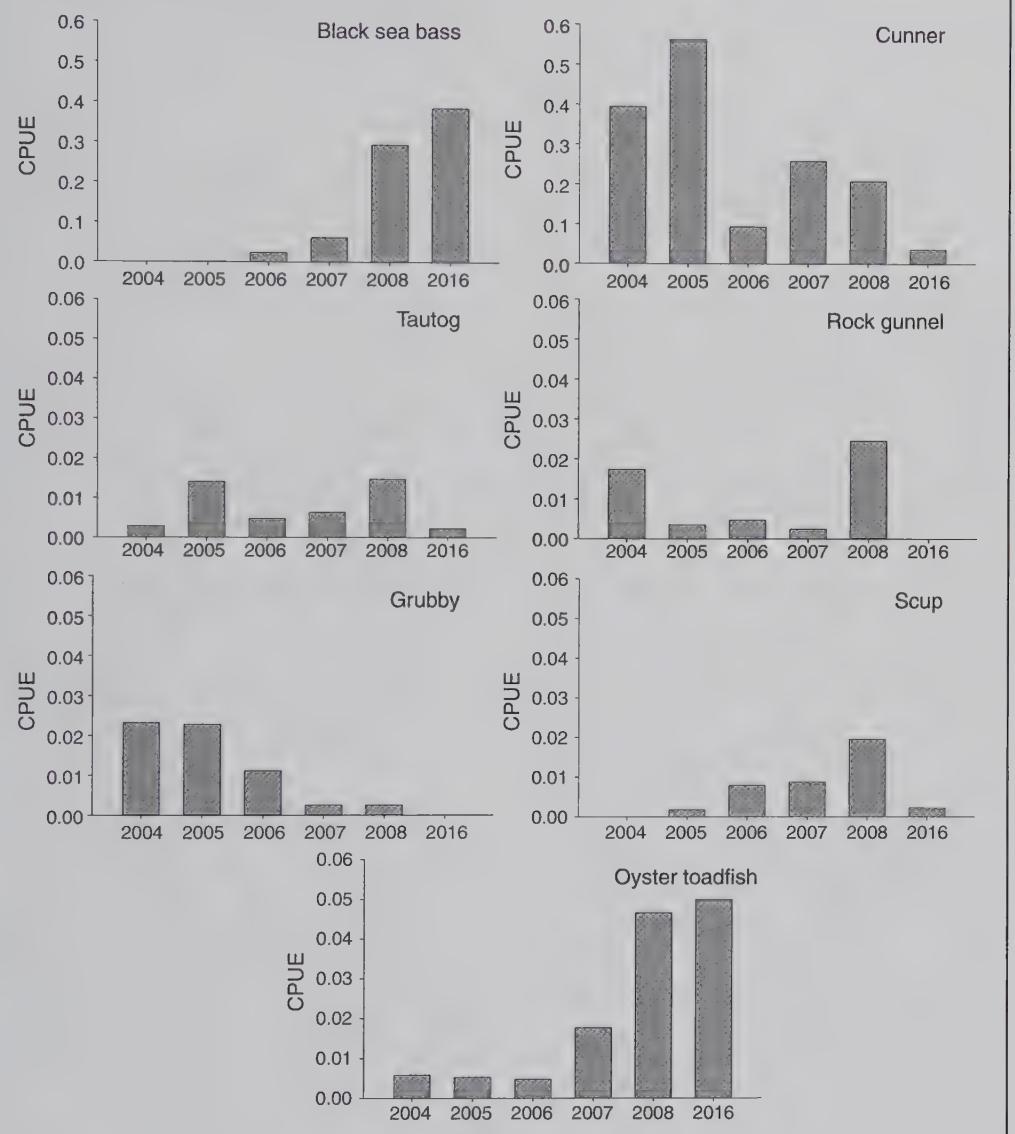

Figure 4

Abundance of juveniles for dominant finfish species caught in traps on a cobble and boulder reef in Long Island Sound during June, July, and August in 2004–2008 and in 2016. Catch per unit of effort (CPUE), used as an index of abundance, was calculated by summing the number of all fish caught and dividing by the total annual fishing effort (number of traps multiplied by number of sampling trips). The dominant species were the black sea bass (*Centropristis striata*), cunner (*Tautoga adspersus*), tautog (*Tautoga onitis*), rock gunnel (*Pholis gunnellus*), grubby (*Myoxocephalus aenaeus*), scup (*Stenotomus chrysops*), and oyster toadfish (*Opsanus tau*). Note that the graphs for black sea bass and cunner have a different range of CPUE values on the *y*-axis (up to 0.6) than graphs for the other species (values up to 0.06).

Fishery Bulletin

Guidelines for authors

Contributions published in *Fishery Bulletin* describe original research in marine fishery science, fishery engineering and economics, and marine environmental and ecological sciences (including modeling). Preference will be given to manuscripts that examine processes and underlying patterns. Descriptive reports, surveys, and observational papers may occasionally be published but should appeal to an audience outside the locale in which the study was conducted.

Although all contributions are subject to peer review, responsibility for the contents of papers rests upon the authors and not on the editor or publisher. *Submission of an article implies that the article is original and is not being considered for publication elsewhere.*

All submissions are subject to a double-blind review to remove the identity of author and reviewer during the review process.

Plagiarism and double publication are considered serious breaches of publication ethics. To verify the originality of the research in papers and to identify possible previous publication, manuscripts may be screened with plagiarism-detection software.

Manuscripts must be written in English; authors whose native language is not English are strongly advised to have their manuscripts checked by English-speaking colleagues before submission.

Once a paper has been accepted for publication, online publication takes approximately 2 weeks.

There is no cost for publication in *Fishery Bulletin*.

Types of manuscripts accepted by the journal

Articles generally range from 20 to 30 double-spaced typed pages (12-point font) and describe an original contribution to fisheries science, engineering, or economics. Tables and figures are not included in this page count, but the number of figures should not exceed 1 figure for every 4 pages of text. Articles contain the following divisions: abstract, introduction, methods, results, discussion, and conclusions.

Notes are generally less than 10 double-spaced typed pages (12-point font), including the Literature cited section. Like articles, notes describe an original contribution to fisheries science. They follow a format similar to that for articles: abstract, introduction, methods, results, and discussion, but the results and discussion sections may be combined and a conclusions section should not be included. They should include no more than 2 figures or tables (2 of each would be too many). They are distinguished from full articles in that they report a noteworthy new observation or discovery—such as the first report of a new species, a unique finding, condition, or event that expands our knowledge of fisheries science, engineering, or economics—and do not require a lengthy discussion. Manuscripts on range extensions will not be considered.

Companion articles should be submitted together and are published together as a scientific contribution. Both articles should address a closely related topic and may be articles that result from a workshop or conference.

Review articles of exceptional quality may be considered occasionally for publication on a case-by-case basis. They address a timely topic that is relevant to aspects of fisheries science. They should include an abstract, but the format of the article, per se, will be up to the author. Please contact the scientific editor to discuss your ideas regarding a potential review article before embarking on such a project.

Perspective essays generally are less than 5 double-spaced typed pages (12-point font) and provide clarification of misused terms or misunderstood topics in fisheries science. Essays are accepted at the discretion of the scientific editor. Opinion pieces on policy will not be considered. They should include an abstract and a list of the literature cited, but no other sections should divide the article. Please contact the scientific editor to discuss your idea before making a submission.

Preparation of manuscript

Title page should include authors' full names, affiliations, mailing addresses, and the senior author's email address.

Abstract should be limited to 200 words (one-half typed page), state the main scope of the research, and emphasize the authors' conclusions and relevant findings. Do not review the methods of the study or list the contents of the paper. Because abstracts are circulated by abstracting agencies, it is important that they represent the research clearly and concisely.

General text must be typed in 12-point Times New Roman font throughout. A brief introduction should convey the broad significance of the paper; the remainder of the paper should be divided into the following sections: Materials and methods, Results, Discussion, Conclusions, and Acknowledgments. Headings within each section must be short, reflect a logical sequence, and follow the rules of subdivision (i.e., there can be no subdivision without at least 2 subheadings). The entire text should be intelligible to interdisciplinary readers; therefore, all acronyms, abbreviations, and technical terms should be written out in full and defined the first time they are mentioned. Abbreviations should be used sparingly because they are not carried over to indexing databases and slow readability for those readers

outside a discipline. They should never be used for the main subject (e.g., species or method) of a paper.

For general style, follow the U.S. Government Publishing Office *Style Manual* (2016, available at website) and *Scientific Style and Format: the CSE Manual for Authors, Editors, and Publishers* (2014, 8th ed.) published by the Council of Science Editors. For scientific nomenclature, use the current edition of the American Fisheries Society's (AFS) *Common and Scientific Names of Fishes from the United States, Canada, and Mexico* and its companion volumes (*Crustaceans, Mollusks, Cnidaria and Ctenophora*, and *World Fishes Important to North Americans*). For species not found in the previously mentioned AFS publications and for more recent changes in nomenclature, use the Integrated Taxonomic Information System (ITIS, available at website), or, secondarily, the California Academy of Sciences *Catalog of Fishes* (available at website) for species names not included in ITIS. Common (vernacular) names of species should be lowercase. Citations must be given for the identification of specimens. For example, "Fish species were identified according to Collette and Klein-MacPhee (2002); sponges were identified according to Stone et al. (2011)."

Dates should be written as follows: 11 November 2018. Measurements should be expressed in metric units, for example, "58 metric tons (t);" if other units of measurement are used, please make this fact explicit to the reader. Use numerals, not words, to express whole and decimal numbers in the general text, tables, and figure captions (except at the beginning of a sentence). For example, "We considered 3 hypotheses. We collected 7 samples in this location." Use American spelling. Refrain from using the shorthand slash (/), an ambiguous symbol, in the general text.

Cite all software, special equipment, and chemical solutions used in the study within parentheses in the general text, including the version number, company name, and the city and state (or nation) of the company headquarters, for example, "SAS, vers. 9.4 (SAS Institute Inc., Cary, NC)."

Word usage and grammar that may be useful are the following:

- *Aging*
  For our journal, the word *aging* is used to mean both age determination and the aging process (senescence). Authors should make clear which meaning is intended where ambiguity may arise.

- *Fish and fishes*
  The plural of the word fish (a collective noun that implies individuals without regard to species) is *fish*.
  Example: The *fish* were collected by trawl net.
  Example: The numbers of *fish* collected that season were less than the numbers from previous years.

  The plural for *fish species* is *fishes* (a contrived plural used by taxonomists to mean several or more *fish species*) or one can use *fish species* (which is preferred in this journal for clarity across disciplines).
  Example: The *fishes* of Puget Sound [biodiversity is implied] or
  Example: The *fish species* of Puget Sound [preferred plural for clarity across disciplines].

- *Crab and crabs, squid and squids, etc.*
  The plural of the word *crab* (i.e., many individuals without regard to species) is *crab*.
  Example: The crab were sorted by weight.
  Example: Many red king *crab* were dying [Many individuals of one species of crab.]

  The plural of *crab species* is *crabs* (a word used by taxonomists) or *crab species* (the latter is preferred in this journal for clarity).
  Example: These *crabs* were selected for treatment. [Different crab species are implied.]
  Example: These *crab species* were selected for treatment. [Preferred word choice for clarity.]
  Example: Snow *crabs* are found throughout the North Pacific Ocean and Bering Sea. [There are 2 species of snow crab; therefore the word *crabs* can be used here.]
  Example: *Two species* of snow *crab* are found throughout the North Pacific Ocean and Bering Sea. [Preferred usage for clarity.]
  Example: Three crabs were selected for treatment. [3 species of crab are implied.]
  Example: Three crab species were selected for treatment. [Preferred word choice for clarity.]

- We use *fisherman* and *fishermen*, not *fisher* and *fishers*, in this journal. One can always use crew member, vessel operator, and angler (the latter for recreational fishing).

- *The definite article with common names of species*
  When the singular common name of a species represents the entire class or group to which it belongs, use the definite article.
  Example: Only one species of the genus *Salmo* is found in the Atlantic Ocean—*the* Atlantic salmon (*Salmo salar*).
  Example: The sonic emissions of *the* bottlenose dolphin are complex.

  For plural common names, this rule does not apply.
  Example: Chinook salmon are found throughout the Pacific Ocean.
  Example: Bottlenose dolphins are found in temperate and tropical waters.

- *Sex*
  For the meaning of male and female, use the word *sex*, not *gender*. Do not write, "fish were sexed." Write, "sex was determined."

- *Participles*
  As adjectives, participles must modify a specific noun or pronoun.
  Example: Using mark-recapture methods, these scientists determined the size of the population. [Correct. The participle *using* modifies the word *scientists*.]

Example: These scientists, based on the collected data, concluded that the mortality rate of these fish had increased. [Incorrect. The scientists were not based on the collected data.]

Example: These scientists concluded, on the basis of collected data, that the mortality rate of these fish had increased. [Correct. The offending participle has been eliminated and an adverbial phrase modifies the verb *concluded*.]

Equations and mathematical symbols should be set from a standard mathematical program (MathType or Equation Editor). Equations formatted in LaTex are not acceptable. For mathematical symbols in the general text (α, χ^2, π, $\pm$, etc.), use the symbols provided by the MS Word program and italicize all variables, except those variables represented by Greek letters and the superscript and subscript parts of variables and expressions. Do not use photo mode when creating these symbols in the general text, and do not cut and paste equations, letters, or symbols from a different software program.

Number equations (if there are more than one) for future reference by scientists; place the number within parentheses at the end of the first line of the equation.

Literature cited section comprises published works and those accepted for publication (in press) in peer-reviewed journals. Follow the name and year system for citation format in this section (i.e., citations should be listed alphabetically by the authors' last names, and then by year if there is more than one citation by the same author. A list of abbreviations for citing journal titles can be found on our website.

Authors are responsible for the accuracy and completeness of all citations. Avoid the use of multiple citations when a single citation sufficiently supports a statement; cite the work that first reported the information that supports a statement, not all of the subsequent works. Literature citation format: Authors (last name, followed by initials for first name and, if given, middle name of first author; then list names of additional authors with initials before last names). Year. Title of article. Abbreviated title of the journal in which it was published. Always include either the range of page numbers (for a journal article) or a total number of pages (for a book or other type of publication). List a sequence of citations in the general text chronologically, for example, "(Smith, 1932; Green, 1998; Smith and Jones, 2015)."

Acknowledgments should be no more than 6 lines of text. Only those who have contributed in an outstanding way should be acknowledged by name. For recognition of other persons or groups, use a general term, such as *crew*, *observers*, or *research coordinators*, and do not include names with these terms.

Digital object identifier (doi) code ensures that a publication has a permanent location online. A doi link (which may include a doi code) should be included at the end of citations of published literature. Authors are responsible for submitting accurate doi links. Faulty links will be deleted at the page-proof stage.

Footnotes are used for all documents that have not been formally peer reviewed and for observations and personal communications, but these types of references should be cited sparingly in manuscripts submitted to the journal.

All reference documents, administrative reports, internal reports, progress reports, project reports, contract reports, personal observations, personal communications, unpublished data, manuscripts in review, and council meeting notes are footnoted in 10-point font and placed at the bottom of the page on which they are first cited. Footnote format is the same as that for formal literature citations. A link to the online source (e.g., [Available from http://www..., accessed July 2017.]), or the mailing address of the agency or department holding the document, should be provided so that readers may obtain a copy of the document.

Tables are often overused in scientific papers; it is seldom necessary to present all the data associated with a study. Tables should not be excessive in size and must be cited in numerical order in the text. Headings should be short but ample enough to allow the table to be intelligible on its own.

All abbreviations and unusual symbols must be explained in the table legend. Other incidental comments may be footnoted with numeral footnote markers. Use asterisks only to indicate significance in statistical data. Do not put a table legend on a page separate from the table; place the legend above the table. *Do not submit tables in photo mode.*

- Note probability with a capital, italic *P*.
- Provide a zero before all decimal points for values less than one (e.g., 0.07).
- Round all values to 2 decimal points.
- Use a comma in numbers of 5 digits or more (e.g., 13,000 but 3000).

Figures must be cited in numerical order in the text. Graphics should aid in the comprehension of the text, but they should be limited to presenting patterns rather than raw data. The number of figures should not exceed 1 figure for every 4 pages of text.

Figure legends should explain all symbols and abbreviations seen in the figure and should be double spaced on a separate page at the end of the manuscript.

Line art and halftone figures should be saved at resolutions >600 dots per inch (dpi) and >300 dpi, respectively. Color is allowed in figures to show morphological differences among species (for species identification), to show stain reactions, to show gradations (such as those of temperature and salinity within maps), and to distinguish

between numerous lines and symbols in graphs. Figures approved for color should be saved in CMYK format.

All figures must be submitted as PDF, TIFF, or EPS files.

- Capitalize only the first letter of the first word and proper nouns in all labels within figures.
- Do not use overly large font sizes for labels in maps and for axis labels in graphs.
- Use the same point size for all labels, except for panel labels (e.g., **A**), which should be slightly larger than other labels (e.g., 11 point versus 8 point).
- Use a sans serif font for all labels. Panel labels (e.g., **A**), however, should be in Times New Roman font.
- Do not use bold fonts or bold lines in figures. Do not use italic fonts. Exceptions include use of italic fonts for labels of bodies of water in maps and a bold font for panel labels (e.g., **A**).
- Do not place outline rules around graphs.
- Do not include vertical and horizontal lines in the background of graphs. Ticks for values on the x-axis and y-axis will suffice.
- Place a north arrow and label degrees latitude and longitude (e.g., 170°E) in all maps. If scale of map requires more than degrees, use degrees minutes, not decimal degrees.
- Place panel labels (e.g., **A**, **B**, **C**) within the upper-left area of each graph or photo in a multi-panel figure, from left to right, then top to bottom. If the letter is not visible against a dark background, put a white box behind it. Do not use white labels.
- Avoid placing labels vertically or diagonally. Y-axis labels can be vertical. Words in horizontal labels can be stacked vertically to fit.
- Use symbols, shading, or patterns (not clip art) in maps and graphs.
- For scale bars in maps, use kilometers. Use the label *km* or *kilometers* (lowercased).

Supplementary materials that are considered essential, but are too large or impractical for inclusion in a paper (e.g., metadata, figures, tables, videos, and websites), may be provided at the end of an article. These materials are subject to the editorial standards of the journal. A URL to the supplementary material and a brief explanation for including such material should be sent at the time of initial submission of the paper to the journal.

- **Metadata, figures, and tables** should be submitted in standard digital format (MS Word or PDF file) and should be cited in the general text, for example, as ". . . was determined (Suppl. Table 3, Suppl. Fig. 1)."
- **Websites** should be cited with a URL in the general text.
- **Videos** must not be larger than 30 MB to allow a swift technical response for viewing the video. Authors should consider whether a short video uniquely captures what text alone cannot capture for the understanding of a process or behavior under examination in the article. Supply an online link to the location of the video.

Copyright law does not apply to *Fishery Bulletin*, which falls within the public domain. However, if an author reproduces any part of an article from *Fishery Bulletin*, reference to source is considered correct form (e.g., Source: Fish. Bull. 117:105).

Failure to follow these guidelines and failure to correspond with editors in a timely manner will delay publication of a manuscript.

Submission of manuscript

Submit a manuscript online at the ScholarOne Manuscripts website for *Fishery Bulletin*. Commerce Department authors must provide proof of internal clearance of their manuscripts with either a completed and signed NOAA Form 25-700 or a copy of the clearance email from the Research Publication Tracking System. For further details on electronic submission, please contact the associate editor, Cara Mayo, at

cara.mayo@noaa.gov.

When requested, the text and tables should be submitted in MS Word format. Each figure should be sent as a separate PDF, TIFF, or EPS file. Send a copy of a figure in the original software if conversion to any of these formats yields a degraded version of the figure.

Questions? If you have questions regarding these guidelines, please contact the managing editor, Kathryn Dennis, at

kathryn.dennis@noaa.gov.

Questions regarding manuscripts under review should be addressed to Associate Editor Cara Mayo.

Fishery Bulletin

Subscription form

Superintendent of Documents **Publications** Order Form

*5178

☐ YES, please send me the following publications:

____ Subscriptions to *Fishery Bulletin*
for $32.00 per year ($44.80 foreign)

The total cost of my order is $ _____ . Prices include regular domestic postage and handling and are subject to change.

_____
(Company or Personal Name) (Please type or print)

_____
(Additional address/attention line)

_____
(Street address)

_____
(City, State, ZIP Code)

_____
(Daytime phone including area code)

_____
(Purchase Order No.)

Charge your order. IT'S EASY!

Please Choose Method of Payment:

☐ Check payable to the Superintendent of Documents
☐ GPO Deposit Account ☐☐☐☐☐☐☐–☐
☐ VISA or MasterCard Account
☐☐☐☐☐☐☐☐☐☐☐☐☐☐☐☐
☐☐☐☐ (Credit card expiration date)

To fax your orders (202) 512-2104

_____
(Authorizing Signature)

Mail to: Superintendent of Documents
P.O. Box 979050, St. Louis, Missouri 63197
Tel. no. (U.S. callers): 866-512-1800
Tel. no. (International callers): 1-202-512-1800

Thank you for your order!

Also available online at
https://bookstore.gpo.gov/products/fishery-bulletin
email: ContactCenter@gpo.gov